Laboratory Study on the Role of Steady Streaming in Oscillatory Sheetflow Transport

(シートフロー漂砂における定常流れの役割に関する実験的研究)

by

KYIKYI LWIN

キー キー ルウィン

A dissertation submitted to the Graduate School of Engineering
in partial fulfillment of the requirements

for the degree of Doctor of Engineering

at

The University of Tokyo

September 2012

Author's Declaration

I hereby declare that I am the sole author of this thesis.
I authorize the University of Tokyo to lend this thesis to other institutions or individuals for the purpose of scholarly research.

Signature

I further authorize the University of Tokyo to reproduce this thesis by photocopying or by other means, in total or in part, at the request of other institutions or individuals for the purpose of scholarly research.

Signature

Examination Committee

Prof. **Shinji Sato**

Assoc. Prof. **Yoshimitsu Tajima**

Assoc. Prof. **Takeyoshi Chibana**

Assoc. Prof. **Fukushi Kensuke**

Assoc. Prof. **Haijiang Liu**

ABSTRACT

Many coastal activities are concerned with the interaction of coastal sedimentary processes and coastal works, such as the construction of structures for shore protection and stabilization, and beach nourishment. It is important to measure sand properties, sediment moving processes and transport rates, as well as the resulted nearshore morphology to understand the sediment transport mechanism under various wave and current conditions. In this study, we are interested in understanding the sediment transport mechanism, especially the influence of wave-induced boundary layer streaming on sediment transport under combined wave and current conditions in the sheetflow regime.

Recently, sediment net transport rate measured through the large wave flume (LWF) experiments presents a more onshore tendency, i.e., a larger onshore net transport, than the result from the small oscillatory flow tunnel (OFT) experiments. Various researchers argue that the wave-induce onshore streaming could be the reason to cause such difference. The objective of this research is to understand the physical features of this phenomenon and answer the question: Does onshore streaming really enhance the onshore sheetflow net sand transport? If so, then, how and how much does it affect the onshore transport? If not, what is the real reason behind? The second is to obtain new insights into the importance of the boundary layer onshore streaming and to understand the transport processes under wave and current conditions.

To achieve the objectives and to measure the sediment net transport rate under sheet flow conditions, laboratory experiments were conducted under the combined asymmetric wave-current conditions to quantitatively evaluate the influence from the onshore streaming. The second order Stokes' wave theory with a velocity asymmetric index of 0.57 was applied for wave generation with three well-sorted sands with medium sand size of D_{50} =0.3 mm (coarse), 0.16 mm (fine) and 0.13 mm (very fine). For fine sand without onshore current, the net transport increases with increasing velocity, and it is directed to the onshore. However, for larger velocity case, the net transport rate decreases and the direction also changes to the offshore. As for the very fine sand, the net transport rate decreases and is directed to the offshore even for a small velocity case. Considering the coarse sand, the net transport is in the onshore direction.

To understand the effect of onshore streaming, a small current U_c of 10 cm/s and 20 cm/s was generated in the onshore direction. Experiment results for small current 10 cm/s indicate the magnitude offshore net transport rate reduces and the direction is to the offshore for the very fine sand and fine sand with large velocity case. When increasing the small current value to 20 cm/s, the net transport rate of fine and very fine sand increases and changes to onshore direction with small velocity case. But for large velocity case, even though the magnitude of offshore net rate reduces, the direction is still directed to offshore with fine sand case. Taking into account the net transport rate measured under the combined wave and current cases, the onshore net transport for coarse sand continuously increases. It is noted that the tendency of increasing of net transport rate is not observed in fine grains when the velocity becomes increases without the contribution of current. In case of the contribution of small onshore streaming, although the magnitude of offshore net transport rate of fine and very fine sand reduces, it still directs to offshore under large velocity case. It indicates that the onshore streaming, indeed, enhances offshore net transport rate for fine sand and very fine sand with large velocity. On the other hand, the small onshore streaming may be partly important for the case of fine sand under small velocity condition.

Sediment particle velocity within the sand-laden sheetflow layer was measured by means of a PIV technique. By averaging the sediment particle velocity over one wave period, the mean flow velocity was also evaluated. From the mean velocity profile under pure wave conditions, it is found that, in case of the coarse sand, an onshore streaming is detected in the pick-up layer and leads to offshore in the upper sheet-flow layer. Nevertheless, in case of fine sand, the profiles show a negative streaming due to the strong phase-lag effect. The positive near-bed streaming is not observed. The large phase-lag can induce a negative (offshore) net transport. Thus, the phase-lag effect seems to play an important role for the sediment sheetflow transport in the OFT test. For coarse sand under combined wave and current conditions, a very small onshore current exists in the pick-up layer ($z< 0$ mm) and the mean flow velocity leads to onshore direction in the sheet flow layer. In the suspension layer, when the elevation is higher than 15 mm, the mean flow changes its direction from onshore to offshore. In the case of fine sand, the time-averaged velocity indicates the streaming is positive in the pick-up layer as well as

in the sheet flow layer. After that, the velocity decreases for increasing the depth (z) mm. Clearly, the additional onshore current in the tunnel does contribute to more onshore sediment transport. Besides that, it is also confirmed that the phase-lag effect plays an important role in the sediment transport under the sheetflow conditions, especially for the fine sand case with large velocity case as it produces offshore net transport rate. Here also, the streaming profiles are very sensitive to sand size.

Furthermore, the measured net transport rates are compared with the results from surface wave under same flow conditions. For very fine and fine sand with onshore streaming, the sediment rate under oscillatory flow tunnel can predict about 75 % of net rates under surface wave with small velocity case. Now, the new experiments indicated the difference of sediment rate between these was about 1.5 times for fine sand with onshore streaming. In addition, the results of coarse sand with streaming produce larger onshore net sediment rate compared to surface wave. It means the contribution of streaming is quite large enough to enhance the more onshore net transport rate for the coarse sand. As a result, the streaming effect is very dependent on sand size.

The maximum erosion depth was estimated from the temporal change of the measured erosion depth. A linear relationship was found between the relative maximum erosion depth δ_{em}/D and the maximum Shields parameter, θ_m. The erosion depth under crest is larger than under trough for fine sand and coarse sand under combined wave and current conditions. The influence of wave period and velocity on erosion depth was also measured for two types of sand.

And then, in order to know how much the distribution of small onshore streaming enhanced the larger net rate, the results of net transport rate with onshore streaming are compared with SANTOSS model which include surface wave effects. In this study, SANTOSS model was also considered as streaming-related model including the streaming effect by analytically to represent the surface wave phenomenon. The comparison results showed that although the results of fine and coarse sand with onshore streaming overestimated compared to the results of streaming-related model, it lies with a factor of two differences.

ACKNOWLEDGEMENTS

First, I would like to express my sincere appreciation and deep sense of gratitude Professor Dr. Shinji SATO for his support and for his careful guidance, encouragement, and kind consideration in enabling me to complete my thesis throughout my studies at the University of Tokyo, Japan. I am also grateful to Associate Professor Yoshimitsu Tajima for helping me with his valuable comments and remarkable guidance. Plus I offer my thanks to Associate Professor Haijiang LIU, who guided and advised to make sheetflow experiments. I also wish to thank him for pointing forward a lot of beneficial opinions, for his helpful advice and good suggestions during the studies at the University of Tokyo.

Second, I would like to thank to MEXT scholarship program for granting opportunity and providing to study in Japan. I am also very thankful to my lab-mates and all of my friends assisting me during my stay in the University of Tokyo.

I would also acknowledge Foreign Student Office and teachers from the University of Toyo who taught me Japanese Language at the department of Civil Engineering for their great assistance.

I am deeply indebted to Honorable Minister U Nyan Tun Aung and former Minister U Thein Swe, Ministry of Transport, for their kind permission to study my doctorate course. Moreover, I would like to take this opportunity to express my sincere appreciation to Prof. Dr. Charlie Than, Rector of Myanmar Maritime University, for giving me a chance to further study in Japan. My special thanks goes to Head of Department (Academic), Daw Khin Kyu Kyu, Head of River and Coastal engineering Department, and all colleagues from Myanmar Maritime University for their constant moral support and words of encouragement all the time.

Finally, I also would like to thank my family for their love and emotional support throughout my studies at the University of Tokyo and for their encouragement in the completion of this thesis.

Table of Contents

LISTS OF FIGURES

LISTS OF TABLES

LIST OF NOTATIONS

A	water particle horizontal excursion distance
A_p	cross sectional areas for cylindrical piston region
A_t	cross sectional areas for rectangular test section
a	semi-excursion or amplitude of the horizontal water excursion
a_p	amplitude of the horizontal excursion for piston
b	width of the tunnel
c	wave celerity
d_g	wave orbital diameter
D	piston diameter
D_E	energy dissipation parameter
D^*	normalized particle size parameter
D_{25}	grain diameter for which 25 % of the sediment by weight is finer
D_{50}	grain diameter for which 50 % of the sediment by weight is finer
D_{75}	grain diameter for which 75 % of the sediment, by weight is finer
$DQ_{fg}\ (k,l)$	minimum quadratic difference
f_{av}	mean values of brightness f
f_c	current friction factor
f_e	friction factor for energy dissipation
f_{cw}	wave-current friction factor
f_w	wave friction factor
$f(i,j)$	a function stands for the brightness value at pixel (i,j)
g	acceleration due to the gravity
g_{av}	mean value of brightness g
H	wave height
H_t	height of the tunnel test section
h	water depth
k	wave number
k_s	roughness height
k_{sc}	roughness height for current

k_{sw}	roughness height for wave
L	wave length
N	counter number
P_i	percentage of the i^{th} fraction of bed material, (i=c, t)phase-lag parameter defined by Ribberink (2010)
p	phase-lag parameter
q	net sediment transport rate
q_b	bedload transport rate
q_{ss}	suspended load transport rate
R_{fg}	cross-correlation between brightness f and g
R_v	velocity asymmetric index
r	Phase lag correction factor
T	wave period
T_c	onshore velocity duration
T_t	offshore velocity duration
t	time
U	amplitude of the water horizontal orbital velocity
U_c	net current velocity
U_p	amplitude of the piston horizontal orbital velocity
U_r	Ursell number
U_{rms}	root mean square velocity
u_c	equivalent sinusoidal velocity amplitude for crest
u_t	equivalent sinusoidal velocity amplitude for trough
u_{max}	maximum free-stream velocity
u_s	sediment horizontal velocity
$u(t)$	time–dependent horizontal orbital velocity directly above the wave boundary layer
$u(z)$	vertical distribution of horizontal velocity
W_t	width of the tunnel test section

w	water particle velocity
w_o	free settling velocity of sand
w_s	sediment vertical velocity
X	horizontal displacement of the moving pattern between two consecutive images
Y	vertical displacement of the moving pattern between two consecutive images
z_o	level where the current velocity is assumed to be zero
z_{um}	level where current velocity U_c is specified
α	linear coefficient
δ_s	sheetflow layer thickness
δ_e	time varying erosion depth
δ_{em}	maximum erosion depth
$\triangle t$	time interval
Γ	parameter introduced by Dibajinia and Watanabe(1992)
ω	angular frequency of the oscillation
ω_{cr}	critical value of ω_i
ω_i	(i=c,t) phase-lag parameter introduced by Dibajinia and Watanabe(1992)
ω_p	angular frequency of the piston
γ_i	(i=c,t) parameter introduced by Dibajnia et al.(2001)
β_i	(i=c,t) parameter introduced by Dibajnia et al.(2001)
θ	time-varying Shields parameter
θ_{cr}	critical Shields parameter
θ_m	maximum Shields parameter
θ_{sheet}	critical Shields parameter for initiation of sheetflow
$\theta(t)$	time-dependent Shields parameter
ε_b	bedload efficiency factor
ε_s	suspended load efficiency factor

Θ_{cr}	critical mobile number
Θ_i	(i=c,t) mobile number
ρ	water density
ρ_s	sediment density
η	ripple height
λ	ripple length
κ	Von Karman constant
σ_f	standard deviation of brightness f
σ_g	standard deviation of brightness g
ν	kinematic viscosity
τ	time-varying bed shear stress
τ_m	amplitude of bed shear stress
Φ	time-average sediment flux
Ω_i	(i=c, t) entrainment of sand carried only by positive or negative velocity defined by Dibajnia and Watanabe (1992)
$\Omega_i^{'}$	(i=c, t) remaining of sand from the previous from positive or negative half cycle to be carried only by next positive or negative velocity defined by Dibajnia and Watanabe (1992)
Ω_{cc}	entrainment of sand carried only by positive velocity defined by Ribberink (2010)
Ω_{tt}	entrainment of sand carried only by negative velocity defined by Ribberink (2010)
Ω_{ct}	remaining of sand from the previous positive half cycle to be carried only by next negative velocity defined by Ribberink (2010)
Ω_{tc}	remaining of sand from the previous negative half cycle to be carried only by next positive velocity defined by Ribberink (2010)

CHAPTER 1

Introduction

1.1. Physical Background

1.1.1. Sediment Transport

As the world's population has been growing continuously, the necessary of land in the coastal region is still increasing. In the world, the coastal regions are the most densely populated areas. The worldwide average width of the coastal zone on the terrestrial side is said to be 60 km. The zone occupies less than 15% of the Earth's land surface, yet it accommodates more than 50% of the world's population (it is estimated that 3.1 billion people live within 200 kilometres from the sea). With three-quarters of the world population expected to reside in the coastal zone by 2025, human activities originating from this small land area will impose an inordinate amount of pressures on the global system. Furthermore, only 40% of the one million km of coastline is accessible and temperate enough to be habitable. The coastal zone is a dynamic area of natural change and of increasing human use. For the view point of ecosystem and human welfare of each country, coastal regions are one of the most important for their strategic location for residential, recreational, and industrial activities. Hence, these coasts are arisen to preserve and maintain the shore against the destructive forces of nature such as strong waves and tsunami.

The sediment on the seabed is transported when it is exposed to large enough forces, or *shear stresses*, by the water movements. These movements can be caused by the current or by the wave orbital velocities or a combination of both, the latter being the most important situation. For the description of the sediment transport along a shoreline or in a coastal area, the relevant parameters are the wave and current conditions, the water-level conditions i.e. tide, storm surge and wave set-up, the sediment characteristics over the area.

Many coastal activities are concerned with the interaction of coastal sedimentary processes such as the construction of structures for shore protection and stabilization, and beach nourishment. It is important to measure sand properties, sediment moving

processes and transport rates, as well as the resulted nearshore morphology to understand the sediment transport mechanism under various wave and current conditions. Sand transport occurs due to the interactions of the sediment lying on the sea bed and by waves and currents. Because of the simultaneous effect of waves and currents, cross-shore sediment transport in the nearshore region is crucially importance. A number of studies on the subject of transport mechanisms have been identified by different approaches of previous researchers. Fig. 1.1 illustrates the schematic diagram of nearshore zones within which different sediment transport modes along the cross-shore profile. As the waves shoal, their profile dramatically change, they become from sinusoidal to skewed wave. Once waves approach breaking and enter the surf zone, they become strongly asymmetric. Therefore, nearshore waves are both asymmetric and skewed, a wave with positive asymmetry and skewness that is forward-leaning in shape and peaked, narrow crests and wide, flat troughs.

Sand transport occurs in different regimes based on their increasing values of the Shields parameter. The three modes are bedload transport, suspended load transport and sheetflow transport. In the surf zone, when the Shields parameter becomes large (>0.8-1.0), the near bed velocities are so large, sand ripples are washed out and the bed becomes plane again. Therefore, the sheetflow transport regime is developed. The sheet flow predominates in the surf zone not only during storms but also even under moderate waves in the field (Watanabe et al., 1991, Dibajnia et al., 1994). Under the sheetflow conditions, sand are transported close to the bed in a thin layer has a thickness in the order of a few mm to cm with high sediment concentrations. The near-bed wave orbital velocities are relatively large and sand is commonly moved and transported in a very thin layer above the bed in the sheet-flow regime in shallow water zones.

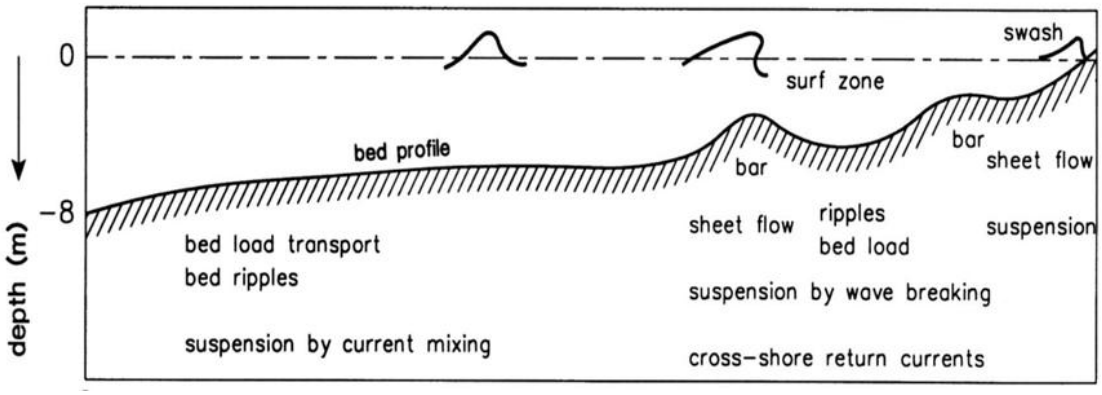

Fig. 1.1. Sand transport mechanisms along a cross-shore profile (Van Rijn,1998b)

1.2. Research Problem

Recently, it is found that under the sheetflow condition, sediment net transport rate measured through the large wave flume (hereafter, LWF) experiments presents a more onshore tendency, *i.e.*, a larger onshore net transport, than the result from the small oscillatory flow tunnel (hereafter, OFT) experiments (Dohmen-Janssen and Hanes, 2002, Schretlen et al., 2009). Various researchers (Nielsen and Callaghan, 2003, Ribberink, 1998, Schretlen et al., 2009, Wouter Kranenburg et.al., 2010) argue that the wave-induced onshore streaming could be the reason to cause such difference between the LWF and OFT experiment results since such onshore streaming develops only under the LWF condition under which the water particle vertical movement is not suppressed as it is under the OFT condition.

Nielson (2006)'s bed-shear stress model incorporates the influence of different wave shapes (velocity- and acceleration skewness) and the surface wave effect with boundary layer streaming. By adding a Wave Reynolds stress (which is a time-averaged shear stress) on top of the stress induced by near bed flow velocities and flow accelerations, the transport rate was measured. From the results, the acceleration effect is more dominant rather than streaming effect.

Taking into account the influence of streaming in the bed shear stress model, Van Rijin (2007) analyzed the model found a relation between the relative roughness and the magnitude and direction of the streaming velocity. In the model, they added an additional positive current velocity at the edge of the boundary layer in case of flat beds and

negative current velocity for ripple beds. The streaming velocity is onshore directed with a large relative roughness under sheet flow conditions and in the case of ripple-bed, the streaming is offshore directed.

Schretlen et al., (2009, 2010) also performed the newly experiment under surface wave conditions to measure and obtain detailed velocity measurements throughout the boundary layer. The results showed that especially under sheet-flow conditions, small wave induced net currents are of large importance for sand transport rates. The difference of sediment transport rate between surface wave and oscillatory flow described that it is the vertical gradient of the wave Reynolds stress in the wave boundary layer which can lead to an additional positive mean flow and bed shear stress under surface waves.

In order to know and answer the question whether the real-wave-induced streaming is indeed the explanation for the differences in sediment transport rates between tunnels and flumes, a numerical model was investigated by Wouter Kranenburg (2010), which gives the possibility to investigate processes in isolation and to quantify their contribution to sediment transport. The mean current profile was compared between the numerical and experimental results of wave flume and oscillatory flow tunnel. Good agreements were well reproduced by the model. In their model, they performed the flume simulations with and without real streaming and then compared the tunnel simulations under the same u^3.The comparison results show that, the flume simulations without real wave streaming show strongly reduced onshore transport rates compared to the earlier flume simulations (with real streaming). But the transport rates still direct to onshore shift compared to the tunnel simulation. They also do not show the tendency of a decreasing growth with increasing u^3 in the case for tunnel simulations with fine grains. These results were consistent with the previous studies (Schretlen et al., 2009, 2010). They concluded that the phase-lag effect seems still to be suppressed or at least overruled by other differences between tunnel and flume. As a result, the additional onshore current in the flume does contribute to onshore sediment transport, but can not be the full explanation of the differences in transport rates in tunnel and flume. Moreover, the real insight into this problem and the physical phenomenon of streaming effect on sediment transport rate are still unclear. Therefore, the research questions of this study are:

1. Does onshore streaming really enhance the onshore sheetflow net sand transport?
2. If not, then, what is the real reason behind? If so, then, how and how much does it affect the onshore transport?
3. Can the mean flow velocity profiles give an explanation about the cause of the increment of onshore net transport rate by the contribution from a small onshore current?

1.3. Scope of the Present Research Work

The general goal of the present study is to improve our understanding of sand transport mechanisms under various wave and current conditions. To assess the effect from a boundary streaming to the net sediment transport, several studies have been performed through experiments and numerical simulations (Nielsen and Callaghan, 2003, Dohmen-Janssen et al., 2002, Schretlen et al., 2009, 2010, Trowbridge and Madsen,1984). However, the real insight into this problem is still unclear. Therefore, comprehensive experimental studies are required to understand the physical feature of this phenomenon.

In this present study, the following objectives have been carried out:

a. To understand the sediment transport mechanism and get the dataset of measurements of net sediment transport rate under asymmetric oscillations and superimposed steady current.
b. To investigate the influence of wave-induced boundary layer streaming on sediment transport under combined wave and current conditions in the sheet flow regime.
c. To gain more understanding on the influences of the streaming components and Lagrangian motion on the model performances
d. To investigate the detailed velocities measurement of sediment particles and time-averaged velocities profiles in the near bed boundary layer by applying PIV(Particle Image Velocimetry) technique
e. To determine the time-varying erosion depth and maximum erosion depth under combined wave –current conditions

1.4. Research Methodology

In order to accomplish the objectives mentioned above and to answer the research questions, the experimental approach is adopted. A series of experiments was conducted in the OFT at the University of Tokyo. To quantitatively evaluate the influence from the onshore streaming, laboratory experiments were conducted under the combined asymmetric wave-current conditions. The second order Stokes' wave theory with a velocity asymmetric index of 0.57 was applied for oscillatory flow generation. The asymmetric flows with a period of T = 3 and 5 s and the maximum onshore velocity u_{max} varying from 0.8 to 1.6 m/s have been applied for three uniform sands with medium sand size of D_{50} = 0.13mm (very fine), D_{50} = 0.16 mm (fine) and 0.3 mm (coarse), respectively.

The movement of sediment processes is recorded by High Speed Video Camera. After that, by using image analysis, the maximum erosion depth and the instantaneous erosion depth for different flow conditions were estimated through recorded images. Temporal and spatial distributions of sediment particle velocities were investigated using Particle Image Velocimetry (PIV). To remove the noise influence in PIV analysis, a Fast Fourier Transform (FFT) algorithm was used to obtain the predominant velocity component, then average over one wave period to achieve the vertical profile of the mean flow velocity, *U (z)*.

The influences of streaming on net transport rate were investigated by applying the analytical sand transport models. Model's validation was carried out by comprehensive comparisons between calculated results and experimental measurements.

1.5. Outlines of the Thesis

In this thesis, a short review of literature of sand transport process, scope and outlines are given in this chapter 1. In chapter 2, a comprehensive review on the previous experimental works concerning the physical background of transport mechanism of uniform sediment under steady and oscillatory flows will be discussed. The different measuring techniques for erosion depth and sediment particles velocities are explained in details in chapter 2. The laboratory experimental set-up, experimental conditions and methodology are expressed in chapter 3. The measurements of PIV and the sediment

transport rates are also illustrated in this chapter. Chapter 4 deals with the experimental results which consist of measured net transport rate, erosion depth, the estimated horizontal velocity of sand particles and the mean velocity profiles under different wave conditions from a PIV technique. Chapter 5 discusses about the analytical model including boundary layer streaming and Lagrangian grain motion effects. In this chapter, the calculated sand transport will be compared with the measured net transport rate in sheet flow conditions under the 2nd order Stroke's wave.

Finally, summary of the research is presented and conclusion will be drawn from the research work. Recommendations and proposed future work will be discussed at the end of the thesis.

CHAPTER 2

Literature Reviews on Previous Researches

2.1. Cross shore sediment transport

2.1.1. General

Cross-shore sand transport refers to the cumulative movement of beach and nearshore sand perpendicular to the shore by the combined action of tides, winds, wave and currents. Cross-shore transport should be well studied because of its importance to beach erosion. Cross-shore transport is mainly caused by the flow velocity of the waves, frequently superimposed on a steady current that will interact with the sand in the seabed.

2.1.2. Sand Transport Modes and Sheet-Flow under Waves

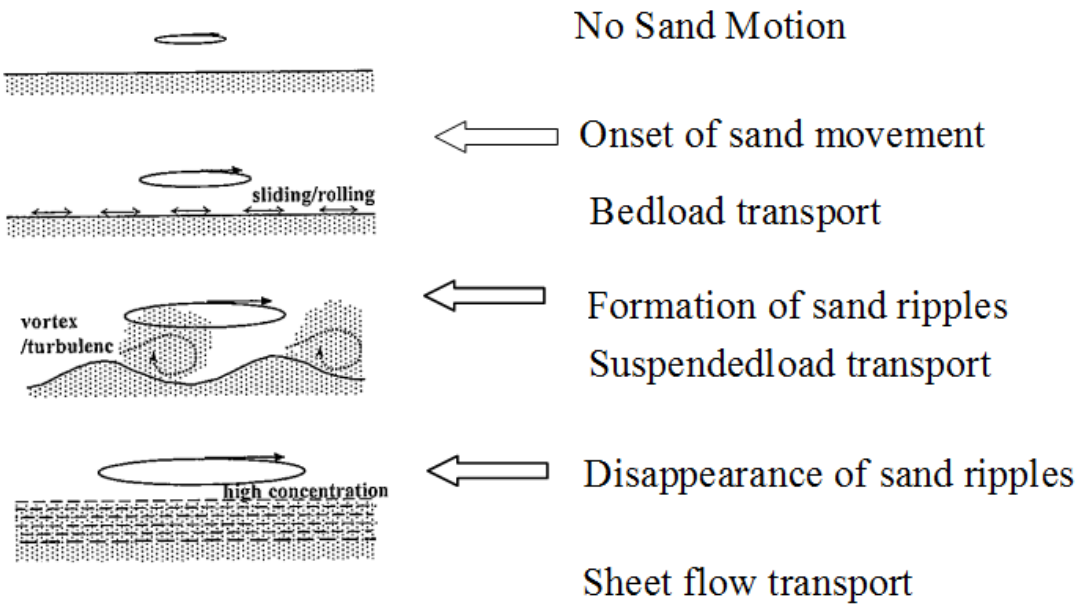

Fig. 2.1. Different modes of sediment transport

The flow field and sediment transport in the bottom boundary layer of sheetflow has been a long time investigation concern for coastal engineers who work in the field of sediment transport. Dynamics of the bottom boundary layer considerably change due to the bed forms. Sand ripples produce flow separation yielding production of turbulence that creates alternation of the velocity distribution in the bottom boundary layer together

with considerable amount of energy dissipation and sand suspension. As the orbital velocity of fluid over rippled bed is increased, the sand ripples lose their height and finally will totally disappear leading to significant amount of sediment motion as sheetflow of sand within a few centimeters of the bottom (Ahmed, 2002).

Outside the surf zone before breaking waves, sediment transport processes are generally concentrated in a layer close to the seabed. Sediment is being moved by the wave orbital motion and transported by wave asymmetry and/or mean currents. Sand transport occurs in three different regimes which are characterized by the bed forms and can be predicted based on the Shields parameter or the mobility number. They are bed load, suspended load and sheet flow transport. The equation (2.1) of dimensionless Shields parameter presents the relation of the initiation of motion, the flow velocity and the sediment size.

$$\theta(t) = \frac{f_w u^2(t)}{2(s-1)gD_{50}} \tag{2.1}$$

where $s = \rho_s / \rho$ is the sediment specific gravity (where ρ_s =density of sediment and ρ = density of water), D_{50} is the sediment size, u is the flow velocity and f_w is the wave friction factor.

There is no sediment motion with very small values of the Shields parameter. With increasing values of the Shields parameter, sediment motion becomes sliding and rolling over each other, but the bed remains flat. It is because of the bed-load is the part of the total load which has more or less continuous contact with the sand bed. Suspended load is the part of the total load which is moving without continuous contact with the bed as the result of the agitation of the fluid turbulence. In suspended load, when the Shields parameter further increases, the bed forms are developed and the appearance of ripples will occur. Further increasing the Shields parameter results that ripples are washed out and the bed becomes plane again. A thin layer with high sand concentrations is moving in a sheet along the bed which is called sheet-flow. The thickness of the sheet-flow layer is generally much larger than a few grain diameters (10-100 grain diameters).The sheet-flow regime occurs when $\theta > 0.8$ (Wilson 1987).

2.2. Quasi-steady and Semi-unsteady Models

2.2.1. Introduction

In coastal engineering practice, studies on sediment transport and the use of the accurate sediment transport model are very essential in order to simulate and predict large-scale and long-term morphological changes. These models have been extensively tested and widely applied to represent the basic hydrodynamic and sediment transport processes. In this chapter, from sections 2.2 to 2.3, detailed descriptions of transport models, which have been used in the present study, are introduced in details.

2.2.2. Classifications of the sand transport models

Generally, sediment transport models can be divided into four different classes:

1. Time-averaged models 2. Quasi-steady models

3. Semi-unsteady models 4. Unsteady models

The time-averaged model and unsteady models will not be discussed in this study.

The different of quasi –steady and semi-unsteady models can be described briefly as follows:

1. Quasi-steady models assume the instantaneous sediment transport rates to some power of the instantaneous near bed flow velocity or bed shear stress (Ribberink, 1998; Nielsen, 2003, 2006).

2. Semi-unsteady models account for the phase lag effects without modeling the detailed time-dependent horizontal velocity and vertical concentration profiles (Dibajnia & Watanabe, 1992; Dohmen-Janssen, et al., 2002).

Another interesting model is SANTOSS transport model (Ribberink et al., 2010) including several effects which is different concerning this subdivision. An extensive description of these transport models is described in the next section. In addition, the Nielsen (2006) sand transport models considering the effect of streaming are studied in this research.

2.2.3 Existing quasi-steady Model

In steady flow, the sand transport rate is proportional to a power (>1) of the near bed velocity. Many sediment transport models were developed by assuming the sediment transport reacts instantaneously to the near bed orbital flow velocity or to the bed shear stress. When the phase lag between bed shear stress and concentration profiles leads to a change in sediment transport (Dibajnia and Watanabe., 1998; Dohmen-Janssen., 1999), unsteady effects will occur. Phase-lag effects become important, especially for fine sediments, high orbital velocities and short wave periods (Dohmen-Janssen., 1999). Due to phase lag effects, the net transport rates might be reduced or even change in direction.

In quasi-steady models, it is assumed that instantaneous sediment transport rate is directly proportional to some power of the instantaneous near-bed oscillatory velocity or bed-shear stress. The sediment transport is computed as a function of bottom shear stress or the near bed velocity. Quasi-steady models (e.g., Bailard,1981; Ribberink, 1998) assume that sand transport reacts immediately to changes in flow conditions. The effect of unsteadiness flow related to entrainment and settling delay effects are not accounted for this kind of model. Some examples for the quasi-steady models are Madsen and Grant (1976), Sleath (1978), Watanabe et al. (1980), Sawamoto and Yamashita (1986), and Ribberink and Al-Salem (1994). The models of Bailard (1981), Sato and Horikawa (1986) and Ribberink (1998) will be described in more details in the next section.

(1) Sato and Horikawa (1986)

Sato and Horikawa (1986) proposed the following formula to estimate the net transport rate, based on the data of oscillatory flow tank experiments in regular and irregular asymmetric oscillations.

$$q(t) = 7 w_0 d (\theta - \theta_c) \theta^{1/2} \tag{2.2}$$

$$\theta = \theta_{on} = \frac{f_w u_c^2}{2(s-1) g D_{50}} \tag{2.3}$$

u_c is the onshore velocity amplitude. This equation is suitable to predict the time-averaged net transport rate over the rippled bed conditions.

(2) Bailard's model (1981)

The quasi-steady model of Bailard (1981) is based on Bagnold's energetic approach (1963). The available fluid power for sediment transport is a constant fraction of the local rate of energy dissipation which can be estimated as, $\omega(t) = \rho c_f |u_b(t)|^3$. The time-varying transport rate is calculated by adding the bed-load transport for a horizontal bed and the suspended load.

$$q(t) = q_b(t) + q_{ss}(t) \tag{2.4}$$

where $q_b(t)$ is bed load transport and given by

$$q_b(t) = \frac{f_w \varepsilon_b u_b^3(t)}{(s-1)g \tan\phi} \tag{2.5}$$

Suspended load $q_{ss}(t)$ can be estimated by,

$$q_{ss}(t) = \frac{f_w \varepsilon_s |u_b^3(t)| u_b(t)}{(s-1)g w_0} \tag{2.6}$$

where s = relative density f_w = wave friction factor; g = acceleration due to gravity; φ = angle of internal friction of the sediment; u_b = horizontal near-bed flow velocity and w_0 = settling velocity of sediment particles. In this model, Bailard used two efficiency factors for bed-load and suspended-load transport which are $\varepsilon_b = 0.1$ and $\varepsilon_s = 0.002$, respectively. Both are obtained by calibration of the net transport rates against field data.

(3) Ribberink's model (1998)

The formula of Ribberink (1998) predicts well for a wide range of oscillatory and steady flows in flat bed conditions (sheet flow). In this model, Ribberink (1998) assumed that the Shields parameter θ is the parameter determining sediment transport motion and the shear stress is the driving force for sediment transport. It is assumed that the instantaneous sediment transport rate is proportional to the difference between the actual time-dependent effective bed shear stress and the critical bed shear stress θ_{cr}. Normalizing the sediment transport rate q_{Rib} by the parameter $\sqrt{(s-1)gD_{50}^3}$, it leads to the following expression for computing sediment transport rate,

$$\vec{\Phi}(t) = \frac{\vec{q_s}(t)}{\sqrt{(s-1)gD_{50}^3}} = m(|\theta'(t)| - \theta_{cr})^n \frac{\vec{\theta'}(t)}{|\theta'(t)|} \tag{2.7}$$

in which $\vec{\Phi}(t)$ = non-dimensional sediment transport rate; *m*, *n* = empirical coefficient; empirical coefficient; $\theta(t)$ = time-dependent Shields parameter and θ_{cr} = 0.05, critical Shields parameter. The values of coefficient *m* and exponent *n* are based on a large data set of steady and oscillatory flows laboratory experiments. Ribberink (1998) found the values of the two coefficients: *m* =11 and *n* =1.65. The time-dependent shear stress is

$$\theta(t) = \frac{f_w |u(t)| u(t)}{2(s-1)gD_{50}} \tag{2.8}$$

The wave friction factor, f_w, is calculated from Swart's formula (1974).

$$\begin{cases} f_w = \exp\left[-5.997 + 5.213\left(\frac{k_s}{a}\right)^{0.194}\right], \frac{k_s}{a} < 0.63 \\ f_w = 0.3, \frac{k_s}{a} \geq 0.63 \end{cases} \tag{2.9}$$

where *a* is the oscillatory flow orbital amplitude.

In case of combined wave-current flow the bed shear stress is derived as

$$\theta(t) = \frac{f_{cw} |u(t)| u(t)}{2(s-1)gD_{50}} \tag{2.10}$$

in which the wave-current friction factor f_{cw} is calculated according to the expression of Madsen and Grant (1976b),

$$f_{cw} = f_c + (1-\alpha) f_w \tag{2.11}$$

in which, $\alpha = \frac{U_c}{u + U_c}$, U_c is current velocity and *u* is the wave velocity amplitude.

The current friction factor is estimated using the following formula which is based on the logarithmic velocity distribution,

$$f_c = 2K^2 \left[\ln\left(\frac{z_{um}}{z_0}\right)\right]^{-2} \tag{2.12}$$

where κ = Von Karman coefficient (= 0.4); z_{um} = height above the sand bed where the

current velocity U_c is prescribed; $z_o = k_s / 30$ is the level where the velocity is assumed to be zero. Both friction factors depend on bed roughness height k_s. The roughness height for pure wave and combined wave and current flow can be estimated as,

$$\begin{cases} k_{sw} = \max\left\{D_{50}, D_{50}\left|(1+6(\left|\overline{\theta}\right|-1\right|\right\} & \textit{for wave} \\ k_{sc} = \max\left\{3D_{90}, D_{90}\left|(1+6(\left|\overline{\theta}\right|-1\right|\right\} & \textit{for current} \end{cases} \tag{2.13}$$

where Dd_{90} is the size at which 90% by weight is finer. The time-averaged absolute magnitude of the Shields parameter $\left|\overline{\theta(t)}\right|$ was described as $\left|\overline{\theta(t)}\right| = \dfrac{f_w \overline{u^2(t)}}{2(s-1)gD_{50}}$.

2.2.4. Existing Semi-unsteady Model

Semi-unsteady sediment transport models are positioned between quasi-steady and unsteady models and it may be a useful and practical alternative to them. This types of model include the effect of the observed phase-lag between the flow velocity and the sediment concentration under waves without the detailed simulation of vertical distribution of time-dependent horizontal velocity and concentration profiles.

When the phase-lag between the sediment concentration and the velocity becomes important, the net onshore transport rate reduces in magnitude or even changes the net transport direction from onshore to offshore especially for fine sand, with large velocities and short wave period cases (Dohmen-Janssen et al., 2002). At that time, the quasi-steady transport model fails to predict the magnitude and direction of the measured offshore net transport rates. Various semi-unsteady models which are taking into account the phase-lag phenomena were introduced to estimate the net sand transport rate under different oscillatory flow conditions. In this section, several semi-unsteady models which include Dibajnia and Watanabe formulae (1996), Dibajnia et al. (2001) and Dohmen-Janssen et al. (2002) are discussed in details.

(1). Model of Dibajnia &Watanabe (1996)

Dibajnia and Watanabe (1992) introduced a transport model for uniform fine sediment under asymmetric oscillation. This model was considered as a semi-unsteady model as it

is able to take into account unsteady effects. Fig. 2.1 is a typical velocity profile of the asymmetric oscillatory flow using in Dibajiania and Watanabe model. If the onshore flow velocity is high, the sediment particles can be stirred up to such a high level that they cannot settle to the bed within the same positive part of the wave-cycle. The sand remaining in suspension from the previous half cycle will be transported in the negative direction during the next part of the wave-cycle. If the settling time of a sediment particle is larger than the part of the wave period, unsteady effects will occur.

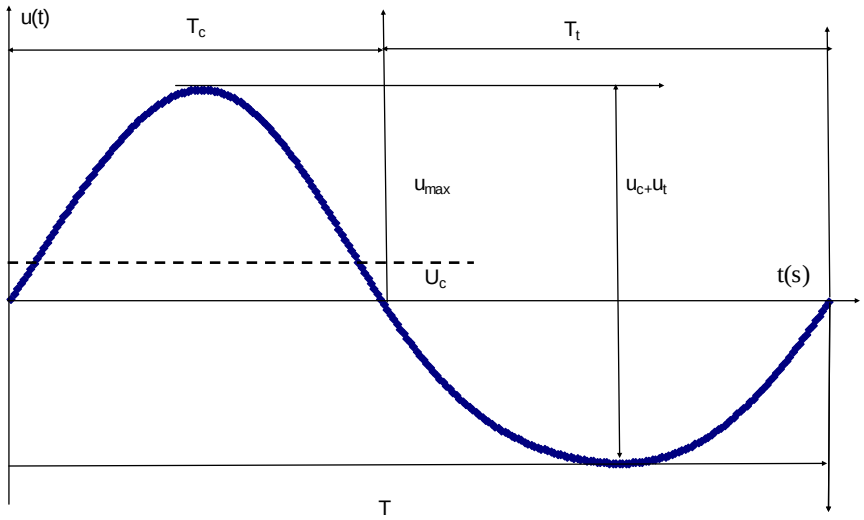

Fig. 2.2. A typical velocity profile of the asymmetric oscillatory flow using in Dibajnia and Watanabe model

Dibajnia and Watanabe used the parameter ω_i to determine the importance of unsteady effects and to represent the ratio of the settling time and the period of the positive and the negative half wave-cycle,

$$\omega_j = \frac{u_j^2}{2(s-1)gw_o D_{50}} \tag{2.14}$$

The subscript j is replaced by either c (crest) or t (trough) representing the onshore (crest) phase and offshore (trough) phase, respectively. The equivalent velocity amplitude under wave crest (u_c) and trough (u_t) for the asymmetric velocity profile can be described by:

$$u_c^2 = \frac{2}{T_c}\int_0^{T_c} u^2 dt \quad u_t^2 = \frac{2}{T_t}\int_{Tc}^{T} u^2 dt \tag{2.15}$$

where T_c and T_t are the duration of the positive and negative part of the wave velocity, respectively. According to Van Rijn (1993), the sediment free settling velocity is w_o

$$w_o = \begin{cases} \dfrac{sgd_{50}^2}{18\nu}, \ for\ 0.01\,mm < D_{50} \le 0.1mm \\ \dfrac{10\nu}{d_{50}}\left(\sqrt{1+\dfrac{0.01sgd_{50}^3}{\nu^2}}-1\right), \ for\, 0.1\ mm < D_{50} < 1.0\ mm \\ 1.1\sqrt{sgd_{50}}\,, \ for\, D_{50} \ge 1.0\,mm \end{cases} \quad (2.16)$$

Dibajnia & Watanabe (1992) defined a non-dimensional parameter Γ to represent the net (non-dimensional) transport rate, giving the difference between the transport during the positive part and the negative part of the wave-cycle,

$$\Gamma = \frac{u_c T_c (\Omega_c^3 + \Omega_t^{'3}) - u_t T_t (\Omega_t^3 + \Omega_c^{'3})}{(u_c + u_t)T} \quad (2.17)$$

where Ω_c represents the amount of sand entrained and transported during the positive half wave-cycle and Ω_c' represents the sand remaining in suspension from the previous positive half wave-cycle and carried by the negative half wave-cycle; Ω_t represents the sand brought into suspension and carried during the negative half wave-cycle; Ω_t' represents the sand remaining in suspension from the negative half wave-cycle and transported by the positive half wave-cycle. They also introduced a new parameter ω_{cr} to extend the applicability of the formula from the sheetflow to the suspended load above ripples. ω_{cr} is equal to unity for sheetflow condition (Dibajnia and Watanabe, 1992) and is equal to 0.03 in the presence of ripples over ripples (Suzuki, et al., 1994). The relation between the parameters Ω_j, Ω_j' and ω_i is described by,

$$if\, \omega_j^{'} \le \omega_{cr} \begin{cases} \Omega_j = \omega_j T_j \sqrt{\dfrac{sg}{D_{50}}} \\ \Omega_j^{'} = 0 \end{cases}$$

$$if\ \omega_j^{'} > \omega_{cr} \quad \begin{cases} \Omega_j = \left[\omega_{cr} + (1-\gamma_j).(\omega_j - \omega_{cr})\right] T_j \sqrt{\dfrac{sg}{D_{50}}} \\ \Omega_j^{'} = \gamma_j.(\omega_j - \omega_{cr}) T_j \sqrt{\dfrac{sg}{D_{50}}} \end{cases} \tag{2.18}$$

In Dibajnia and Watanabe (1996) model, they extended their model to estimate the net transport rate for different sediments with mixed-sizes and densities by introducing a parameter P_j that accounts the weight ratio of each sand in the mixture. Finally, the generalized formula for transport rate of each component is,

$$q_{(DW96),j} = P_j.0.0015 w_o D_{50}.sign(\Gamma)\left|\Gamma\right|^{0.5} \tag{2.19}$$

(2). Model of Dibajnia et al. (2001)

In Dibajnia et al. (2001) model, the dimensionless net transport rate, Φ, is modified based on the transport formula of Dibajnia and Watanabe (1996) as,

$$\Phi = \frac{q}{w_s D_{50}} = 0.0019 \frac{u_c T_c (\Omega_c + \Omega_t^{'}) - u_t T_t (\Omega_t + \Omega_c^{'})}{(T_c + T_t)\sqrt{sgD_{50}}} \tag{2.20}$$

where Ω_j is $\quad if\ \omega_j^{'} \le \omega_{cr} \quad \begin{cases} \Omega_j = \omega_j T_j \sqrt{\dfrac{sg}{D_{50}}} \\ \Omega_j^{'} = 0 \end{cases}$ (2.21)

$$if\ \omega_j^{'} > \omega_{cr} \quad \begin{cases} \Omega_j = \left[\omega_{cr} + (1-\gamma_j).(\omega_j - \omega_{cr})\right] T_j \sqrt{\dfrac{sg}{D_{50}}} \\ \Omega_j^{'} = \gamma_j.(\omega_j - \omega_{cr}) T_j \sqrt{\dfrac{sg}{D_{50}}} \end{cases} \tag{2.22}$$

where ω_{cr}=1.2, and $\omega_j = (\theta_j - \theta_{cr})\dfrac{D_{50}}{w_s T_j}$ and $\theta_j = \dfrac{u_j^2}{2sgD_{50}} = \dfrac{\psi_j}{f_w}, \psi_j = \dfrac{f_w u_j^2}{2sgD_{50}}$

Ω_j (and not $\Omega_j^{'}$) are set to be as follows,

$$if\ \psi_j < \psi_{sheet} \quad \Omega_j = \left(\frac{\psi_j - \psi_{cr}}{\psi_{sheet} - \psi_{cr}}\right)^3 .\Omega_j \tag{2.23}$$

$$\gamma_j = \beta_j^* . \beta_j^{'}$$

in which

$$\begin{cases} \beta_j^* = 1 \quad if\ \dfrac{T_{pj}}{T_j} \ge 2 \ , \end{cases}$$

$$\beta_j^* = \frac{6T_{pj}}{T_j} - 2 \quad if \ \frac{1}{3} < \frac{T_{pj}}{T_j} < \frac{1}{2} \ , \ \beta_j^* = 0 \qquad if \ \frac{T_{pj}}{T_j} \le 2 \tag{2.24}$$

$$\begin{cases} \beta_c' = 1, \ if \ \dfrac{u_t}{u_c} \ge \dfrac{1}{4} \\ \beta_c' = 4\dfrac{u_t}{u_c}, \ if \ \dfrac{u_t}{u_c} < \dfrac{1}{4} \end{cases} \quad , \begin{cases} \beta_t' = 1, \quad if \ \dfrac{u_c}{u_t} \ge \dfrac{1}{4} \\ \beta_t' = 4\dfrac{u_c}{u_t}, \quad if \ \dfrac{u_c}{u_t} < \dfrac{1}{4} \end{cases} \tag{2.25}$$

In Dibajnia et al. (2001) model, the critical values of Shields and mobility numbers for initiation of motion are as follows: $\theta_{cr} = 0.05$, Ψ_{cr} =5 and Ψ_{sheet} = 0.8, respectively.

(3). Model of Dohmen-Janssen (2002)

Dohmen-Janssen et al. (2002) developed a new semi-quasi transport model, which is closely based on the existing quasi-steady model of Ribberink (1998). In this model, they account the phase-lag effects. The phase lag correction factor, *r* is linked to the calculated net transport rates of model of Ribberink (1998). The factor *r* is the ratio of the net sand transport rate with phase-lag effects and to the net rate without phase-lag effects of Ribberink (1998) model.

$$r = \frac{\overline{q_{(DM)}}}{\overline{q_{(RB)}}} = \frac{U_c^3 + \frac{1}{2}U_c U_1^2 + \frac{1}{2}U_c U_1^2 F_1(p)}{U_c^3 + \frac{3}{2}U_c U_1^2} \tag{2.26}$$

The free-stream velocity for sine waves with an imposed net current is described as: $u(t) = u_0 + u_1 \sin(\omega t)$. In which, the net transport rate of Ribberink ($q_{(Rib)}$) can be calculated from Eq. (2.7). The phase-lag factor *r* is a function of phase-lag parameter *p*. If phase-lag effects are not important, then *r* = 1 and the Dohmen-Janssen (2002) model returns to the quasi-steady model of Ribberink (1998). $F_1(p)$ is function of phase lag parameter *p*.

$$F_k(p) = \frac{P_k \cos\varphi_k + Q_k \sin\varphi_k}{(P_k^2 + Q_k^2)^{\frac{3}{2}}}, \ k = 1,2 \tag{2.27}$$

where

$$G(p)=\frac{P\cos\varphi_k+Q\sin\varphi_k}{(P^2+Q^2)^{\frac{3}{2}}},\ k=1,2$$

$$P_k=\frac{1}{2}+\left[\frac{1}{6}+(kp)^2\right]^{\frac{1}{4}}\cos(\frac{1}{2}\alpha_k),\ k=1,2$$

$$Q_k=\left[\frac{1}{16}+(kp)^2\right]^{\frac{1}{4}}\sin(\frac{1}{2}\alpha_k),\ \ k=1,2$$

$\alpha=\arctan(4kp),\ k=1,2$ and $\varphi_k=\arctan(-\frac{Q_k}{P_k}),k=1,2$.

The phase lag parameter is

$$p=2\pi\frac{\delta}{w_oT},k=1,2 \tag{2.28}$$

where the sheetflow layer thickness ,δ, is expressed,

$$\delta=\begin{cases}35\,D_{50}.\theta_m,\ D_{50}<0.21mm\\ 13\,D_{50}.\theta_m,\ D_{50}\geq 0.21mm\end{cases} \tag{2.29}$$

The reduction factor r for the formulae of the 2nd -order Stokes waves with an imposed net current is,

$$r=\frac{\overline{q_{(DM)}}}{\overline{q_{(RB)}}}=\frac{U_c^3+\frac{1}{2}U_cU_1^2+\frac{1}{2}U_cU_2^2+\frac{1}{2}U_cU_1^2F_1(p)+\frac{1}{2}U_1^2U_2F_1(p)+U_cU_2^2F2(p)+\frac{1}{4}U_1^2U_2F2(p)}{U_c^3+\frac{3}{2}U_cU_1^2+\frac{3}{2}U_cU_2^2+\frac{3}{4}U_1^2U_2}$$

2.2.5. SANTOSS Sand Transport Model

The other sand transport model, SANTOSS model (Ribberink, et al., 2010), is based on the semi-unsteady model concept of Dibajinia and Watanabe (1992) by making several modifications in which it incorporates the influences of phase-lag and different wave shapes, and the influence of surface wave effect.

Ribberink et al. (2010) stated that the SANTOSS model should cover all the wave and current related sediment transport rates within the wave boundary layer. The modified net transport rate is expressed for oscillatory flow condition. The net transport rate is,

$$q = \frac{\sqrt{|\theta_c|}T_c(\Omega_{cc} + \Omega'_{tc})\frac{\theta_c}{|\theta_c|} - \sqrt{|\theta_t|}T_t(\Omega_{tt} + \Omega'_{ct})\frac{\theta_t}{|\theta_t|}}{T}\sqrt{(s-1)gD_{50}^3} \qquad (2.30)$$

where Ω_{cc} and Ω_{tt} represent the sand loads that are entrained during positive and negative half cycle and transported during the same half –cycle. Ω_{ct} and Ω_{tc} represent the sand loads that are entrained during positive and negative half-cycle and transported during the next half - cycle. To get a non-dimensional half-cycle transport rate, firstly the load contributions are estimated in the following manner. The different sediment loads becomes,

$$if\ P_c \le P_{cr} \begin{cases} \Omega_{cc} = \Omega_c \\ \Omega_{ct} = 0 \end{cases} \qquad (2.31)$$

$$if\ P_c > P_{cr} \begin{cases} \Omega_{cc} = \frac{1}{P_c}\Omega_c \\ \Omega_{ct} = \frac{1}{P_c}\Omega_c \end{cases} \qquad (2.32)$$

$$if\ P_t > P_{cr} \begin{cases} \Omega_{tc} = \frac{1}{P_t}\Omega_t \\ \Omega_{tt} = \Omega_t \end{cases} \qquad (2.33)$$

$$if\ P_t \le P_{cr} \begin{cases} \Omega_{tt} = \Omega_t \\ \Omega_{tc} = 0 \end{cases} \qquad (2.34)$$

where P_{cr}= 1 is the critical value

Above the equation, when the phase lag parameter *P* exceeds the P_{cr}, there is an exchange of sand from one half cycles to the next. Again, the sand load entrained in the flow during each half cycle related to the Shields parameter θ_i, where subscript (*i*) either '*c'* for crest or '*t*' for trough. So, it can be written as,

$$\begin{cases} if\ |\theta_i| \le \theta_{cr},\ \Omega_j = 0 \\ if\ |\theta_i| > \theta_{cr},\ \Omega_j = m(|\theta_i| - \theta_{cr})^n \end{cases} \qquad (2.35)$$

in which the critical Shields number, θ_{cr} is calculated following Soulsby (1997),

$\theta_{cr} = \frac{0.3}{1+1.2D} + 0.055(1-\exp(-0.02D))$ and the coefficients *m* and *n* are calibration coefficients. D_{50} is the medium grain diameterThe phase lag parameter P_i represents the ratio of a representative sediment stirring height and the sediment settling distance:

$$\begin{cases} P_j = 8\dfrac{\delta_{si}}{2(T_j - T_{pj})w_s} \; if\ \eta = 0 \quad for\ sheetflow\ regime \\ \\ P_j = 9.3\dfrac{\eta}{T_j w_s} if\ \eta > 0 \qquad for\ ripples\ conditions \end{cases} \tag{2.36}$$

in which η is the ripple height and δ_{si} the sheet flow layer thickness. Although the sheet flow layer thickness δ_{si} is calculated according to Eq. (2.28) of Dohmen-Janssen et al. (2002) model, the coefficient of multiplier for fine sands is reduced from 35 to 25 in this model.

The calculation of Shields parameter and friction factor for combined wave and current can be seen in Eq. (2.37). The wave roughness height for the mobile bed roughness for sheet flow conditions and presence of ripples conditions as follow:

$$\begin{cases} k_{sw} = \max\left\{d_{50}, d_{50}\left|(1+\mu(|\theta|-1\right|\right\} + p\eta^2 \Big/ \lambda \\ \\ k_{s\delta} = \max\left\{3d_{90}, d_{50}\left|(1+\mu(|\theta|-1\right|\right\} + p\eta^2 \Big/ \lambda \end{cases} \tag{2.37}$$

where λ is the ripple length, p = 0.4 and the parameter μ is :

$$\mu = \begin{cases} 6, if\ D_{50} \le 0.015mm \\ \\ [6+10^3 D_{50} - 0.15)\dfrac{(1-6)}{(0.2-0.15)}, if\ 0.15 < d_{50} < 0.2 \\ \\ 1, if\ D_{50} \ge 0.2\ mm \end{cases} \tag{2.38}$$

In case of oscillatory flows with acceleration skewness, the net transport formula can be estimated as,

$$q = \frac{\sqrt{|\theta_c|}T_c(\Omega_{cc} + \dfrac{T_c}{2T_{cu}}\ \Omega_{tc}^{'})\dfrac{\theta_c}{|\theta_c|} - \sqrt{|\theta_t|}T_t(\Omega_{tt} + \dfrac{T_t}{2T_{tu}}\Omega_{ct}^{'})\dfrac{\theta_t}{|\theta_t|}}{T}\sqrt{(s-1)gD_{50}^3} \tag{2.39}$$

In addition, SANTOSS model was modified for progressive surface waves considering the additional flow mechanisms with the wave-Reynolds stress, the Lagrangian grain motion and the vertical velocity.

2.2.6. Streaming-related bed shear stress Model

(1). Nielsen and Callaghan (2003)

In the recent years, practical wave-dominated cross-shore sand transport models have been developed by considering the boundary layer streaming effect. Nielsen (2003) developed a model by considering the influence from wave shape and boundary layer streaming for wave dominated cross-shore sand transport. The analytical results (Nielsen and Callaghan, 2003) for sediment transport rates indicated the streaming effect is less important than acceleration effect which is more significant to further increase in net transport rate.

Nielsen (2001) uses a Meyer-Peter and Müller (1948) formula to relate the sediment transport rate to the shear stress induced by near bed flow velocities and flow accelerations. This model is approached on quasi-steady features which can predict the onshore net transport rate. To incorporate the influences of streaming, Nielsen (2006) adds an additional time-averaged shear stress $-\rho(\widetilde{\tilde{u}\tilde{v}})_\infty$ in terms of wave friction factor, f_e, and wave number, k.

$$-\rho(\widetilde{\tilde{u}\tilde{v}})_\infty = \rho\frac{1}{4\sqrt{2}}kA^3\omega^2 f_e \tag{2.40}$$

where A is the near-bed semi-excursion distance, $\omega = \frac{2\pi}{T}$, f_e is,

$$f_e = \exp\left[5.5(\frac{r}{A})^{0.2} - 6.3\right] \tag{2.41}$$

$$r = 170\sqrt{\hat{\theta}_{2.5} - 0.05}D_{50} \tag{2.42}$$

And then, the non-dimensional bed shear stress is calculated as the Shields parameter,

$$\theta(t) = \left|\frac{|u_\theta|u_\theta - (\widetilde{\tilde{u}\tilde{v}})_\infty}{(s-1)gD_{50}}\right| \tag{2.43}$$

in which $u_\theta(t) = \sqrt{\frac{1}{2} f_{2.5}} \left[\cos\varphi_\tau u_\infty(t) + \sin\varphi_\tau \frac{u_\infty(t+\partial t) - u_\infty(t-\partial t)}{2\omega_p \partial t} \right]$

Later, Nielsen (2006) pointed out the difference between the large wave flume experiments and oscillatory flow tunnel is due to the boundary layer streaming and/or Lagrangian mass transport of sediment. According to Longuet-Higgins (2005), the mean bed shear stress must be related to energy dissipation, $D_E = \overline{\tau_b} c$,where $c = L/T$, wave celerity. Then, the streaming related bed shear stress can be estimated as,

$$(\overline{\tilde{u}\tilde{v}})_\infty = \frac{D_E}{\rho c} = \frac{2}{3\pi} A^3 \omega^2 f_e / c \tag{2.44}$$

Finally, the modified instantaneous sediment transport rate is calculated as,

$$\Phi(t) = \frac{q_s(t)}{\sqrt{\Delta g D_{50}^3}} = 12(|\theta(t)| - 0.05)\frac{u_\theta(t)}{|u_\theta(t)|} \quad for\ \theta(t) > 0.05 \tag{2.45}$$

$$= 0 \quad for\ \theta(t) < 0.05$$

2.3. Wave Induced Boundary Layer Steaming in Surface Wave

2.3.1. Background

To gain more understanding relevant processes for the interaction of sand, detailed measurements of sediment transport under different flow conditions have been carried out in large-scale experimental facilities such as Large Wave Flume (LWF) and Oscillatory Flow Tunnel (OFT). Even though oscillatory flow tunnels are able to simulate surface waves well and provide a good approximation of the flow experienced at the sea bed, some fundamental differences still remain. From the large-scale experimental results, the following differences between OFT experiments and LWF (real surface waves) were found by Dohmen-Janssen and Hanes (2002), Ribberink *et al.* (2008) and Schretlen *et al.* (2009). Various studies argue that the boundary layer streaming is likely to be of most significance rather than the other differences between OFT and surface waves.

-In surface wave, Lagrangian motion can occur a fluid particle in a wave will move with larger forward velocities during the wave crest than the backwards velocities during the wave trough. The Lagrangian mean velocities are absent in OFT.

- In a tunnel, the pressure is in phase with its gradient, which is in phase with the

acceleration. Under surface waves, the phase of the pressure is shifted 90°, compared to the pressure gradient and is in phase with the velocity, rather than the acceleration.

- The vertical orbital velocities are present in LWF while OFT has no vertical velocity. Boundary layer streaming is an onshore-directed constant current in the boundary layer is only present under surface waves due to the vertical orbital velocities. Eulerian mean velocities result from the vertical and horizontal orbital velocities are not exactly 90° out of phase in the boundary layer, it gives rise to an onshore directed mean velocity, close to the bed (Longuet-Higgins, 1953). The producing of positive streaming in the wave boundary layer was shown in Fig. 2.3.

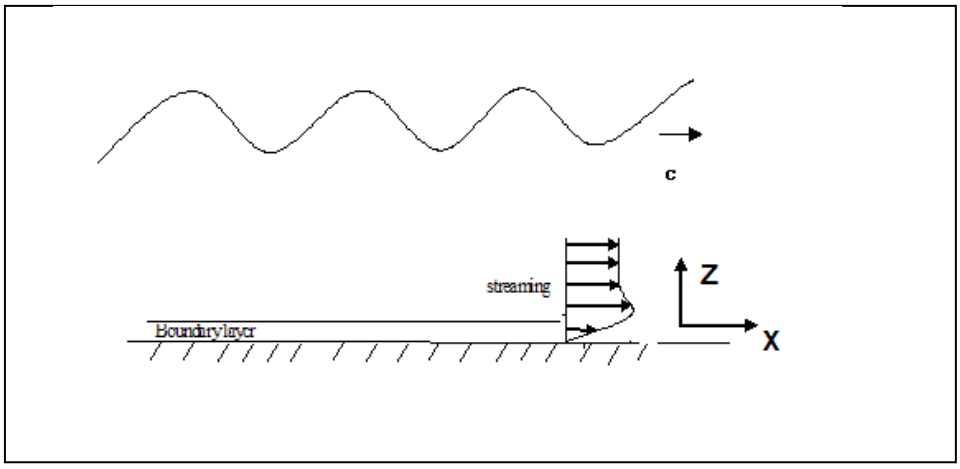

Fig. 2.3. Onshore streaming in real surface wave (Longuet-Higgins,1958)

And also, according to Longuet-Higgins (1953), the streaming velocity at the edge of the boundary layer can be calculated using the following equation (2.46) for flat beds conditions with constant viscosity. Fig. 2.4 shows the streaming profiles of Longuet-Higgins (1953).

$$u_{str}(z) = \frac{U_1^2}{4c}\{3 + e^{2\beta z} - 2e^{\beta z}[(\beta z - 1)\sin\beta z + (\beta z + 2)\cos\beta z]\} \qquad (2.46)$$

where u_{str} is the streaming velocity, $c = \frac{L}{T}$ is wave celerity, $\beta = (2\nu/\omega)^{1/2}$ and $U_1 = \frac{H\omega}{\sinh(kh)}$,respectively.

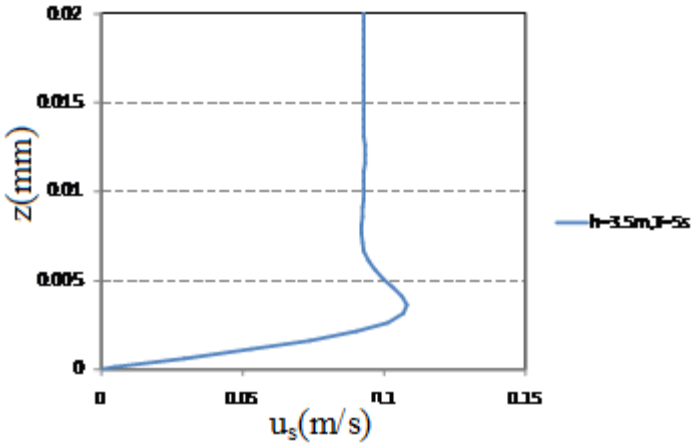

Fig. 2.4. Vertical profile of streaming profile ((Longuet-Higgins,1953)

2.3.2. Relative Importance of two streaming mechanisms

As discussed above, surface waves can induce a steady current known as the boundary layer streaming. There are two types of boundary layer streaming. Holmedal and Myrhaug (2009) clearly identify the two important mechanisms causing streaming. The first one streaming is caused by turbulence asymmetry in successive wave half-cycles (beneath asymmetric forcing). This type of streaming can be offshore directed which occurs both under surface waves and in OFT. The other type of streaming caused by the presence of a vertical wave velocity within the seabed boundary layer was explained by Longuet-Higgins (1958). This type of streaming (hereafter LH streaming) can only occur in surface waves. It leads into the onshore directed mean velocity in the boundary layer. The LH streaming is the dominant mechanism acting on the sediments, which leads to a net sediment transport in the direction of wave propagation (Holmedal and Myrhaug, 2009).

2.3.3. Lagrangian velocity

The fundamental differences between the oscillatory flow and surface wave were already described in details. Lagrangian grain motion is one of the important mechanisms under surface wave. At the edge of the boundary, Longuet-Higgins (1953) found the boundary

steady streaming velocity (Eulerian velocity) $\overline{u_{L,\infty}} = \frac{3}{4}\frac{U_0^2}{c}$ as well as Longuet-Higgins (1957) observed the horizontal mass transport velocity(Lagrangian velocity), $\overline{u_{L,\infty}} = \frac{5}{4}\frac{U_0^2}{c}$. In addition, the mass transport velocity is in the direction of wave propagation, it means always positive. In real wave, the particles move with the wave propagation at the wave crest which takes a longer wave period to spend to travel to the onshore part. On the other hand, the wave moves against the wave direction at the wave trough which takes a shorter time to travel the offshore part. As a result, Eulerian flow velocity (steady streaming) and also the mass transport velocity (Lagrangian velocity) enhance the onshore net transport rate under surface waves.

2.3.4. Roughness –induced streaming

The effects of surface roughness transitions on steady turbulent boundary layers have been extensively studied experimentally, numerically, and theoretically. Recently, Fuhrman (2011) presented the *k-ω* turbulence model to simulate the varying bottom roughness in oscillatory wave boundary layer and measured the time-averaged velocity, bed shear stress, and turbulence quantities. The numerical results were compared with experiments results performed by Fredsoe *et al*. (1993). The experiments which involved the sudden bottom roughness transition over beds (from pebble-bed rough section to smooth sand section) were conducted in oscillatory flow tunnel. The author made the validation of the numerical model by comparing against measured period-averaged velocity profiles from Fredsøe *et al*. (1993). It described that an oscillatory flow over a sudden change in roughness will effect in differences between successive half-cycles in the vicinity of the roughness change. The near-bed fluid leaving the smoother section will have unnaturally large velocity as it enters the rougher section, when compared to an another flow over a bed having uniformly larger roughness, during the negative half-cycle, where the flow is directed toward the rougher section, On the other hand, during the positive half-cycle: it means the flow directed toward the smoother section, the near-

bed flow coming off the rougher section will be illustrated by reduced velocity gradients (and thereby velocities), when compared to flow over a uniformly smoother bottom.

From the results of time- averaged velocity characteristics due to these described differences in the two half-cycles, it can be seen that the near bed flow was in the direction of larger roughness. It means that the near bed flow can induce negative streaming towards the larger roughness section compared to smooth section. This type of streaming is referred to roughness–induced streaming due to bottom roughness variations in the bed. This flow is consecutively seemingly compensated by a circulation current in the direction of the smoother section higher up in the profile.

2.4. Effect of streaming on net transport rate

Using large wave flume facility, the sheetflow mobile bed experiments can also be performed (Ribberink *et al*., 2000; Dohmen-Janssen and Hanes, 2002, 2005). Dohmen-Janssen and Hanes (2002) performed sheet flow experiments in the 300-m long wave flume at Hannover (GWK, Hannover) and investigated the sediment movement differences under the large oscillatory water tunnel (LOWT) and the large wave flume (LWF). They found net transport rate under the LWF is 2.5 or 2.0 times larger than LOWT under the same $\overline{u^3}$ conditions and they contributed this phenomenon is due to the onshore directed boundary layer streaming that is present under progressive waves but is not present in tunnel flow.

In order to get the detailed measurements of mean flow velocity profiles inside the wave boundary layer, Schretlen *et al*., (2010) also performed high resolution measurements of boundary layer flow and all results are compared to oscillatory flow tunnel experiments (Ribberink *et al*., 2008 and Campbell *et al*., 2006) with similar hydrodynamic and sediment characteristics. Fig. 2.5 shows the mean velocity profiles for of medium (D_{50} = 0.25 mm) and fine (D_{50} = 0.14 mm) sand with wave period T= 5 s under same wave conditions. In LWF, the magnitude of this onshore directed velocity varies between the different wave conditions but the trend is similar for both types of sand. In the case of OFT data, the mean profiles for medium sand is different with the fine sand. Again, in this figure, the trend of the mean profiles is comparable between the

tunnel and surface wave experiments; it shows different behavior especially in the pick-up layer and sheet flow layer. In surface wave, the onshore streaming detected in the pick-up layer and sheet flow layer for two types of sand. In oscillatory flow, the negative streaming was observed in the pick- up layer. They explained that the reason is the wave Reynolds stress in the wave boundary layer, which is present under surface waves but is absent in oscillatory flows. Further comparison between surface wave and oscillatory flow is that the erosion depth under the wave crest ($\delta_{e,crest}$) is almost the same as the erosion depth under the wave trough ($\delta_{e,trough}$) for fine sand in tunnels (Ribberink *et al.*, 2008). But, in the surface wave experiments, $\delta_{e,crest}$ is greater the $\delta_{e,trough}$, which directly leads to a net onshore mean velocity in the lowest levels of the sheet-flow layer.

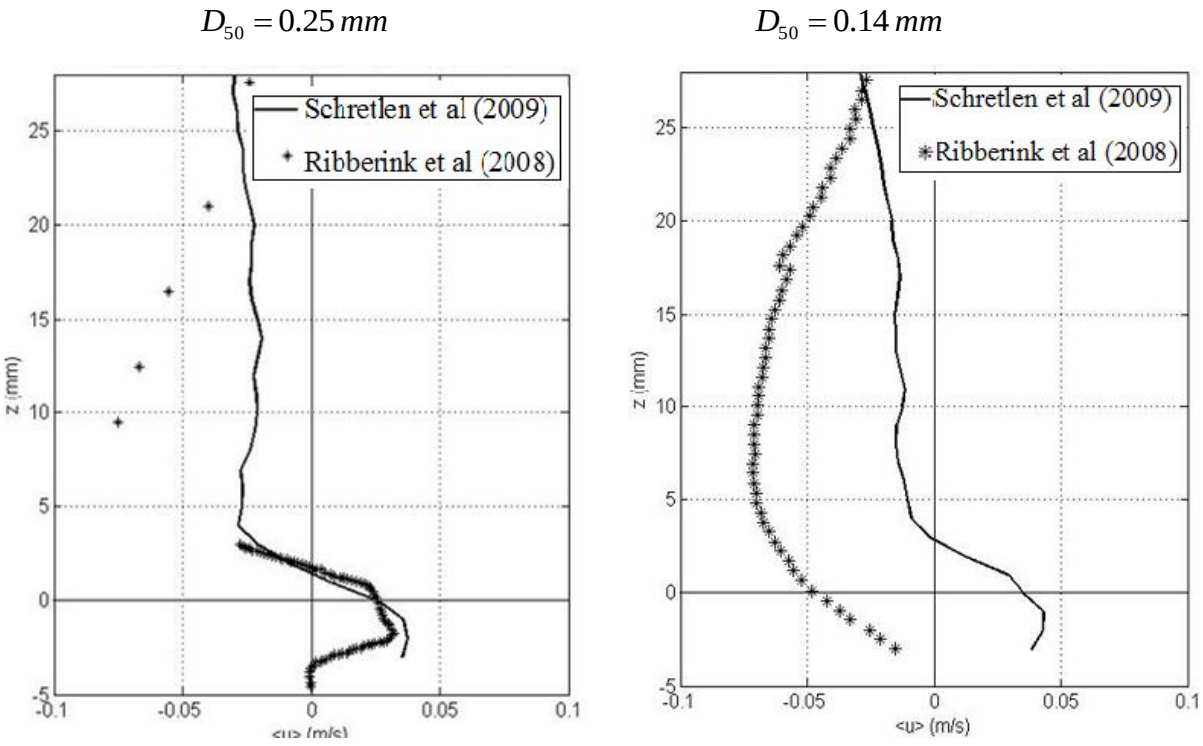

Fig. 2.5. Mean flow velocity measurements inside the wave boundary layer (Schretlen *et al.*, 2010)

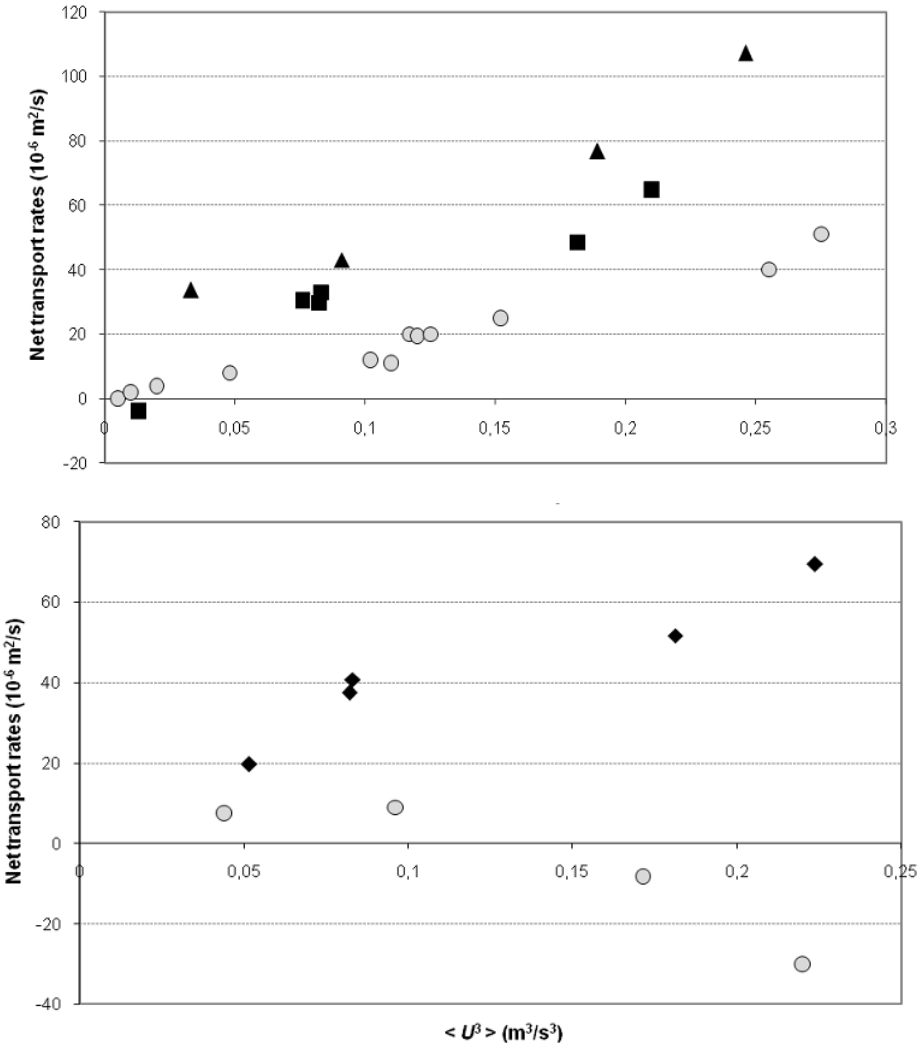

Fig. 2.6. Measured net sand transport rates for medium and fine sand in OFT and LWF (Schretlen *et al.*, 2010)

Schretlen et.al. (2009) measured net sand transport rates from the new experiments, and compared to existing oscillatory flow tunnel measurements (Ribberink et al. 2008). The comparison results of surface wave and oscillatory flow were presented in fig. 2.6 for both types of sand. The upper panel is for medium sand and the lower one is for fine sand. The black date represent for surface wave and the circles for fine sand. Fig. 2.6 shows that the comparison results of the medium sand (D_{50}=0.25 mm) transport rates in LWF are higher than those in OFT under similar sand and wave conditions. In the case of fine sand (D_{50}=0.14 mm), the net transport rate in LWF shows continuously increases but in OFT, the net transport rates a slight increase. After that, it decreases and becomes negative (offshore net rate) with an increase of flow velocity, $<u^3>$. It is because of the domination of phase lag effects for

fine sand conditions in OFT. It also indicates that the difference in mean current between surface waves and oscillatory flows may dominate the transport process and is therefore decisive for the net sand transport rates.

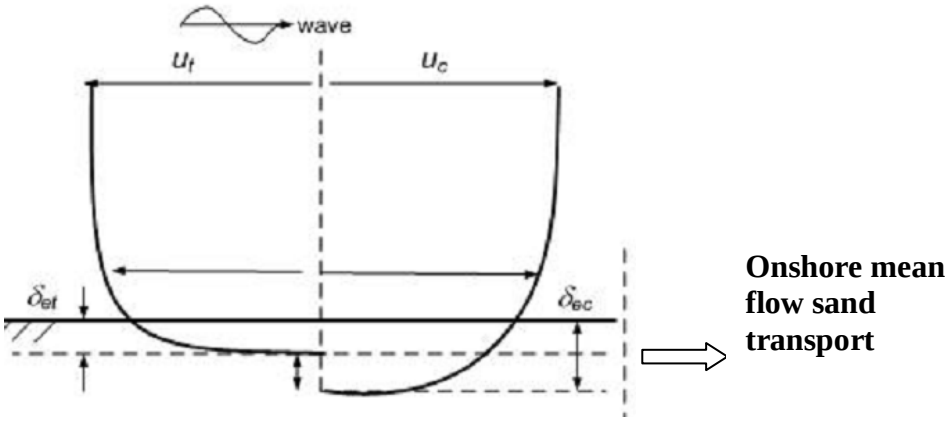

Fig. 2.7. Schematic representation of how a difference in crest and trough erosion depth ($\delta_{e(crest)} > \delta_{e(trough)}$) (Schretlen *et al.*, 2009)

In addition, the other difference between fine sand surface wave and tunnel experiments is that the erosion depth under the wave crest ($\delta_{e(crest)}$) is almost the same as the erosion depth under the wave trough ($\delta_{e(trough)}$) in tunnels due to the phase-lag effects (Ribberink *et al.*, 2008) although the free-stream velocity skewness is comparable. However, the erosion depth under the crest is always larger than under the trough in the surface wave experiments which directly leads to a net onshore grain motion in the lowest levels of the sheet-flow layer. This difference in erosion depth behaviour is due to the contribution of the positive mean wave-Reynolds stress component to the time-dependent bed-shear stress. It leads to a higher bed-shear stress under the wave crest and smaller under the trough for surface waves in comparison with oscillatory tunnel flows (Schretlen *et al.*, 2009). Fig. 2.7 showed schematically how this leads to a mean flow and transport in onshore direction for a velocity-skewed wave. This difference in erosion depth behavior can also be explained by the contribution of the positive mean wave-Reynolds stress component to the time-dependent bed-shear stress.

2.5. Reviews on the Measurements of Sediment velocity

As mention before, because the sheet flow layer is present in a very thin layer (a few mm's) above the sand bed with high concentration, measurements of sediment particles velocity under the sheetflow conditions are still relatively difficult.

Considering the sand transport process and the change of bottom morphology, sediment particle velocity measurements under the sheetflow conditions are important. Previously, several researchers measured the sediment particle velocity by using different measuring techniques. Horikawa *et al*. (1982) was the first to measure the sediment velocity under the sheetflow conditions. They used a motor-driven 35 mm camera, and the sediment velocity was determined by tracing individual particles on successive images in the suspension layer. To avoid the sidewall effects, the interior particles were used to decide the velocity. While in the lower sheet flow layer, it means 2mm above the original bed level, an extrapolation procedure was used. Velocity amplitude was obtained by curve fitting and the phase was decided by photographic technique.

Asano (1995) measured the motion of light plastic particles under oscillatory sheetflow conditions with a high-speed video camera, and also with a 35 mm motor-driven camera as an auxiliary.

Ahmed and Sato (2001) recorded the experimental processes by using High Speed Video Camera (HSVC) and applied the Particle Image Velocimetry (PIV) technique to estimate the particle velocities at different elevations. An exponential relationship between the image brightness values and sediment concentration was proposed. Liu (2005) also measured the sediment particles velocity by using HSVC and applied the PIV technique.

Wright (2002), O'Donoghue and Wright (2004b) used newly developed Ultrasonic Velocity Profiler (UVP) for the velocity measurements (details see in O'Donoghue and Wright, 2004b). The UVP is possible to measure a detailed velocity profile for 128 measurement points along the beam axis, from the free stream, throughout the wave boundary layer, into the upper sheet-flow layer. Schretlen (2009) performed the experiment in Large Wave Flume and measured flow velocity measurements. They applied the same method used in O'Donoghue and Wright (2004b).

2.5.1. PIV Technique

PIV technique has been rapidly developed and used to measure instantaneous velocity vector fields. PIV can carry out two-dimensional instantaneous velocity measurements.

PIV is the method acquiring velocities at grid points using high-density distribution patterns of subsequent particle images. Correct pairs of elements of particle clouds are obtained in two consecutive frames based on the similarity of image brightness distribution patterns in the two frames by calculating the values of cross-correlation or minimum quadratic difference as shown in the sketch below Fig. 2.5. The basic of cross-correlation method is to compare the interrogating window (first image at $t=t_o$), $f(i, j)$, with a window that has the same size of the interrogating window and moves within the search window (second image at $t = t_0 + \Delta t$), $g(i+k, j+l)$. The matrices, $f(i, j)$ and $g(i+k, j+l)$ are considered here to be the brightness values at the pixel (i, j) and $(i+k, j+l)$ in limited areas of size $n \times n$ pixels of a digitized PIV record as shown in Fig. 2.5. Once the maximum correlation is achieved, the new position of the pattern is defined. The formulation of the cross-correlation is,

$$R_{fg}(k,l) = \frac{\sum_{i=n/2}^{n/2}\sum_{j=-n/2}^{n/2}\left[\left(g(i+k, j+l) - g_{av}\right) - \left(f(i,j) - f_{av}\right)\right]}{(n+1)^2 \sigma_f \sigma_g} \tag{2.47}$$

where $R_{fg}(k, l)$ is the correlation between the two functions of f and g, σ_f and σ_g are the standard deviation of f and g which can be estimated as,

$$\left.\begin{aligned} \sigma_f &= \sqrt{\frac{\sum_{i=n/2}^{n/2}\sum_{j=-n/2}^{n/2}\left[\left(f(i,j) - f_{av}\right)\right]^2}{(n+1)^2}} \\ \sigma_g &= \sqrt{\frac{\sum_{i=n/2}^{n/2}\sum_{j=-n/2}^{n/2}\left[\left(g(i+k, j+k) - g_{av}\right)\right]^2}{(n+1)^2}} \end{aligned}\right\} \tag{2.48}$$

in which f_{av} and g_{av} are the mean values of g and f. The present study followed the parabolic peak fit method used by Ahmed and Sato (2001) to determine the location of the pattern in the order of sub-pixel. Three points are utilized to calculate the exact location of the particle cloud pattern (X, Y).

$$X = \left\{ l + \frac{R_{fg}(k,l-1) + R_{fg}(k,l+1)}{2\left[R_{fg}(k,l-1) - R_{fg}(k,l) + R_{fg}(k,l+1)\right]} \right\} \times \textit{image scale} \tag{2.49}$$

$$Y = \left\{ l + \frac{R_{fg}(k-1,l) + R_{fg}(k+,l1)}{2\left[R_{fg}(k-1,l) - R_{fg}(k,l) + R_{fg}(k+1,l)\right]} \right\} \times \textit{image scale} \tag{2.50}$$

If we know the time interval between the two images $\triangle t$ and image scale,the sediment particle velocities can be determined using these equations,

$$u_s = \frac{X}{\Delta t} \quad , \quad v_s = \frac{Y}{\Delta t} \tag{2.51}$$

Gui and Merzkirch (1996) firstly introduced Minimum Quadratic Difference (MQD) algorithms. The basic of MQD approach is to compare the patterns between the two images to satisfy the minimum quadratic difference, $DQ_{fg}(k,l)$. Once the minimum value is achieved, the new position is defined in the order of one pixel, *k* and *l*. To determine the displacement of sand particles between two successive images, Ahmed and Sato (2001) developed the original formulation of MQD proposed by Gui and Merzkirch (1996) by subtracting the mean brightness. The MQD formulation by Ahmed and Sato (2001) was used in this study.

$$DQ_{fg}(k,l) = \frac{1}{(n+1)^2} \sum_{i=n/2}^{n/2} \sum_{j=-n/2}^{n/2} [(g(i+k, j+l) - g_{av}) - (f(i,j) - f_{av})]^2 \tag{2.52}$$

where $DQ_{fg}(k,l)$ is the minimum quadratic difference.

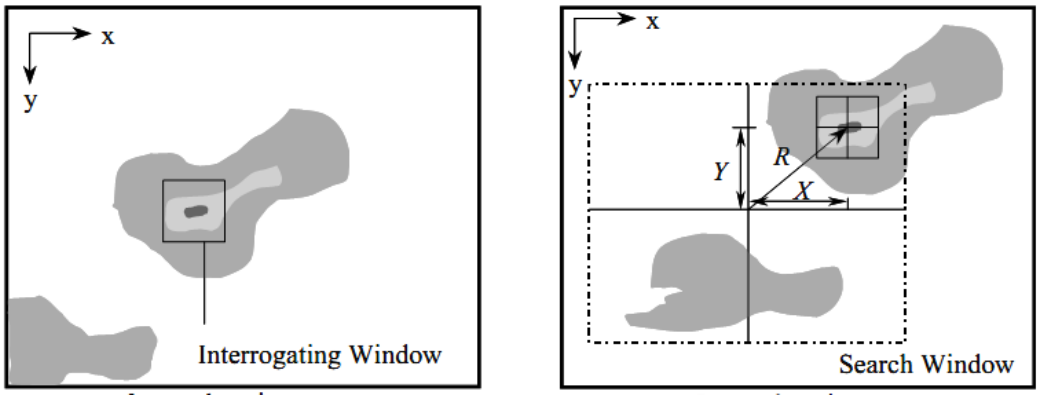

First image at $t = t_0$ Second image at $t = t_0 + \Delta t$

Fig. 2.8. Displacement between two analogous particle clouds pattern (Ahamed and Sato, 2001)

2.6. Reviews for Measurements of Erosion depth

The varying of the level of the immobile bed between a minimum z_{min} and a maximum z_{max} can be seen during the wave cycle due to the sediment pick-up and deposition processes. The maximum erosion depth, δ_{em} , is the vertical distance between the original bed level, $z = 0$, and $z = z_{\min}$. Although the erosion depths are small for

typical sand sizes in wave-generated sheetflow conditions, it is one of the interesting parameter for transport process in oscillatory sheetflow.

Asano (1992) used large but light plastic particles with diameter 4.17 mm and 1.24 in specific gravity to investigate the sheetflow behaviors. Some parts of sediment and water in the flume were dyed to visualize easily. From the measurement of temporal variations of the erosion depth, Asano found the linear relationship between the maximum erosion depth δ_{em} and the maximum Shields parameter θ_m ,

$$\frac{\delta_{em}}{d} = 8.5(\theta_m - \theta_{cr}) \tag{2.53}$$

Zala Flores and Sleath (1998) proposed one parameter *S* which is the ratio of inertial to gravity force which can be considered as a relative local flow acceleration (Sleath , 1994). The erosion depth not only depends on the Shields parameter but also the parameter *S*.

$$S = \frac{\rho u \omega}{(\rho_s - \rho)} \tag{2.54}$$

For large values of (S >~0.2), plug flow may occur and the erosion depth increased suddenly under such condition. But at small value of *S*, the mobile layer reacts instantaneously to the flow velocity and he found that the maximum erosion depth has a linear relationship with the maximum Shields parameter that has the same form like Asao (1992).

$$\frac{\delta_{em}}{d} = 3\theta_m \tag{2.55}$$

Dohmen-Janssen et al., (2001) measured the maximum erosion depth with three different kinds of sands with $D_{50} = 0.13mm$(fine), $D_{50} = 0.21mm$(medium) and $D_{50} = 0.32mm$ (coarse) under combined wave-current sheetflow conditions. The erosion depth was recorded using a normal video camera through the glass wall. From the experiment results, they found the measured erosion depth of fine sand is larger than for medium and coarse sand. It still holds the linear relationship between the erosion depth and Shields parameter.

$$\begin{cases} \dfrac{\delta_{em}}{d} = 7.8\theta_m \quad d = 0.13mm \\ \dfrac{\delta_{em}}{d} = 4.5\theta_m \quad d \geq 0.21mm \end{cases} \tag{2.56}$$

O'Donoghue and Wright (2004a) performed sheetflow experiments under sinusoidal or the 2nd-order Stokes waves conditions with three uniform sands and four mixed sands. They measured detailed time-varying erosion depth $\partial_e(t)$ under different sinusoidal or asymmetric waves. Authors found that there was a phase shift of $0.1\theta_m$ between the instantaneous erosion depth and the free-stream velocity or the instantaneous Shields parameter, $\theta(t)$. The following linear relationship between $\theta(t)$ and $\partial_e(t)$ can be established,

$$\frac{\delta_e(t)}{d} = 2.8\theta(\omega t - 0.1\theta_m) + 5.5(\theta_m - 1) \tag{2.57}$$

From this expression, the maximum erosion depth can be estimated as,

$$\frac{\delta_{em}}{d} = 8.3\theta_m - 5.5 \tag{2.58}$$

where d is the medium grain diameter, θ_{cr} is the critical Shield parameter for the inception movement of the sediment particles. Time-varying Shields parameter, $\theta(t)$ under the oscillatory flow conditions is defined as,

$$\theta(t) = \frac{\tau(t)}{\rho(s-1)gd} = \frac{\frac{1}{2} f_w u_b(t)^2}{(s-1)gD_{50}} \tag{2.59}$$

in which $\tau(t)$ is bed shear stress, $u_b(t)$ is the near bed horizontal free-stream velocity above the wave boundary layer, $s = \rho_s / \rho$ is the sediment specific gravity where ρ_s, ρ are the sediment and water particle density, respectively, g is the acceleration due to gravity, f_w is the wave friction factor and the value of f_w = 0.01. Then, the maximum Shields parameter, θ_m, corresponds to the maximum flow velocity,

$$\theta_m = \frac{\tau_m}{\rho(s-1)gd} = \frac{\frac{1}{2} f_w u_b{}^2}{(s-1)gD_{50}} \tag{2.60}$$

where τ_m and u_b are the amplitude of bed shear stress and free-stream velocity, respectively.

CHAPTER 3

Laboratory Experimental Set-up and Methodology

3.1. Introduction

3.1.1. General

At present, the knowledge is already obtained about net cross-shore sediment transport and transport processes under sheet-flow conditions. Sand transports are very difficult to measure directly in the field. Therefore, most of the measurements are carried out in laboratory experiments using different facilities, such as the wave flumes or water tunnels which are either small-scale or full-scale experiments. Based on the extensive review of previous experimental studies and knowledge obtained from these large-scale laboratory experiments, several experiments have been conducted in the oscillatory flow tunnels (OFT). Also, although most of these experiments are performed with sinusoidal and velocity skewed flows, the studies of boundary layer streaming, which is induced by surface waves, are rare.

Previous studies (Dohmen-Janssen and Hanes, 2002, Ribberink *et al*., 2008 and Schretlen *et al*., 2009) suggested that the effect of boundary streaming may dominate for cross-shore sediment transport is therefore decisive for the net sand transport rates. Therefore, to know the effect of boundary layer streaming, experiments were performed on skewed velocity with superimposed a small onshore current in OFT.

3.1.2. Objectives of Present Experiment Work

The overall objective of the new experiments is to obtain quantitative data for net transport rates under sheet-flow conditions with different sands. Although there is a quite number of experimental data under sheet flow conditions, experimental data on sand transport in combined wave-current for the 2^{nd} order Stroke's wave conditions are less. Therefore, in this study, new experiments were performed under combined wave and current in the Small Oscillating Flow Tunnel.

During the experiments, the successive images recorded by HSVC were used to analyze the sand transport process. To investigate streaming effect on sediment transport, sediment particle velocities was measured to achieve the vertical profile of the mean flow velocity, *U (z)*.

3.2. Experimental Facilities

3.2.1. Oscillatory Flow Tunnel

Experiments were performed in an Oscillatory Flow Tunnel (OFT) at University of Tokyo. This facility can perform the experiments under the original scale of the horizontal orbital motion near the bed. (In March 2002, the OFT was elongated to the present length scale).

The oscillatory motion, generated in an oscillating water tunnel is supposed to represent the near-bed orbital motion under the surface wave. However, in the oscillatory flow tunnel, there is no free surface and it is enclosed by the conduit. A schematic diagram of the Oscillatory Flow Tunnel (OFT) and its dimensions are shown in Fig.3.2. The OFT consists of a loop of closed conduits and a hydraulically-driven piston. The tunnel is equipped with a 5.7 m long rectangular horizontal test section with a height of 24 cm and a width of 7 cm. A 40 mm deep flat sand bed is situated at the center of the test section with mild slopes at both ends. Sands are filled into the test section forming an initially flat bed. The test section is surrounded by a glass sidewall on the observational side, a black painted wooden board on the opposite side and detachable ceilings. Sand traps made of honeycombs are installed at both ends of the test section in order to collect the sand that would be transported away from the test section. In addition, an onshore or offshore steady current imposed with the oscillatory flow is generated by a circulation system which is controlled by a pump. Two discharge meters are installed on both sides of the current circulation section. Adjusting the discharge of the water flux inside the system, different current velocities can be generated. The current velocity U_c inside the test section can be calculated,

$$U_c = \frac{Q}{bh} \tag{3.1}$$

where Q is the discharge rate, b and h are the width and height of the test section, respectively.

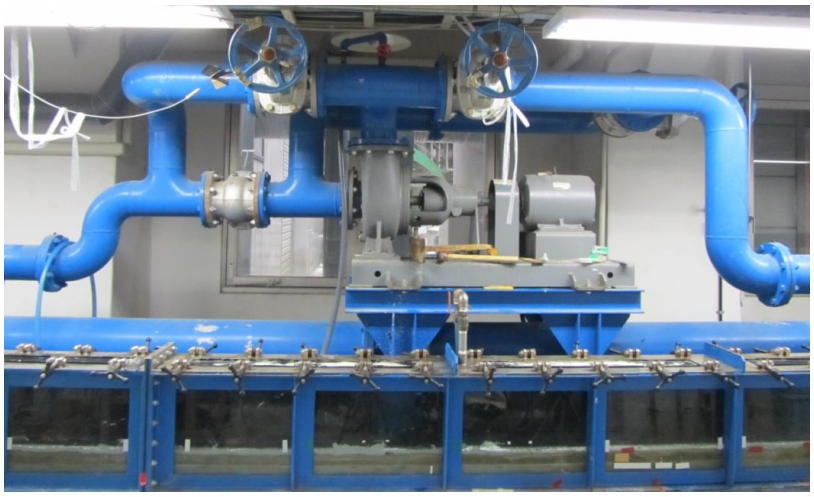

Fig. 3.1. Photo of Oscillatory Flow Tunnel

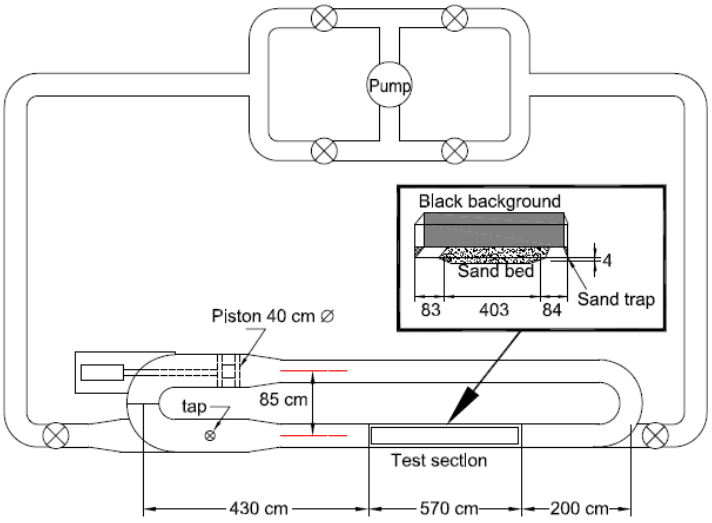

Fig. 3.2. Schematic diagram of the oscillatory flow tunnel (all dimensions are in cm)

3.2.2. Simulation of Orbital Motions and Calibration Experiments

In this section, the mechanism to generate the oscillating flow inside the tunnel is presented together with the calibration experiments. The present oscillatory flow water tunnel consists of a loop-shape closed conduit and a piston-type wave generator shown in Fig. 3.2. The piston's movement is controlled by the electronic signals from PC. In the oscillatory flow tunnel, any kinds of oscillatory flow conditions can be obtained by providing the proper time-varying signals of piston displacements. Signals such as regular symmetric or asymmetric waves, i.e., simple periodical waves with constant wave height and direction can be generated using Stokes or Cnoidal wave theory which can be easily generated from the existing program code. Using

such kind of oscillatory flow tunnel, two kinds of asymmetric waves can be generated: the velocity asymmetric waves and the acceleration asymmetric waves.

To be the inputting voltage electronic signals, the displacement data should be adjusted into the range of [-1, 1]. Then, through an amplifier, the time series electronic datasets of piston's displacement under various flow conditions can be achieved. Calibration experiments were performed to generate the new velocity profiles for the velocity asymmetric wave. From the calibration process, it can get the relationship between Counter number, N and the maximum velocity of water particle, U . In calibration experiments, adjusting a certain value of counter number, N through piston controller, corresponding maximum amplitude of the actual displacement of the piston is determined for the 2^{nd} –order Stroke's waves of two different wave periods of 3, and 5 sec. As the water mass is conserved, the following relationship for the flow flux is applicable, $A_p U_p = A_t U$ where and U_p and U are the amplitude of the horizontal orbital velocity for piston and water particle respectively. $A_p = \pi/4D^2$ and $A_t = H_t W_t$ are the cross sectional areas for cylindrical piston region and rectangular test section respectively, where D =39.8 cm is the diameter of the piston and, W_t = 7.0 cm, H_t =24.0 cm are the width and height of the test section. A typical velocity profile resulting from the piston displacement is shown in Fig. 3.4. The linear relationship of the resulted calibration of counter, N, and the maximum velocity is shown in Fig. 3.3 and the linear calibration relationship is written below.

$$N = \alpha . u_{\max}$$

where N= Counter Number, u_{max}= maximum free –stream velocity and is coefficient.

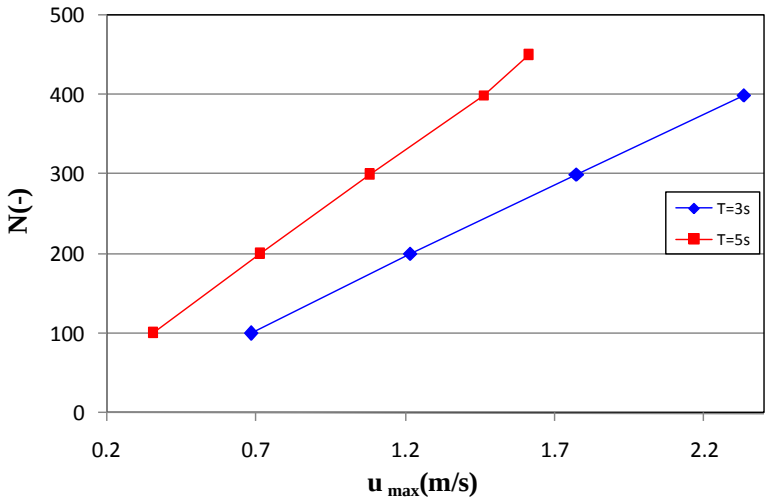

Fig. 3.3. Calibration of N and u_{max}

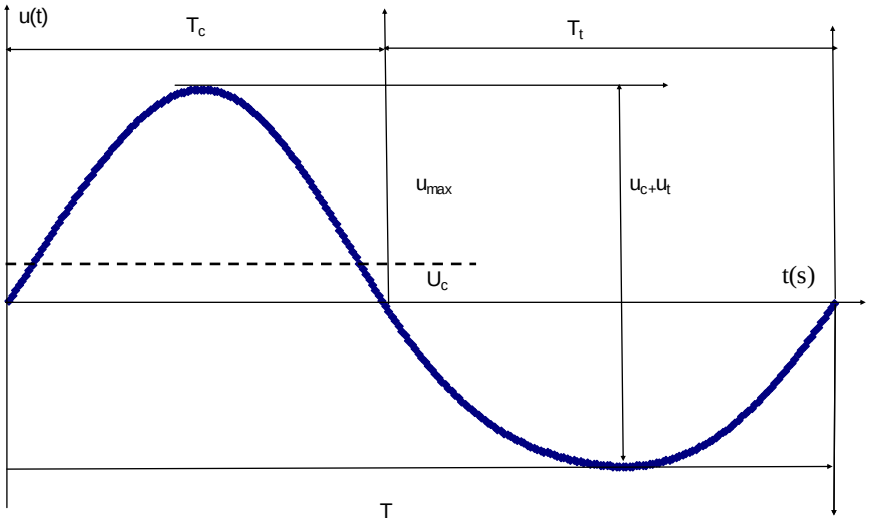

Fig. 3.4. Typical velocity profile of asymmetric oscillation and definitions

The resulted calibration of counter, *N*, with different flow condition are listed in Table 3.1. After inputting the time-series data file under the relative wave condition for certain wave height, period and water depth, corresponding oscillatory flow can be generated inside the water tunnel by adjusting the counter number on the amplifier.

Table 3.1. Counter numbers used for the 2nd – order Stroke's wave experiments

T=3s						
u_{max}(m/s)	0.8	1.0	1.2	1.4	1.6	1.8
N (-)	135	169	202	236	270	303

T=5s						
u_{max} (m/s)	0.8	1.0	1.2	1.4	1.6	1.8
N (-)	221	276	331	386	441	496

3.3. Experimental Set-up

3.3.1. Sediment properties and measuring instruments

Experiments were performed with three different three well-sorted sands with a medium sand size of D_{50} =0.13 mm (very fine), 0.16 mm (fine) and 0.3 mm (coarse). The sieve analysis of these sands was provided in Fig. 3.5. From the sand distribution curve, we can obtain the Trask's sorting coefficient,

$S_o = \sqrt{D_{75}/D_{25}} = \sqrt{0.21/0.13} = 1.27$, where D_{75} and D_{25} are the grain diameter for which 75% and 25% of the sediment by weight is smaller respectively.

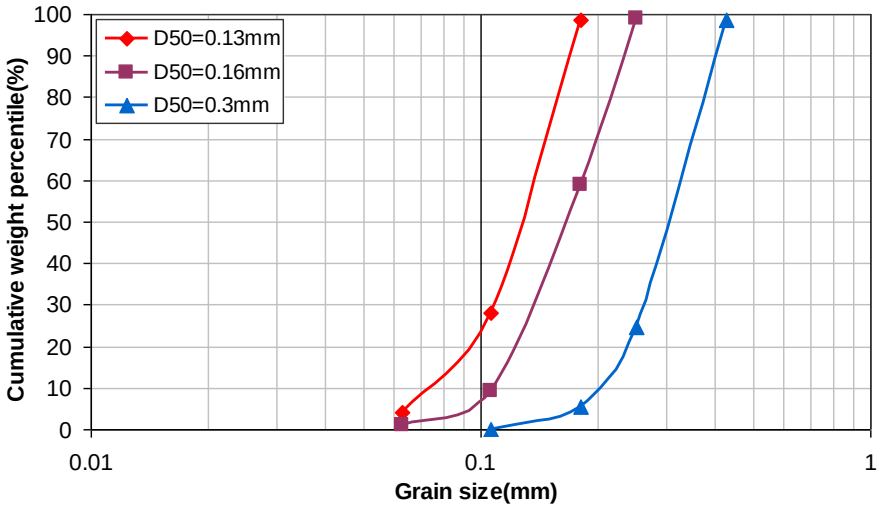

Fig. 3.5. Grain size distribution curves of the three sands in the experiments

The measuring procedures were performed by an enhanced PIV technique. The layout sketch of PIV experiment was shown in Fig. 3.6. By installing the HSVC (High Speed Video camera) very close to the glass sidewall, the experiments were conducted in OFT. Two light sources are adjusted so as to illuminate the tracers (fine sand). By putting a black background, only the sand particles will become sources of light due to the reflection. The oscillations are generated to the steady state before recording each case. (HSVC) produces 420 frames in one second and records the experimental processes. The size of the frame is 220 by 168 pixels. A typical visualized image utilized in the PIV technique including an image scale was shown in Fig. 3.7.

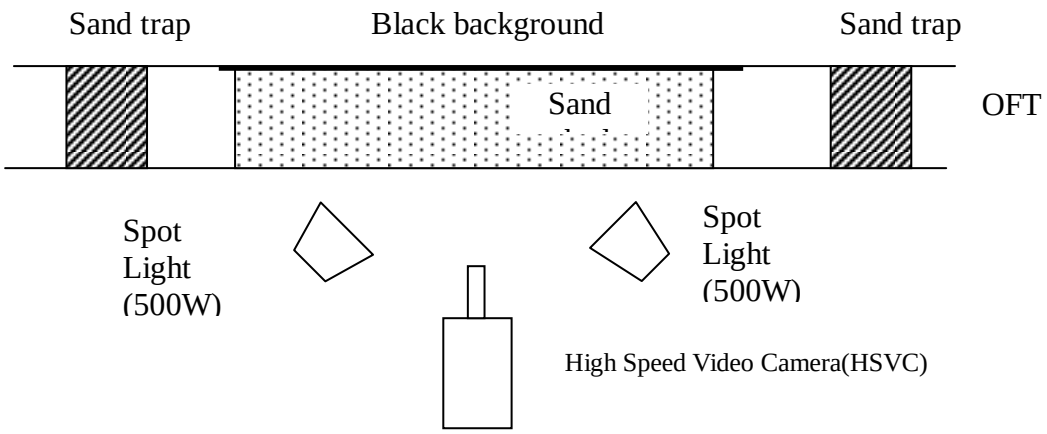

Fig. 3.6. Experimental apparatus utilized for image analysis (top view)

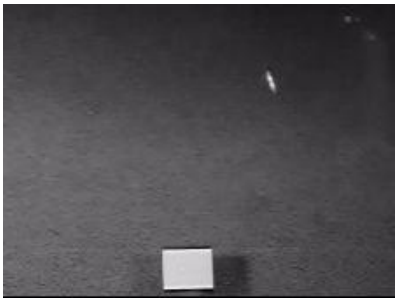

Fig. 3.7. Typical visualized image

3.3.2. Experimental Conditions

To quantitatively evaluate the influence of the onshore streaming to the sheetflow sand transport, laboratory experiments were conducted under the asymmetric wave and current conditions, and the corresponding net sand transport rate was recorded. The new experiment mainly focused on the 2nd -order Stokes asymmetric waves with superimposed current conditions. The free–stream velocity of 2nd -order Stokes wave can be determined by: $u(t) = u_1 \sin(\omega t) - u_2 \cos(\omega t)$.where: u_1 and u_2 = the velocity amplitude of the first and second order components of the horizontal velocity and $\omega = 2\pi/T$, the angular frequency of the wave. *A* velocity asymmetric index, $R_v = 0.57$ was used. It is defined as,

$$R_v = u_c /(u_c + u_t) = (u_1 + u_2)/2u_1 \tag{3.2}$$

where u_c and u_t are crest velocity and trough velocity magnitudes, $u_1 = 0.5(u_c + u_t)$ and $u_2 = 0.5\ (u_c - u_t)$, respectively. In total, 40 cases were carried out to measure the net sediment transport rate. Sheetflow transport regime was confirmed for all experimental conditions. According to Longuet-Higgins (1957), onshore streaming

velocity for the 2nd-order Strokes wave theory can be estimated as:

$$U_c = \frac{3}{4c}\left(\frac{a\omega}{\sinh(kh)}\right)^2 \tag{3.3}$$

where a is the wave amplitude, ω is the angular frequency, k is the wave number, h and c are the wave height and wave celerity, respectively. In this study, the assumed water depth and wave height are 3.5 m and 1.2 m based on the wave flume data Schretlen *et al*., (2009). To understand the effect of onshore streaming, a small onshore steady current U_c of 10 cm/s and 20 cm/s which is calculated based on Eq. 3.5 was superimposed in the same direction with wave propagation, *i.e.*, the onshore direction. Experimental conditions for all tests are tabulated in Table 3.2, 3.3 and 3.4. In addition, temporal variations of erosion depth and maximum erosion depth were measured under asymmetric oscillatory flow and combined wave-current flow. In order to know the effect of sand size and the effect of streaming on the erosion depth, two kinds of sediments with fine and coarse sand were used for the experiments. PIV technique was applied to estimate the time- dependent and time-averaged sediment particles velocities.

Table 3.2. Test conditions for very fine sand (D_{50}=0.13mm)

Test	T (s)	D_{50} (mm)	u_{max} (cm/s)	U_c (cm/s)	U_1 (cm/s)	U_2 (cm/s)	R_v (-)
T5VF1	5	0.13	80	0.0 10 20	70.20	9.8	0.57 -
T5VF2	5	0.13	90	0.0 10 20	78.9	11.1	0.57
T5VF3	5	0.13	100	0.0 10	87.7	12.3	0.57
T5VF4	5	0.13	120	0.0 10	105.3	14.7	0.57
T5VF5	3	0.13	1.0	0.0	87.7	12.3	0.57
T5VF6	3	0.13	1.2	0.0	105.3	14.7	0.57

Table 3.3. Test conditions for fine sand (D_{50}=0.16mm)

Test	T (s)	D_{50} (mm)	u_{max} (cm/s)	U_c (cm/s)	U_1 (cm/s)	U_2 (cm/s)	R_v (-)
T5F1	5	0.16	80	0.0 10	70.20	9.8	0.57 -
T5F2	5	0.16	100	0.0 10 20	87.7	12.3	0.57
T5F3	5	0.16	120	0.0 10 20	105.3	14.7	0.57
T5F4	5	0.16	140	0.0 10 20	122.8	17.2	0.57
T5F5	5	0.16	160	0.0 10 20	140.4	19.6	0.57
T3F5	3	0.16	100	0.0 10 20	87.7	12.3	0.57
T3F2	3	0.16	120	0.0 10 20	105.3	14.7	0.57

Table 3.4. Test conditions for coarse sand (D_{50}=0.3mm)

Test	T (s)	D_{50} (mm)	u_{max} (cm/s)	U_c (cm/s)	U_1 (cm/s)	U_2 (cm/s)	R_v (-)
T5C1	5	0.3	120	0.0 10 20	105.3	14.7	0.57
T5C2	5	0.3	140	0.0 10 20	122.8	17.2	0.57
T5C3	5	0.16	160	0.0 10 20	140.4	19.6	0.57
T3C4	3	0.16	120	0.0 10 20	105.3	14.7	0.57
T3C5	3	0.16	140	0.0 10 20	122.8	17.2	0.57

3.3.3. Experimental Procedures

The following flow chart figure describes the experimental procedures to obtain the net transport rate, the temporal distribution of the erosion depth, and the sediment velocity. The necessary detail procedures are also explained in the following paragraph.

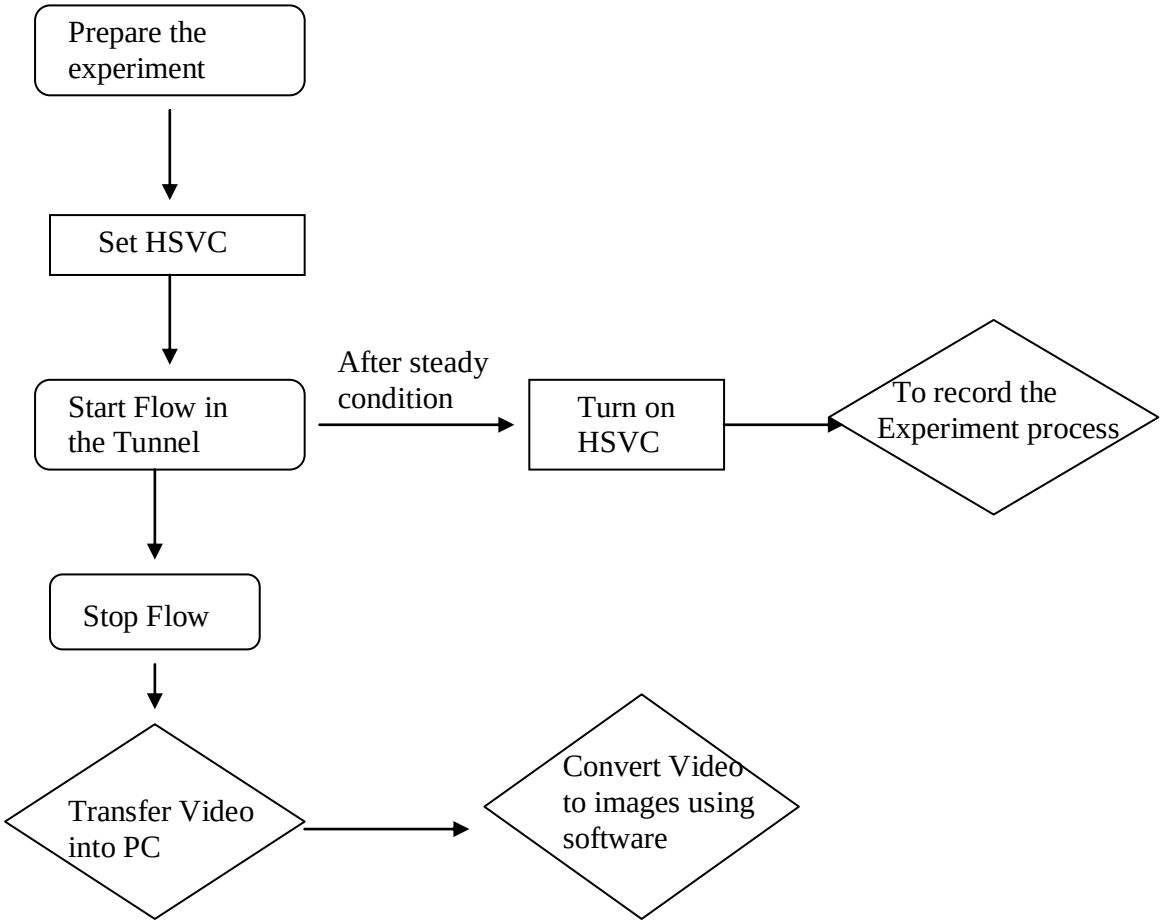

Fig. 3.8. Flow chart of the experimental procedures

For the preparing the experiments, first inject the water up to half of the oscillatory flow tunnel, and then put the required amount sand into the tunnel. Close the tunnel with detachable ceilings and successively fill water until all the air bubbles are driven out the tunnel. For the second step to set HSVC system, two spotlights are put at suitable positions and used tripod to fix the HSVC and adjust the proper elevation for recording. Make the HSVC lens axis perpendicular to the tunnel sidewall. And then, we can start the flow in the tunnel. After the oscillations are operated to the steady state, turn on the HSVC to record the experimental process. At the same time, use a flash to record the time. After that, it stops the oscillating flow. Finally, the video is transferred into PC and converted the video frames into bitmap images using computer software. Image analysis achieved by using Matlab.

3.4. Present Experimental measurements

3.4.1. Measurement for Net Transport Rate

In experiments for measuring net rate, a wooden plate was initially placed in the middle of the test section to separate onshore and offshore parts. Then, the dry sand was filled in each side and assured an initially flat bed. Most of the experiments were operated for about (20-30) oscillation cycles. After operating the oscillatory flow, sands remained at each part and stored inside sand traps were taken out carefully. Subsequently, each part of sands was placed in an oven to dry completely for 24 hours. Finally, the dried sand was weighted and the net transport rates were calculated based on the mass difference between the two parts after a recorded experimental duration Δt_{exp} .

$$q_{meas} = \frac{\Delta M_{on} - \Delta M_{off}}{2b\rho_s \Delta t_{\exp}} \tag{3.6}$$

where

q_{meas}= the measured net sand transport rate,

ΔM_{on} and ΔM_{off} = the sand mass difference of the onshore and offshore parts before and after experiment

b = the width of the tunnel, and

ρ_s = the sediment density.

Δt_{exp} .=experimental duration

The experimental error was estimated through Ahmed and Sato (2001),

$$error = \frac{\Delta M_{on} + \Delta M_{off}}{\Delta M_{on} - \Delta M_{off}} \tag{3.7}$$

3.4.2. Horizontal Sediment Particle Velocity Measurements by using PIV

Sediment particle velocity within the sand-laden sheetflow layer was measured by means of a PIV technique. The enhanced PIV technique developed by Ahmed and Sato (2001) is used in the present study to calculate the sand particle velocity. High Speed Video Camera (HSVC) produces 4200 frames per one second. After setting a black wood board as the background in the oscillating tunnel, the sand particles become the only light source due to reflection in the recorded images. Using such images, we can perform the PIV technique to estimate the sediment particles velocity. Then, the video was transferred into PC and converted the video frames into bitmap images using computer software. The frames were captured up to 2100 bitmap files for wave period 5 s (420 frames x 5.0 s) and 1260 bitmap files for wave period 3 s (420 frames x 3.0 s). The size of the frame is 220 by 168 pixels in which each pixel has the gray value or brightness value, in the range from 0 to 255. To calculate the image scale (pixels correspond to metric measure), a tape with known size (10mm x 8 mm) was glued at the area of interest.

3.4.3. Present measurements of Maximum erosion depth

Sediment is being picked up from the bed which is going up and down during the wave cycle. In the present study, image analysis was used as a non-intrusive method to know this variation of bed level. The change of bed level was recorded by using the (HSVC) which was installed very close to the glass side wall. And then, the recordings were analyzed to investigate the difference of top of bed level at zero and maximum velocity. The difference of bed level is defined as the maximum erosion depth. The difference values of brightness between two successive images obtained from the HSVC was used to determine the erosion depth. The brightness values are enlarged 20 times to be clear the difference between the unmovable bed and mobile bed layer.

Fig. 3.9 shows a distinctive image of sand bed around flow reversal and at the moment of maximum velocity which is used to determine the maximum erosion depth $\delta_{em,}$. Fig. 3.10 presents a typical image at different phases of 60° interval which is used to measure instantaneous time-varying erosion depth. The black block in the middle

of the images is a tape to calibrate the image scale. Measured time-varying erosion depth for the asymmetric flow conditions of u_{max} =1.4 m/s, T= 5 s and D_{50} = 0.3 mm are shown in Fig. 3.10 together with free-stream velocity.

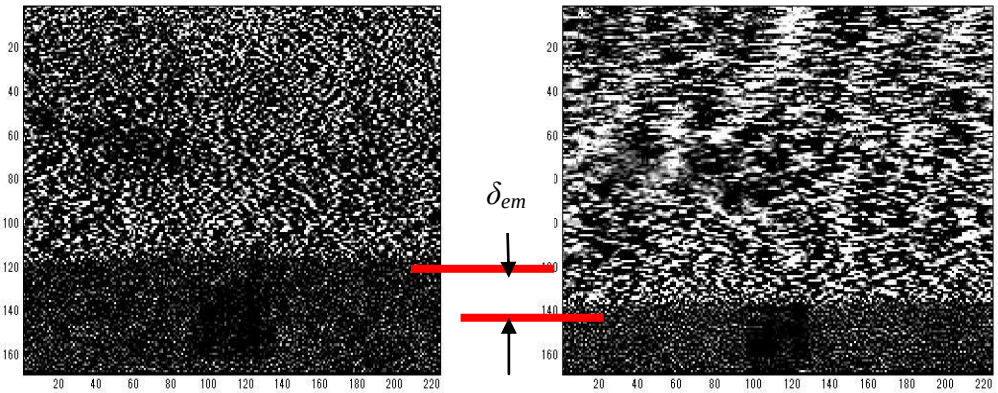

Fig. 3.9. Erosion depth at the moment of maximum velocity and around flow reversal (All dimensions are in mm)

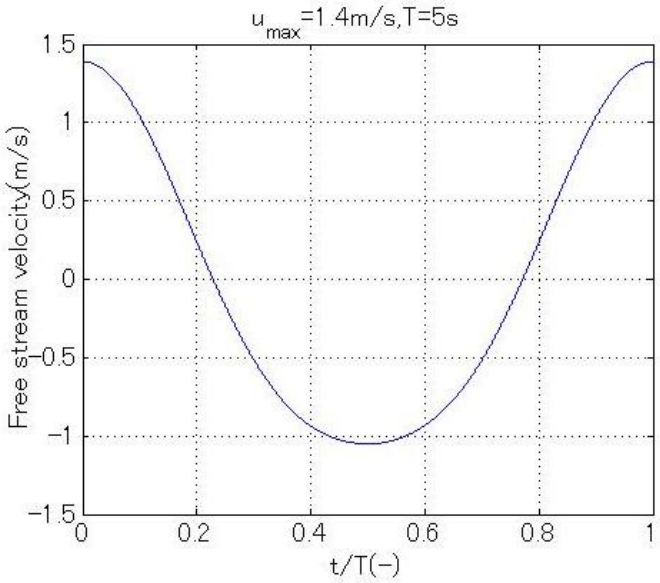

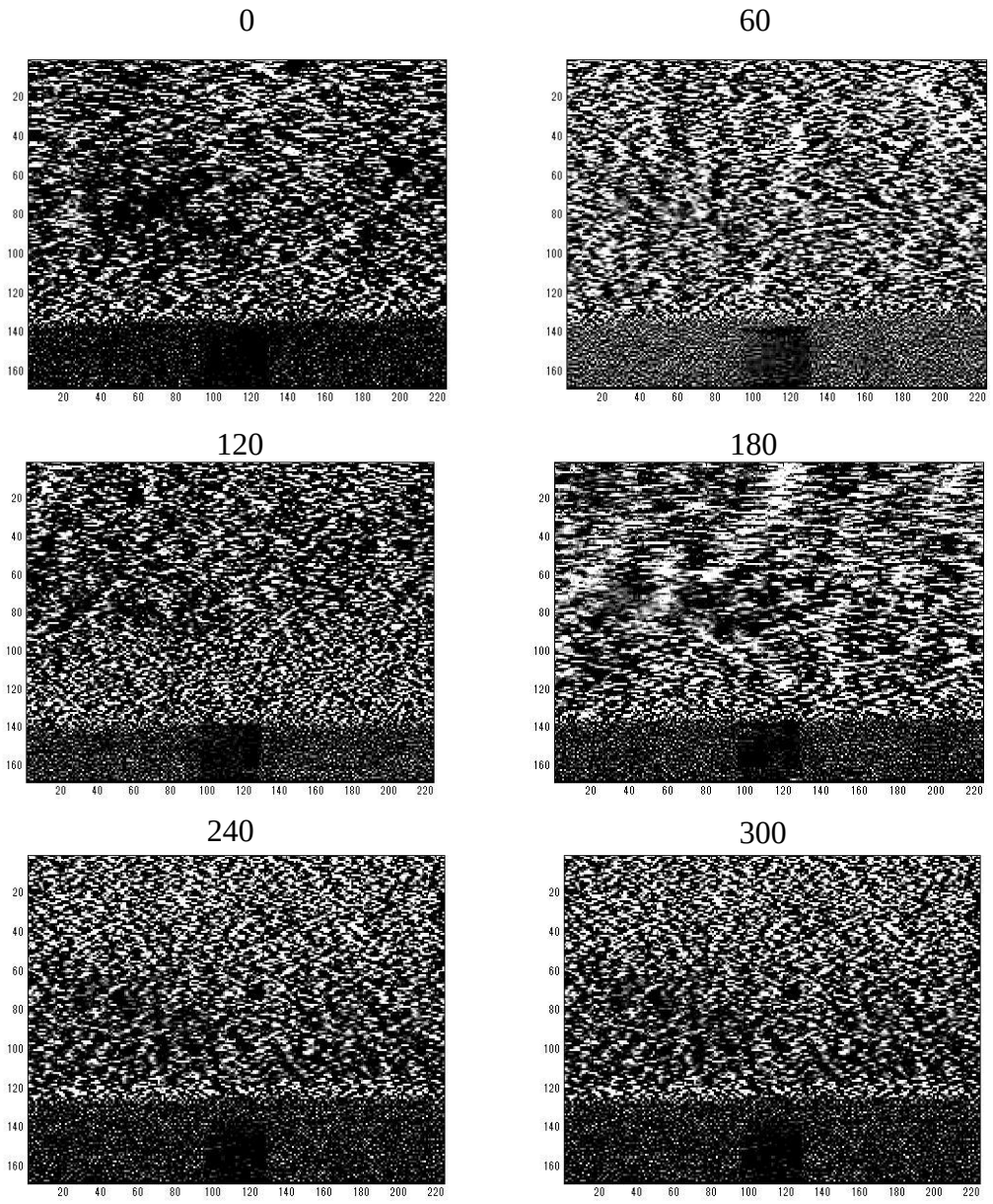

Fig. 3.10. Measurement of the instantaneous erosion depth under different phases

CHAPTER 4

Experimental Results and Discussions

4.1. Introduction

In this chapter, the main results of all experimental series, which include the values of measurements of net transport rate under different flow conditions, are presented. Section 4.3 describes about grain-size effects as well as steady streaming effects on the sediment transport processes for three types of sand. Section 4.4 deals with the measurements of sediment particle velocities at different elevations by means of PIV technique. This section also expresses the results of vertical profiles of the mean flow velocity, *U (z)*, for different sand sizes and wave period conditions. The variation of turbulence intensity was also measured. In section 4.5, it discusses about the maximum erosion depth and time-varying erosion depth under different flow conditions.

4.2. Objectives of present experiments

The main objective of these experiments was to understand the moving mechanism of the uniform sediments and to obtain the quantitative experimental data set of net transport rate. Therefore, the experiments with uniform sands were performed in the oscillatory water flow tunnel under sheetflow and asymmetric conditions and net sediment transport rates were measured. In addition, in order to assess the effect of onshore streaming on sediment net rate, the time-dependent horizontal sediment velocities and mean flow velocity were investigated under different flow conditions by using an enhanced Particle Image Velocimetry (PIV) technique.

4.3. Net transport rates of uniform sand

To achieve the objectives of the influence of streaming on net transport and to know the reason of difference net transport rate between the oscillatory flow tunnels and surface waves, sand transport was measured and compared the results between without onshore current and with onshore current .

Experimental conditions and results for all net sand transport rates of three types of sands associated with measurement error are tabulated in Tables 4.1, 4.2 and 4.3. In total, 40 cases were carried out with asymmetric waves and combined asymmetric wave and current conditions. For very fine and fine sand cases, the net transport rate

was determined by averaging the results of 2 or 3 tests. For coarse sand cases, the measurement of net rate was not repeated and only one time measurement is made because the error due to the sand loss is small. The name of test condition, oscillation period T, the amplitude of free-stream velocity and the imposed current U_c with respective average net transport rate per unit width, q_{net} are described in each table.

Table 4.1. Measured net transport rate of very fine sand (D_{50} =0.13mm)

Test	T (s)	D_{50} (mm)	u_{max} (m/s)	q_{net} (cm^2/s)		q_{net} (cm^2/s)		q_{net} (cm^2/s)	
				U_c=0 (cm/s)	Error (-)	U_c=10 (cm/s)	Error (-)	U_c=20 (cm/s)	Error (-)
T5VF1	5	0.13	0.8	-0.17	0.3	-0.12	0.5	0.27	-0.35
T5VF2	5	0.13	0.9	-0.35	0.2	-0.25	0.4	0.28	-0.29
T5VF3	5	0.13	1.0	-0.37	0.2	-0.35	0.3	-	-
T5VF4	5	0.13	1.2	-0.83	0.1	-0.63	0.3	-	-
T5VF4	3	0.13	1.0	-0.4	0.08	-	-	-	-
T5VF4	3	0.13	1.2	-0.94	0.17	-	-	-	-

Table 4.2. Measured net transport rate of fine sand (D_{50} = 0.16 mm)

Test	T (s)	D_{50} (mm)	u_{max} (m/s)	q_{net} (cm^2/s)		q_{net} (cm^2/s)		q_{net} (cm^2/s)	
				U_c=0 (cm/s)	Error (-)	U_c=10 (cm/s)	Error (-)	U_c=20 (cm/s)	Error (-)
T5F1	5	0.16	0.8	0.05	-0.3	0.28	-0.1	-	-
T5F2	5	0.16	1.0	0.09	-0.4	0.38	-0.2	0.41	-0.14
T5F3	5	0.16	1.2	-0.18	0.2	0.31	0.2	0.56	-0.22
T5F4	5	0.16	1.4	-0.57	0.1	-0.45	0.3	-0.25	-0.2
T5F5	5	0.16	1.6	-0.93	0.1	-0.83	0.3	-0.6	-0.28
T5F5	3	0.16	1.0	-0.14	0.1	0.26	-0.27	0.18	0.5
T5F5	3	0.16	1.2	-0.4	0.07	0.39	-0.27	0.6	-0.24

Table 4.3. Measured net transport rate of coarse sand (D_{50} =0. 3mm)

Test	T (s)	D_{50} (mm)	u_{max} (m/s)	q_{net} (cm^2/s)		q_{net} (cm^2/s)		q_{net} (cm^2/s)	
				U_c=0 (cm/s)	Error (-)	U_c=10 (cm/s)	Error (-)	U_c=20 (cm/s)	Error (-)
T5C1	5	0.3	1.2	0.27	-0.03	1.22	-0.01	1.3	-0.03
T5C2	5	0.3	1.4	0.55	-0.02	1.56	-0.01	1.6	-0.06
T5C3	5	0.3	1.6	0.8	-0.02	1.6	-0.02	1.85	-0.02
T5C1	3	0.3	1.2	0.27	0.06	0.85	-0.05	1.13	-0.03
T5C2	3	0.3	1.4	0.31	-0.05	0.9	-0.09	1.37	-0.06

4.3.1. Influence of steady streaming

In order to know the influence of oscillatory flow velocity and the contribution of onshore current on net transport, the net transport rate is plotted against the flow velocity. The measurements of net rate are presented as a function of flow velocity amplitude for three types of sands with the wave period of 3s and 5 s under with and without onshore current conditions.

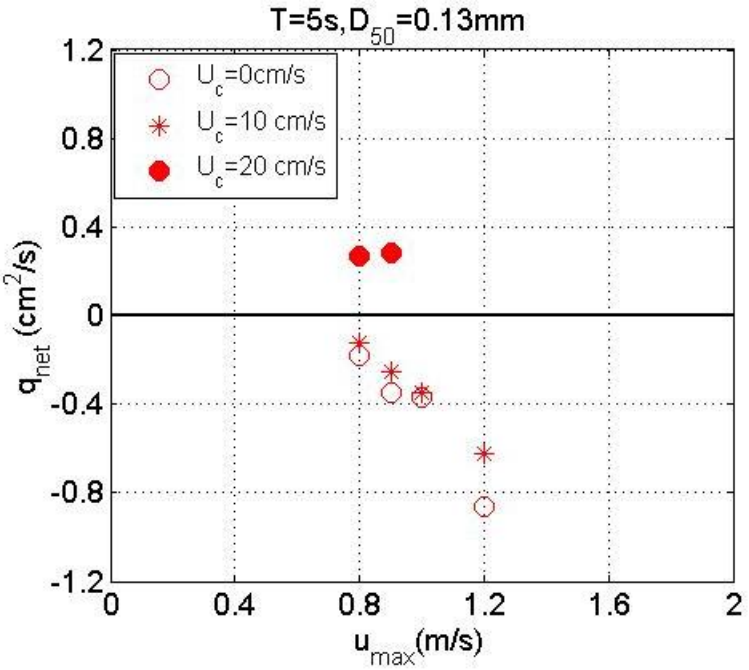

Fig. 4.1. Net transport rate as a function of flow velocity (T= 5s, D_{50}=0.13mm)

Fig. 4.1 shows the net sand transport rates for very fine sand case. The positive value represents the onshore sediment transport rate and negative one is the offshore

net transport rate. The net sand transport goes to offshore direction even under the small velocity, and its magnitude increases with the increasing velocity. Taking into account the net transport rate measured under the combined wave and current cases, onshore steady streaming enhances the onshore sand transport. For instance, magnitude of the offshore net transport reduces for the very fine sand case with the onshore current U_c =10 cm/s. Further increasing the magnitude of onshore current to U_c = 20 cm/s, the offshore net rate significantly decreases and its direction changes to onshore (empty marks to solid marks) in the case of very fine sand.

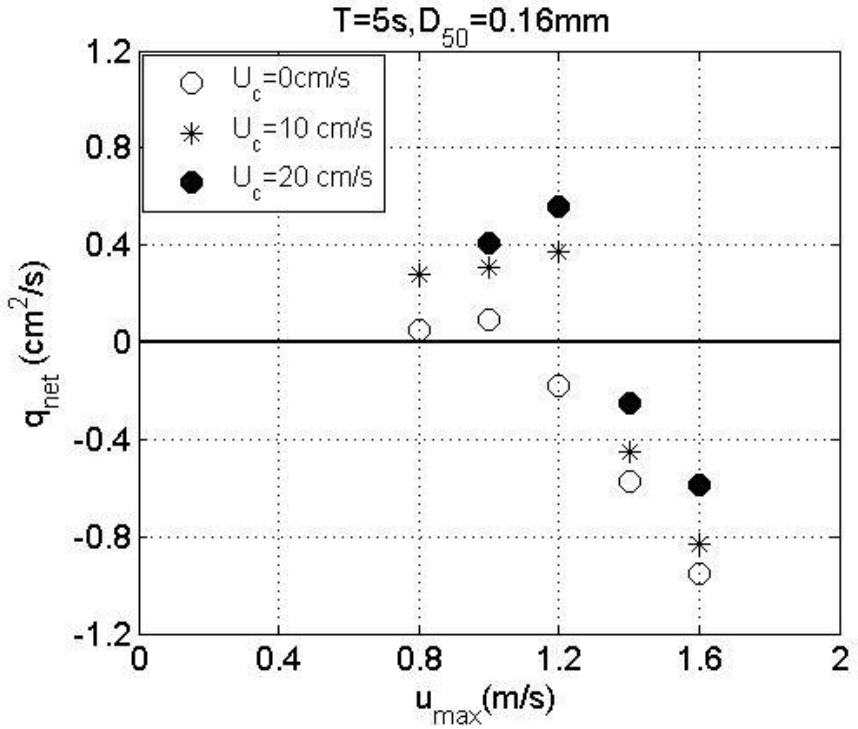

Fig. 4.2. Net transport rate as a function of flow velocity (T= 5s, D_{50}=0.16mm)

The measured net transport rates for fine sand case are illustrated in Fig. 4.2. When the oscillatory flow was of long period of 5 s, the sand was suspended up to an elevation higher than in the short wave period, and was transported mainly by the onshore current flow. Hence, the direction of the net transport agreed with that of the current flow. It indicates that, for fine sand concerning the small velocity condition, the net transport rate presents a rather small value in the onshore direction. The measurements demonstrate a reduction in net transport rate and it changes to the offshore direction with the increasing wave velocity. In the case of combined wave and current, the more onshore net rate is occurred with small velocity case. In addition, when the velocity further increases, even though the offshore net value reduces, the

direction is still offshore. It can be explained that the phase-lag effect of fine sand in the sheetflow transport regime. The phase-lag effect enhances the offshore sand movement which becomes significant under the condition of small sand size, short wave period and large free-stream velocity (Dohmen-Janssen *et al.* 2002).

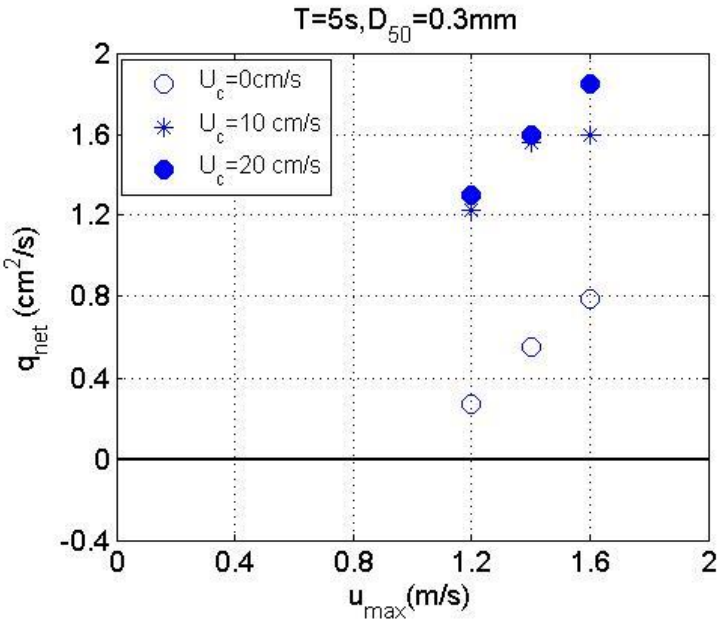

Fig. 4.3. Net transport rate as a function of flow velocity (T= 5s, D_{50}=0.3mm)

In Fig. 4.3, without and with onshore streaming, the results for coarse sand net sand transport with respect to the free-stream velocity illustrate the similar trend with previous studies (Dibajiia and Watanebe, 1996, Dohmen-Janssen, *et al.*, 2001 and Ahmed and Sato, 2003). First, considering the coarse sand without onshore streaming, the net transport is always directed to the onshore and the onshore net transport for coarse sand continuously increases with increasing flow velocity. It is because when the velocity is larger, the entrainment of sand into the flow is also stronger and higher and sand has enough time to settle to the bed as the settling velocity is larger. So, the net sediment is transported to the onshore direction before the occurrence of negative velocity. And also, the bed load is dominant rather than suspension load in coarse sand. As mention in chapter 2, if sand transport behaves quasi-steady, net transports increase for increasing flow velocity. The sand transport of coarse sand behaves quasi-steady behavior

Here also, to understand the effect of onshore streaming, a small current of U_c = 10 and 20 cm/s was generated in the same direction with the wave propagation. The experiment results show a larger onshore net transport rate compared to without

current case. Even though we contribute the larger positive onshore current, the results between U_c = 10 and 20 cm/s shows no significant difference for the flow velocity case of u_{max}=1.2 m/s and 1.4 m/s. It seems the effect of larger current is not dominant in case of coarse sand. For the longer wave period of coarse sand with U_c= 10 cm/s, bedload transport was predominant and most of the sand was carried by both the wave flow and the onshore current and transported into the onshore direction. With the addition of onshore current of U_c=20 cm/s, the increment of net transport rate is almost the same. Although the larger current was contributed, the wave is more dominant and the sand transported during positive velocity as well as the suspended sand during negative velocity distributed to the onshore direction.

The measured net transport rates of short wave period T= 3 s is presented in Figs. 4.4 and 4.5 which includes the results for fine sand and coarse sand. Without onshore streaming, the net rates for fine sand decrease and the direction is offshore with increasing velocity. It might also be caused by the phase-lag effect of short wave period. Considering the effect of onshore streaming, the net rates significantly increase and it leads to onshore direction. It showed that for the cases of onshore steady flow (U_c= 10 and 20 cm/s), the sand suspended during the large onshore flow velocity was transported into the shoreward direction. In which, the phase-lag effect of fine sand is not important while the onshore current is superimposed with the wave. And the magnitude of net transport rate changes from offshore to onshore in case of fine sand.

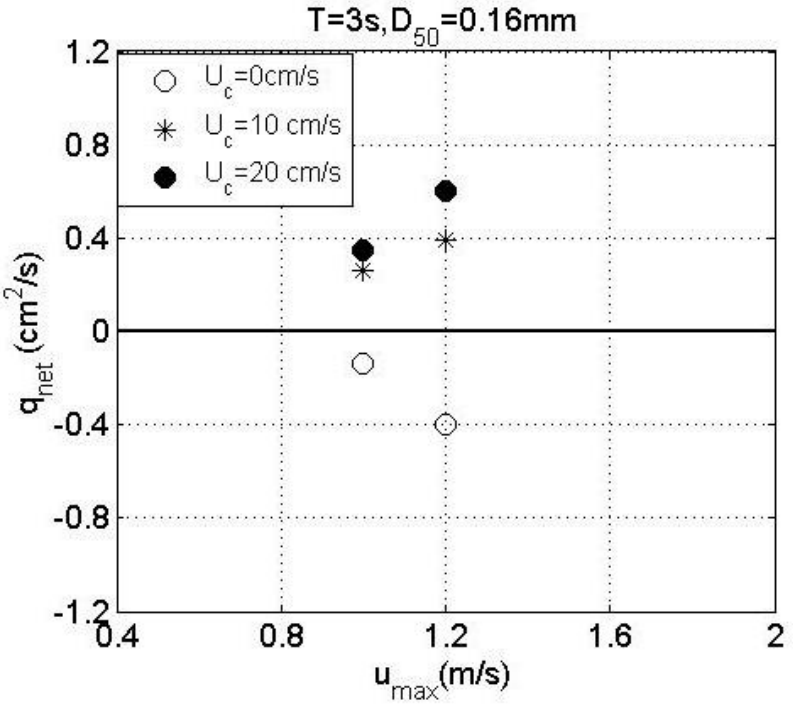

Fig. 4.4. Net transport rate as a function of flow velocity (T= 3s, D_{50}=0.16mm)

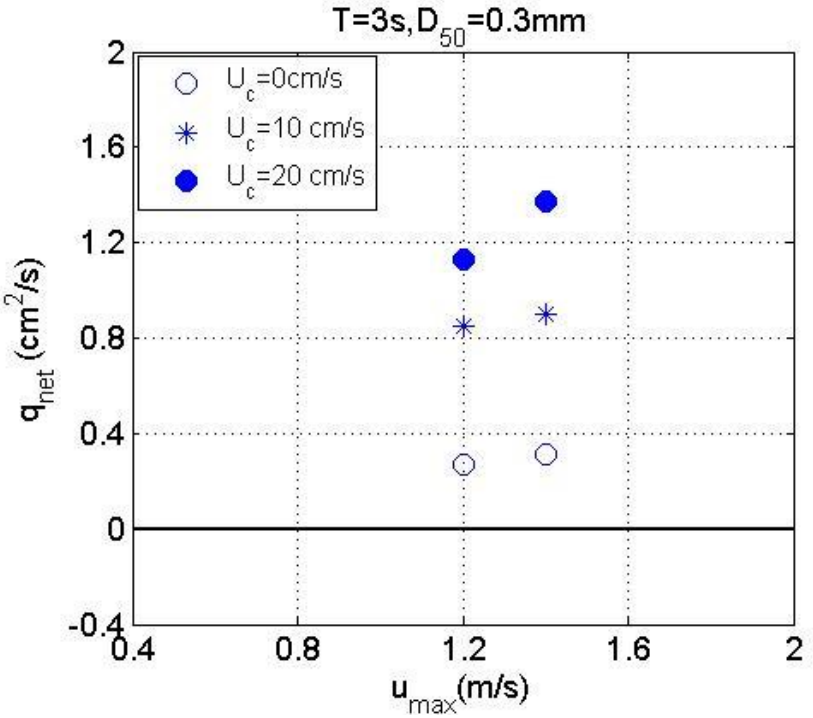

Fig. 4.5. Net transport rate as a function of flow velocity (T= 3s, D_{50}=0.3 mm)

Fig. 4.5 describes that the sand transport rates with coarse sand continuously increase with increasing velocity. The distribution of net transport rate is similar to that of wave period of 5 s. However, the significant increment between U_c =10 cm/s and 20 cm/s is arisen in short wave period. It is noted that the short wave period leads

to decrease of suspension in a case of current prevailing. Thus, for shore wave period with larger onshore current, bedload is more significant and more sediment net rate is transported in the direction of wave compared to longer wave period.

It is concluded that in general, the measured net transport rates with an onshore streaming produce a larger onshore net transport compared to without streaming for all cases. Hereafter, such difference on the net sand transport rate owing to the steady streaming is referred to as the streaming-induced net transport rate. A positive value of such net transport rate corresponds to an enhancement of the net sand transport in the onshore direction.

4.3.2. Streaming-induced Net Transport Rate

Dohmen-Janssen *et al.* (2002) suggested the phase-lag effect in the sheetflow transport regime enhances the offshore sand movement. As aforementioned, the onshore streaming, in general, supports the onshore sand movement. Therefore, investigation on the sediment transprot under the combined wave-current flow conditions can be regarded as an interaction between these two factors, the wave factor and the current factor. Fig. 4.6 illustrates the relationship between the streaming-induced net transport rate and the free-stream velocity for wave period T = 5 s under the conditions of U_c =10 and 20 cm/s. In the case of U_c =10 cm/s, taking into account the effect of sand size, it is confirmed that under the same velocity condition, streaming-induced onshore net transport is the most significant in case of the coarse sand for which the phase-lag effect prone to offshore movement is minimum. Fine sand with a large phase-lag effect demonstrates a small increase on the net transport rate.

On the other hand, for the same sized sand, increase of the onshore net transport rate due to boundary streaming is related to the free-stream velocity in a fairly complex pattern. When the free-stream velocity is small, increasing velocity enhances the onshore net transport under which the boundary streaming plays a more important role on the sand movement since the phase-lag effect is insignificant for such small velocity cases. Whereas, for a larger velocity, *e.g.*, u_{max} >0.9 m/s for very fine sand, >1.2 m/s for fine sand and >1.4 m/s for coarse sand, enhancement on the onshore net transport rate decreases. Under such kinds of velocity conditions, the phase-lag effect leading to an offshore net transport becomes crucial. Onshore transport due to a small streaming current could not overturn such trend from the

phase-lag effect. In another words, the wave factor is more important than the current factor in these cases. As a result, increase on net sand transport owing to the boundary streaming tails off for the large velocity cases. However, further increasing the onshore streaming to 20 cm/s for all cases, the streaming-induced net transport rate returns increasing the net rate and leads to the onshore direction which indicates influence from the streaming becomes predominant.

As a result, steady onshore boundary streaming, in general, supports the onshore sheetflow transport. However, for small sand cases, the enhancement on the offshore transport owing to the significant phase-lag effect may occur under certain velocity conditions. Further investigation is needed to scrutinize this phenomenon.

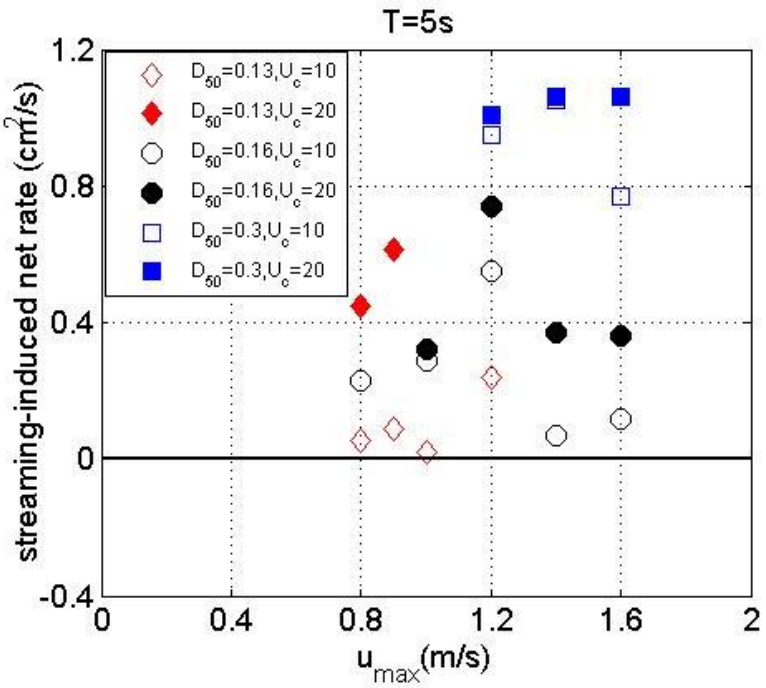

Fig.4.6. Streaming-induced net transport rate as a function of flow velocity (T=5s)

Fig. 4.7 plots the streaming-induced net transport rate against the free-stream velocity for wave period T = 3 s. Again, considering the effect of flow velocity, streaming-induced onshore net transport of fine sand with U_c =10 cm/s increases with increasing flow velocity. But, in case of coarse sand with U_c =10 cm/s, the streaming-induced net rate is almost the same for two different flow velocity. Under the same velocity condition with u_{max} = 1.2 m/s with U_c =10 m/s, the streaming-induced net transport rate of fine sand is larger than coarse sand. The current factor enhances the larger streaming –induced net rate of fine sand compared to coarse sand. At that time,

the phase-lag effect is not significant for fine sand with short wave period. The entrainment of sand is larger due to the high velocity and available settling velocity is enough to settle back even though the variation in velocity is faster before the flow reversal. Thus, it distributes the onshore net transport under combined wave and current conditions.

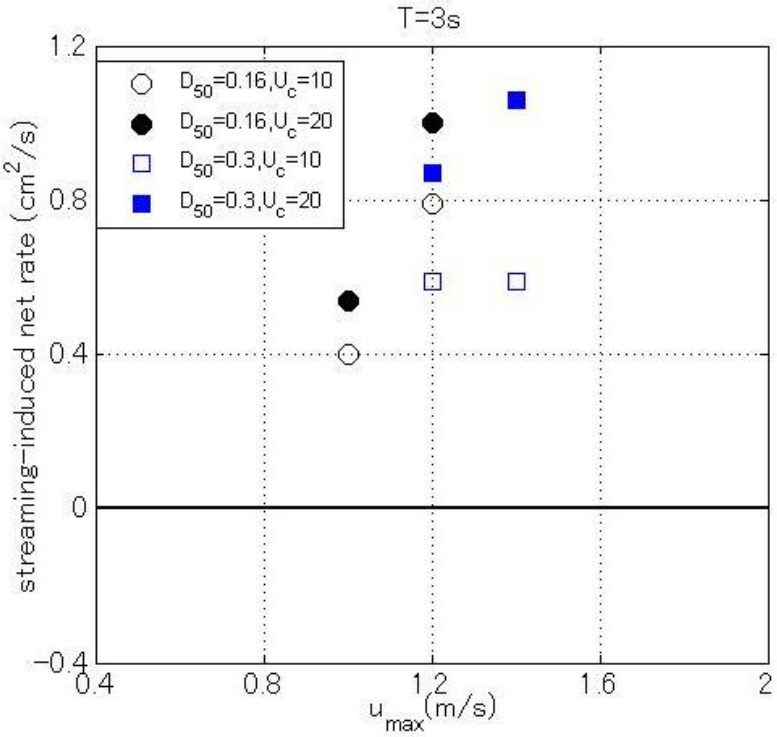

Fig. 4.7. Streaming-induced net transport rate as a function of flow velocity (T=3s)

4.3.3. Influence of grain-size on net transport rates

In Figs. 4.8 and 4.9, the measured net sand transport, $< q_s >$ is shown as a function of the third-order moment of the time-dependent velocity, $< u^3 >$, for three types of sand experiments (D_{50} = 0.13, 0.16 and 0.30 mm) with different onshore streaming U_c = 0,10 cm/s with wave period of T = 5 s.

All the results from the new experiments shows the trend of net sand transport rate is also decreasing with increasing velocity moment, $< u^3 >$, for very fine sand without and with streaming case. Taking into account fine sand, a small increase of net rate occurs with small velocity case and then the net transport rate decreases and becomes negative with an increasing flow velocity, $< u^3 >$ in the case of without and with onshore streaming case. The increasing of net transport rates is occurred with increasing the third-order velocity moment, $< u^3 >$, for coarse sand case. Taking into

considering the influence of grain size, the net transport rates of very fine grains results are smaller than of fine and coarse sand for all experimental runs. Phase-lag effects are more pronounced in the higher velocity regime with fine sand. Although it cannot know whether the phase–lags are present between the instantaneous transport rate and the instantaneous flow velocity, it can be investigated the net transport rates are strongly reduce and the direction leads to offshore for the case of large flow velocity, fine grain sand (Dohmen-Janssen *et al.*, 2002). It can be concluded that grain-size plays a very important role in sediment transport processes.

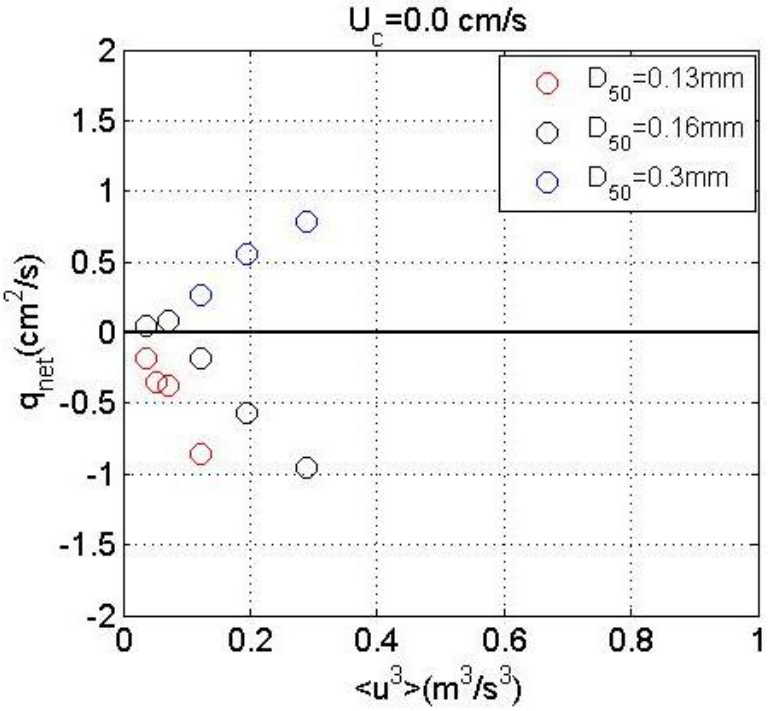

Fig.4.8. Relation between net transport rates and third-power velocity moment ,$<u^3>$ with wave period T = 5s (U_c=0 cm/s)

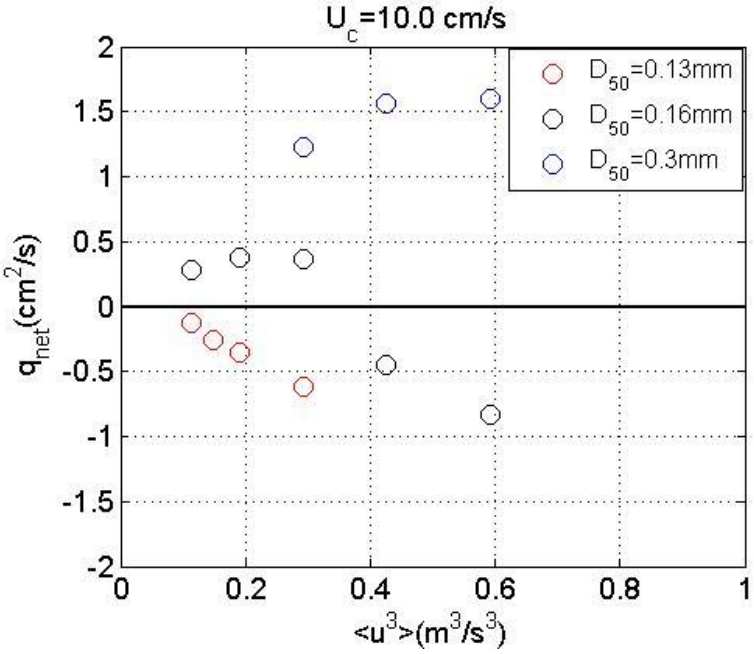

Fig.4.9. Relation between net transport rates and third-power velocity moment,$<u^3>$ with wave period T = 5s (U_c=10 cm/s)

4.3.4. Comparison of measured net transport rate with surface wave

Figs. 4.10, 4.11 and 4.12 give about the results of measured net sand transport rates from the new experiments compared to the results of previous flume measurements under the same condition of third- power velocity moment, $< u^3 >$, for three different types of sand (D_{50} = 0.13 mm,0.16 mm and 0. 3 mm).

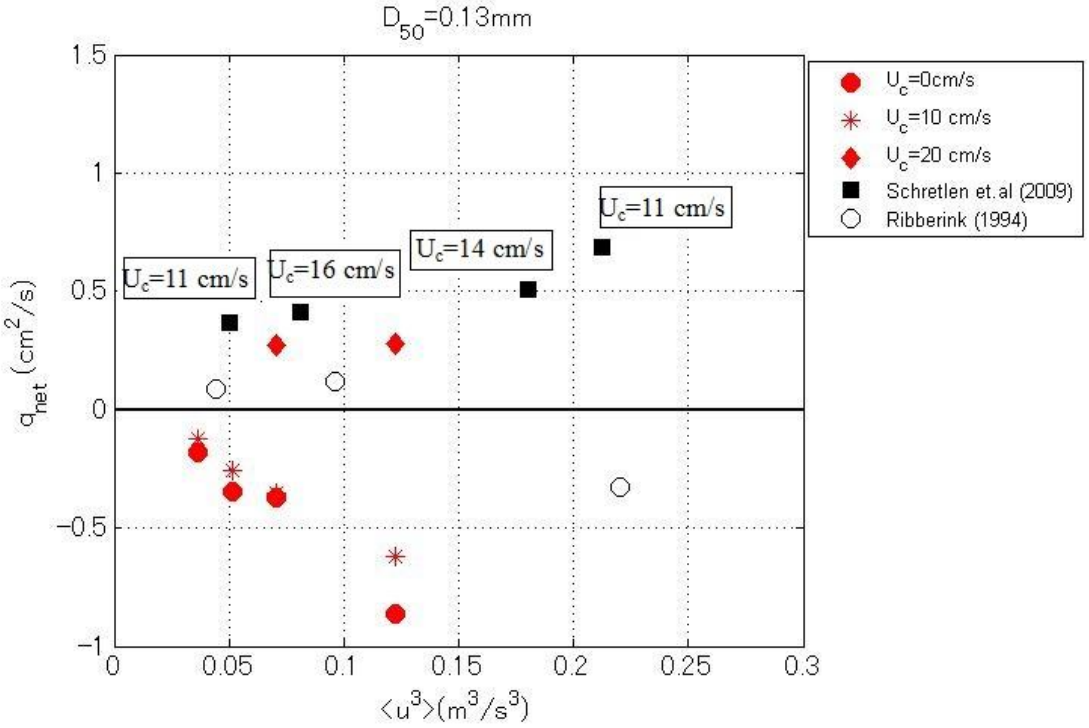

Fig. 4.10.Comparison between measured sand transport rates from oscillatory flow tunnel experiments and flume experiments (D_{50} = 0.13mm)

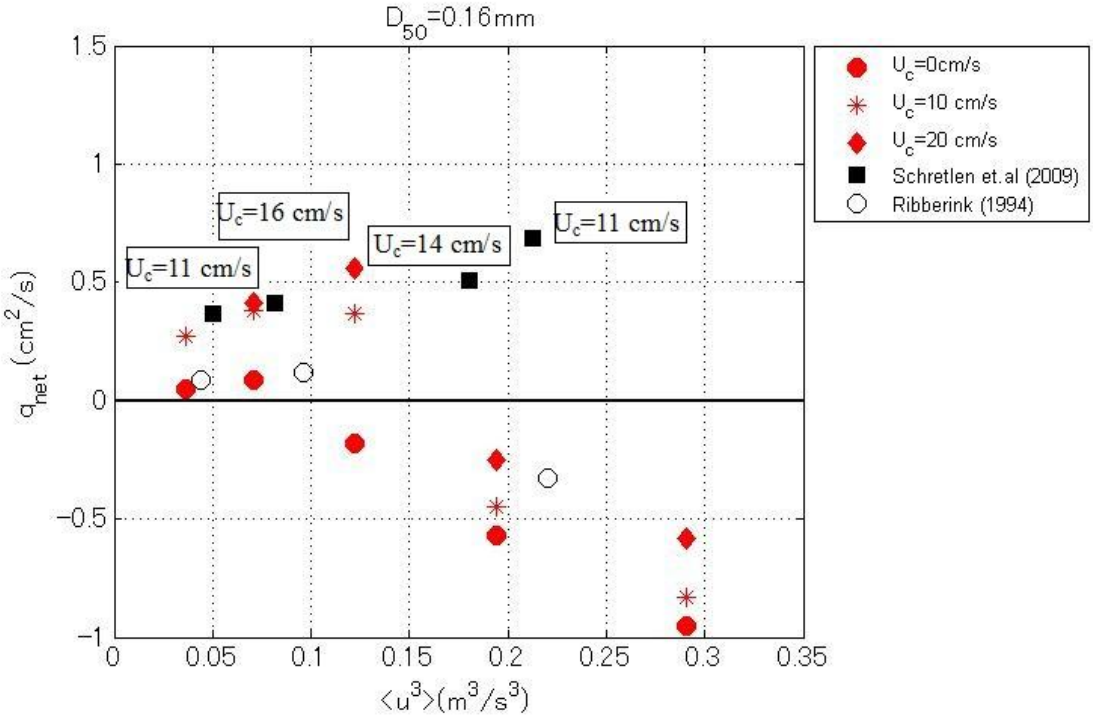

Fig. 4.11.Comparison between measured sand transport rates from oscillatory flow tunnel experiments and flume experiments (D_{50} = 0.16mm)

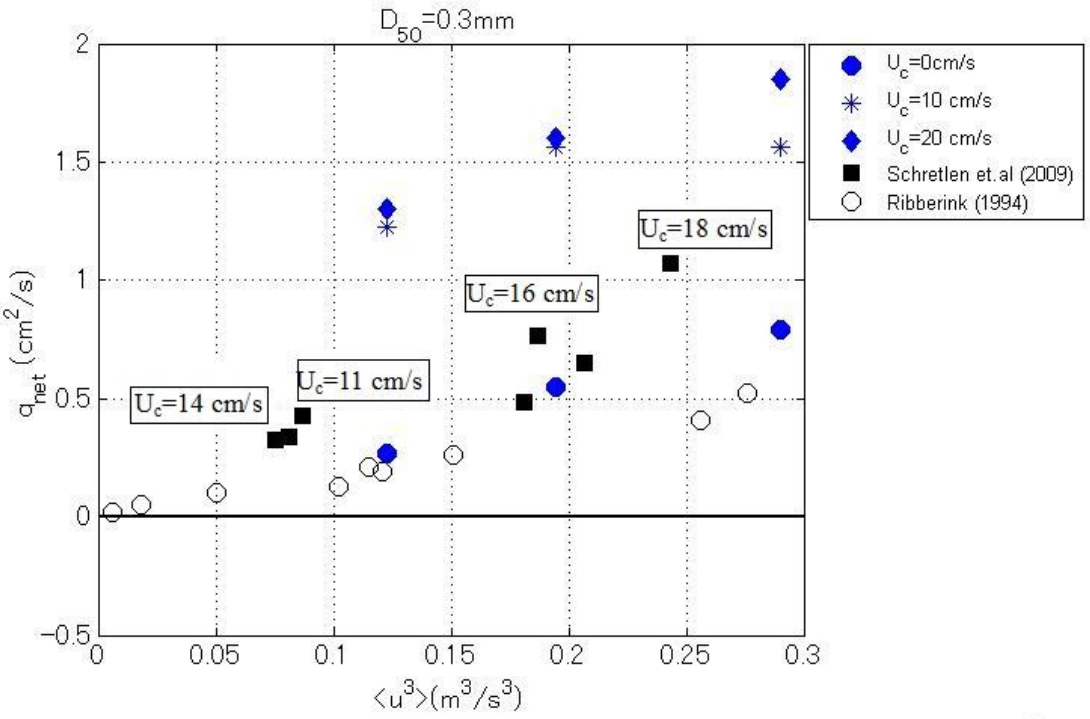

Fig. 4.12.Comparison between measured sand transport rates from oscillatory flow tunnel experiments and flume experiments (D_{50} = 0.3mm)

The comparison can be made between surface flow and oscillatory flow for three types of sand. The surface wave data was presented with corresponding onshore streaming. Fig. 4.10 shows that the net transport rates of very fine sand are smaller than surface waves in case of no streaming; it is consistent with the previous studies. Considering the calculation of small onshore streaming of *Uc*=20 cm/s, the net sand rates are comparable between oscillatory flow tunnel and large wave flume data. Previously experimental results, the net transport rates under surface waves are about a factor of 2.5 larger than in uniform horizontal oscillatory flows (Dohmen-Janssen and Hans, 2002, Ribberink, *et al*., 2000). Now, probably, the new experiments predict the difference is not too much between oscillatory flow and large wave flume with small velocity case, $<u^3>$. In the case of fine sand onshore streaming, 20 cm/s, the net transport rate is almost the same with the surface wave. The fine sand experiments under surface waves do not change the direction and show a continuous increase of positive transport with increasing velocity, $<u^3>$. However, the present results of very fine and fine sediment transport rates become offshore when the velocity, $<u^3>$, increases in the oscillatory flow experiment. It means that the onshore streaming of 10 and 20 cm/s only enhanced the onshore net transport rate for the very fine and fine

and with the small velocity case. On the other hand, in case of large velocity case, the contribution of onshore streaming should be larger than 20 cm/s.

The comparison results for coarse sand are also presented in Fig. 4.12. From oscillatory flow tunnel experiments with U_c = 0 cm/s, the net transport rates for surface wave are larger than the oscillatory flow data which is similar characteristics with the former results. At present, the larger onshore net rate is expected by the contribution of U_c = 10 and 20 cm/s in the case of oscillatory flow. The net transport rates of coarse sand in OFT are significantly larger than those in surface waves for both case of U_c = 10 and 20 cm/s. Thus, considering the coarse sand, the onshore streaming could be smaller than the value of 10 cm/s. Hence, the contribution amount of onshore streaming is a function of sand size and free-stream velocity. In this study, the value of onshore streaming was only considered as a constant value of 10 and 20 cm/s. It means the contribution of streaming is quite large enough to enhance the more onshore net transport rate for the coarse sand. As a result, the streaming effect is very dependent on sand size.

Moreover, it shows that the difference in boundary streaming between surface waves and oscillatory flows may partly dominate the transport process. The additional onshore current in the tunnel does contribute to more onshore sediment transport. At the same time, it is also confirmed that the phase-lag effect plays an important role in the sediment transport under the sheetflow conditions, especially for the fine sand case. Generally speaking, by distribution the small onshore current, the net sediment rates of horizontal oscillatory flows can predict 75 % of those for surface waves with the fine sand. Therefore, not only the streaming effect but also the other differences seem still to be present between surface wave and oscillatory flow conditions. Still now we cannot give the full explanation of the differences of transport rates in oscillatory flow and surface wave. Further investigation is needed to understand more details.

4.4. Sediment Particle Velocities

4.4.1. Intercomparison among different window sizes

Sediment particle velocity within the sand-laden sheetflow layer was measured by means of a PIV technique developed by Ahmed and Sato (2001) is used in the present study to calculate the sand particle velocity. In PIV technique, choosing of the window size is somewhat important. Choosing the inappropriate interrogating

window size, it will make inaccuracy its position at the next time step to move within the search window. Therefore, the inter-comparison between different window sizes is investigated and the results are presented in Fig. 4.13. The top of the figure is the variation of the free-stream velocity and the lowers are the sediment velocity variation at the level of z =0 mm and z = 5 mm using different window sizes.

Clearly, velocity fluctuation can be noticed around the maximum velocity and smoothly variations are occurred around flow reversals for all window sizes. The results for small interrogating (15 by 15 pixels) and searching windows (29 by 29 pixels) size show spike noises frequently occur along the velocity variation. Small window size makes mistake easily to match between two successive images during calculation. Therefore, by increasing the window size of interrogating window (21 by 21 pixels) and searching windows (41 by 41 pixels) size, the frequently noise will disappear other than small window size but still has some spike noise. After using large interrogating window (31by 31 pixels) and searching windows (53 by 53pixels) size, those frequent spike values almost disappear. But at the same time, using the larger window size the calculated velocity magnitude is smaller than that of the other two window sizes. After analyzing the window size, in the present study, the enhanced PIV method was applied to calculate the particle velocity using with medium interrogating (21by 21 pixels) and searching window (41by 41 pixels) size.

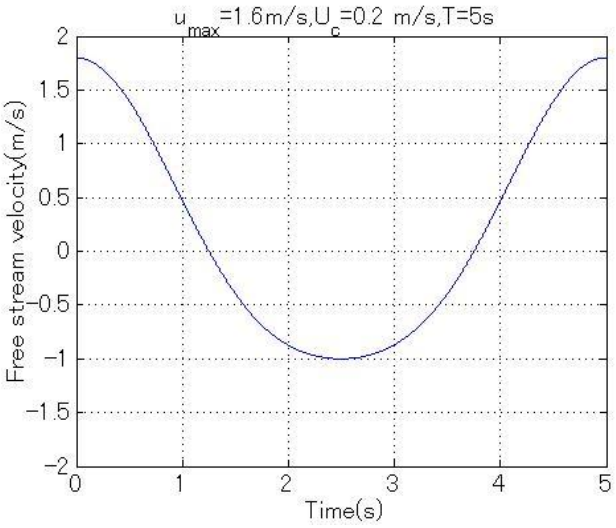

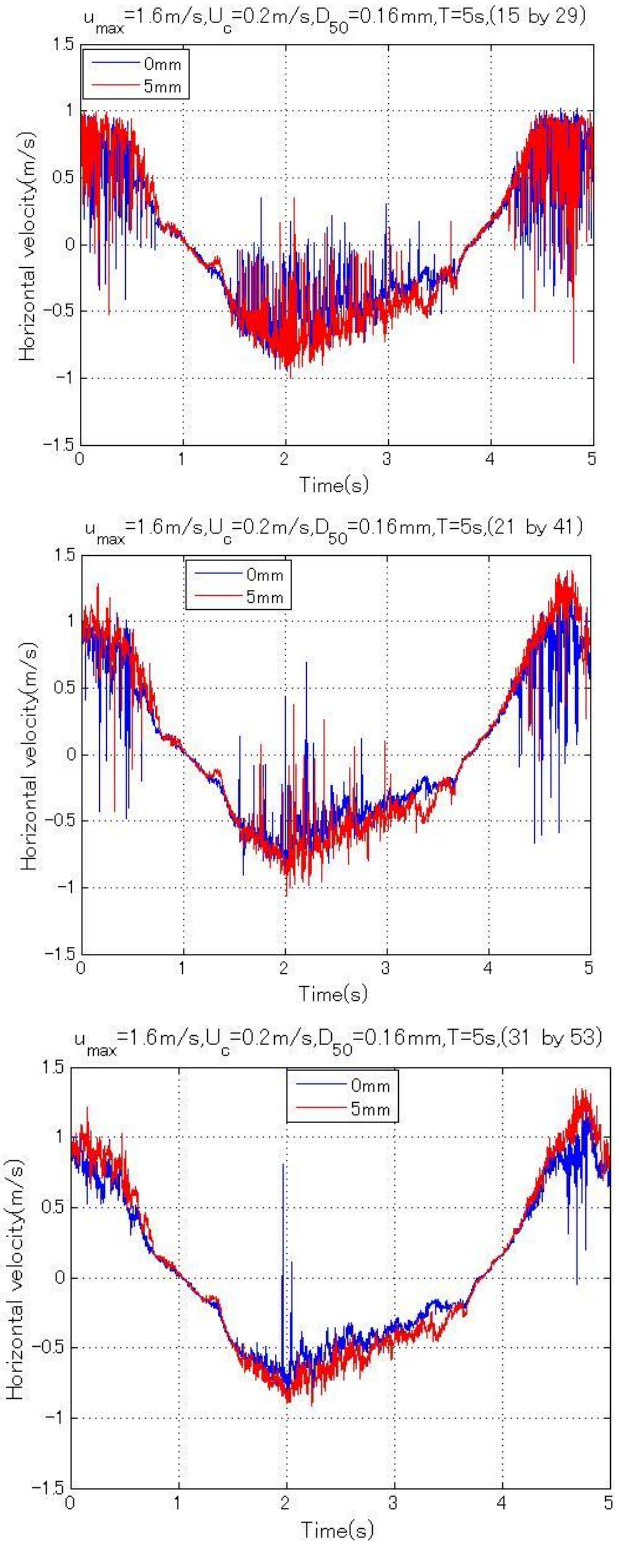

Fig.4.13. Comparison between different interrogating and searching window sizes

4.4.2. Horizontal velocity of Sediment particles

As mentioned before, because the sheet-flow layer is present in the few mm's to cm's above the sand bed, we expected that the small wave induced net currents inside the wave boundary layer are to be of large importance for the total sheet flow sediment transport. Therefore, one of the main objectives of the new experiments was to obtain detailed velocity measurements throughout the boundary layer into the sheet-flow layer. Present experimental results of measured net transport showed that onshore sheetflow sand transport was enhanced by small onshore currents superimposed to skew velocities. Here, we introduced a small onshore current and performed experiment under combined wave and current conditions in OFT. Therefore, it is worth to investigate the current profiles for these conditions to understand whether this can give an explanation about the reason of the increment of onshore net transport rate due to the addition of small onshore current. Figs. 4.14 and 4.15 show the results of near-bed velocity measurements of the 2nd-order stroke's wave with T = 5 s and different velocities. The positive values stand for onshore velocities, the negative values offshore velocities.

The temporal variation of the velocities at five different levels from 2 mm below the initial bed level up to 10 mm above the initial bed level was estimated. Generally, the shapes of particle velocity are similar to that of the free stream flows. The results for a fine sand case are presented in Fig. 4.13 and for coarse sand in Fig. 4.14. When increasing elevation, velocity amplitudes increase gradually. The sediment particle velocity may reach about 72 % of free stream velocity when the level is further away (z = 25mm) from the bed. At the initial bed level (z = 0 mm), the velocity decreases rapidly due to the high sediment concentration.

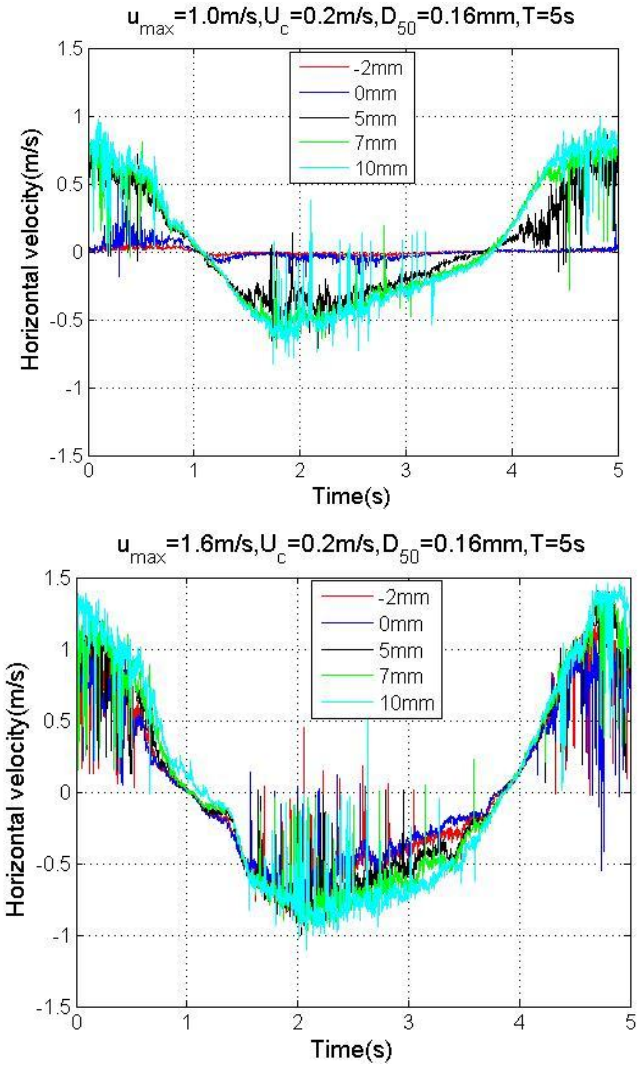

Fig. 4.14. Horizontal particles velocity for fine sand

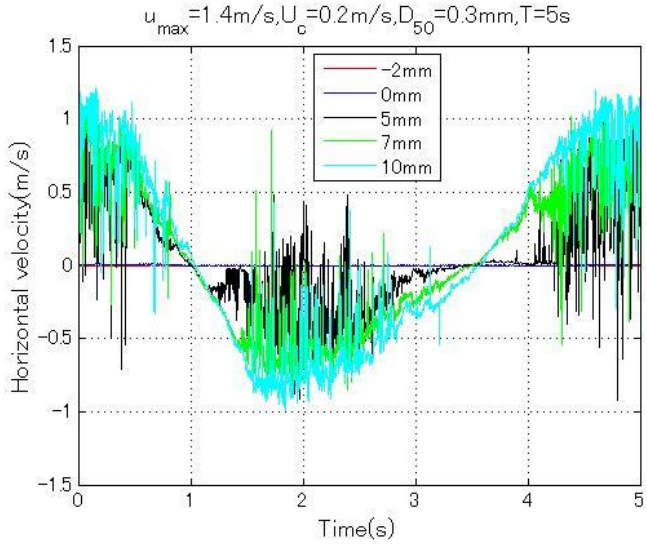

Fig. 4.15. Horizontal particles velocity for coarse sand

From the time-dependent velocity variations, the vertical distributions of horizontal velocity at different phases can also be estimated. Figs.4.16 and 4.17 illustrate the vertical profiles for sediment velocity at different phases with 30° interval with fine sand and coarse sand of T= 5s. With the decrease in velocity magnitude from the free stream downwards to the bed, the velocities phase-lead can also be observed. The upper panel is for onshore phases and bottom is offshore phases.

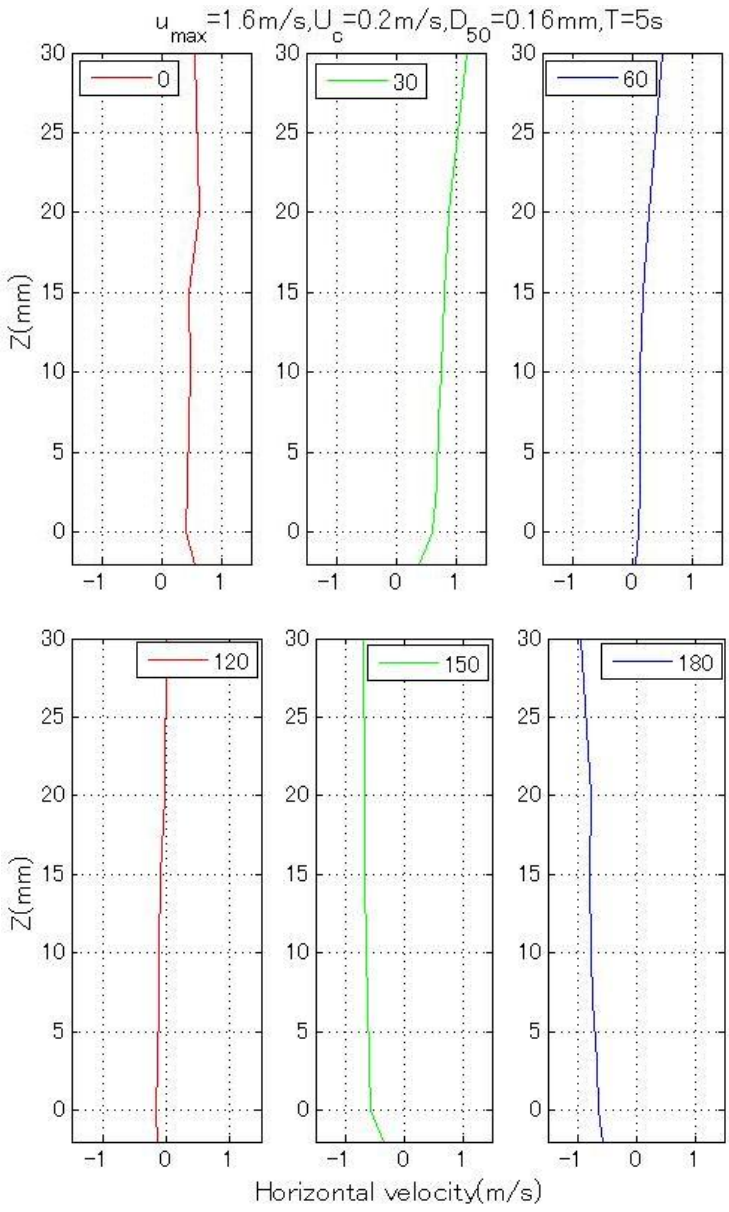

Fig.4.16. Velocity profiles at six phases during one wave period for D_{50}=0.16mm

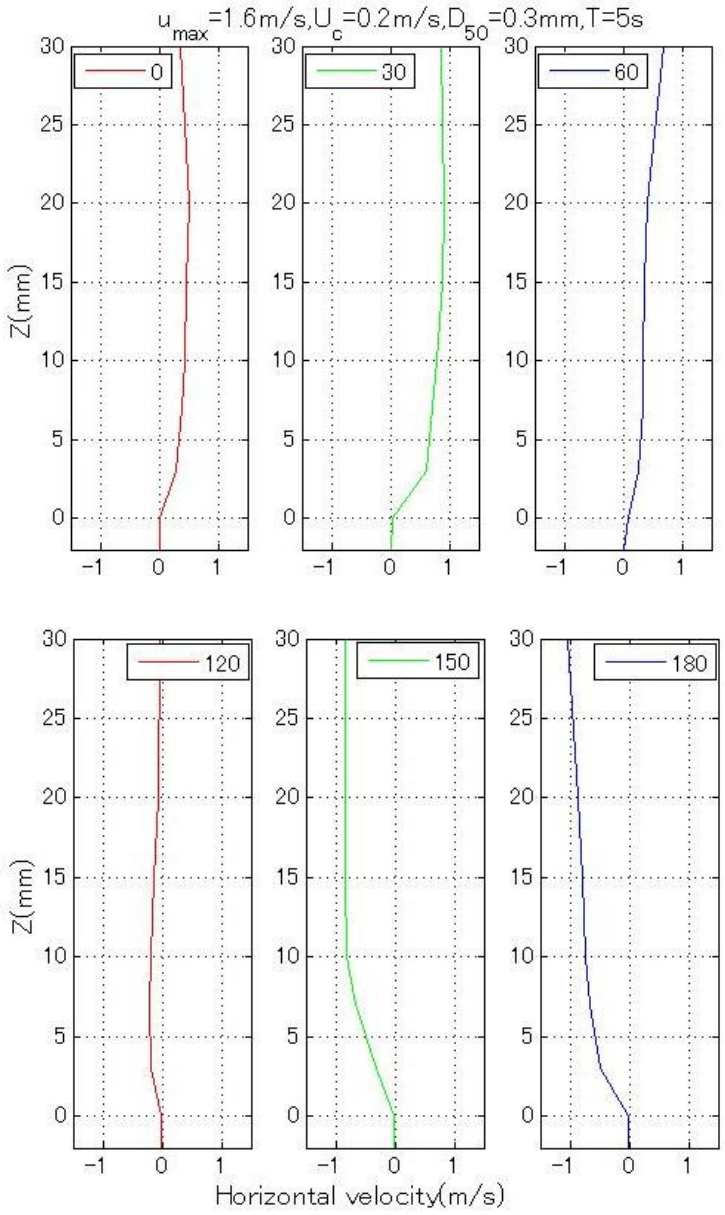

Fig.4.17. Velocity profiles at six phases during one wave period for D_{50}=0.3mm

4.4.3. Turbulence Quantites

In this study, also the trubulence intensities u'^2 were measured and it can be calculated as,

$$\overline{u'^2} = \overline{(u-\bar{u})^2} \tag{4.1}$$

where u is the instantaneous horizontal velocity, $\bar{u}$ is the mean velocity using the FFT algorithm. Fig. 4.18 illustrates time-varying turbulence distribution at four levels with a cut-off frequency being 7 Hz. It is found that the turbulence intensity is large around the maximum velocity and it is small around the flow reversals for all

levels. Liu (2005) mentioned that the erosion process occurs when the turbulence intensity is large and at flow reversals the deposition process dominates.

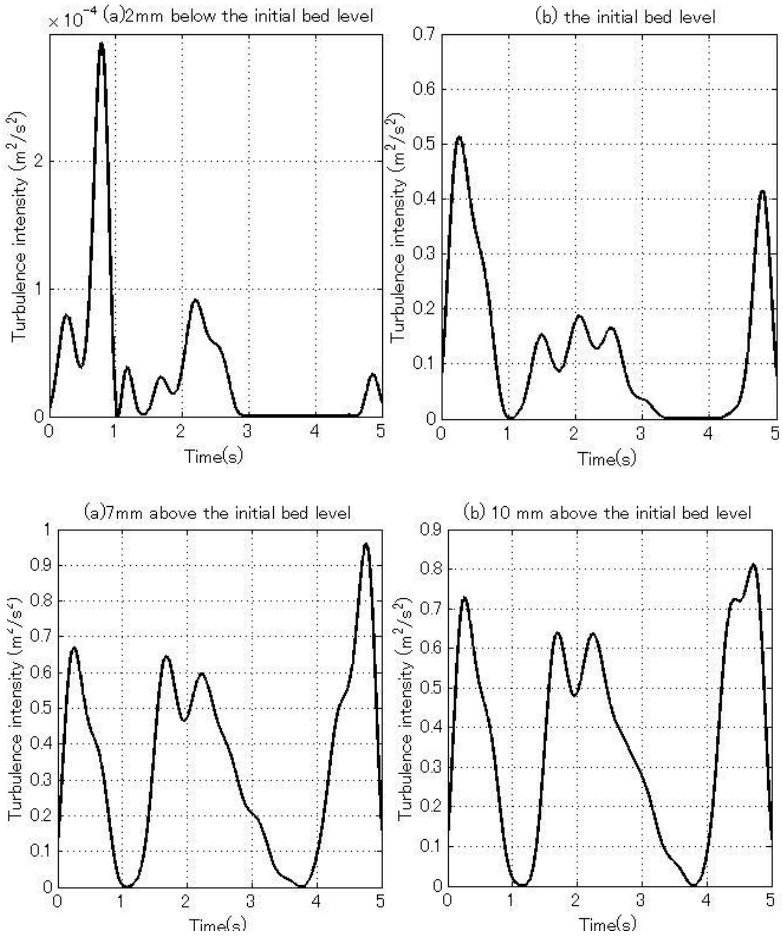

Fig. 4.18. Horizontal turbulence intensity distribution at different levels

u_{max} =1.6 m/s, T =5 s, D_{50} =0.3 mm

4.5. Time –averaged velocity profiles

4.5.1. Mean flow velocity for Wave

To remove the noise influence in PIV analysis, a Fast Fourier Transform (FFT) algorithm was used to obtain the predominant velocity component then average over one wave period to achieve the vertical profile of the mean flow velocity, *U (z)*. Fig. 4.19 presents the instantaneous horizontal velocity distribution at five different levels obtained by using the Fast Fourier Transform (FFT) algorithm for two types of sand.

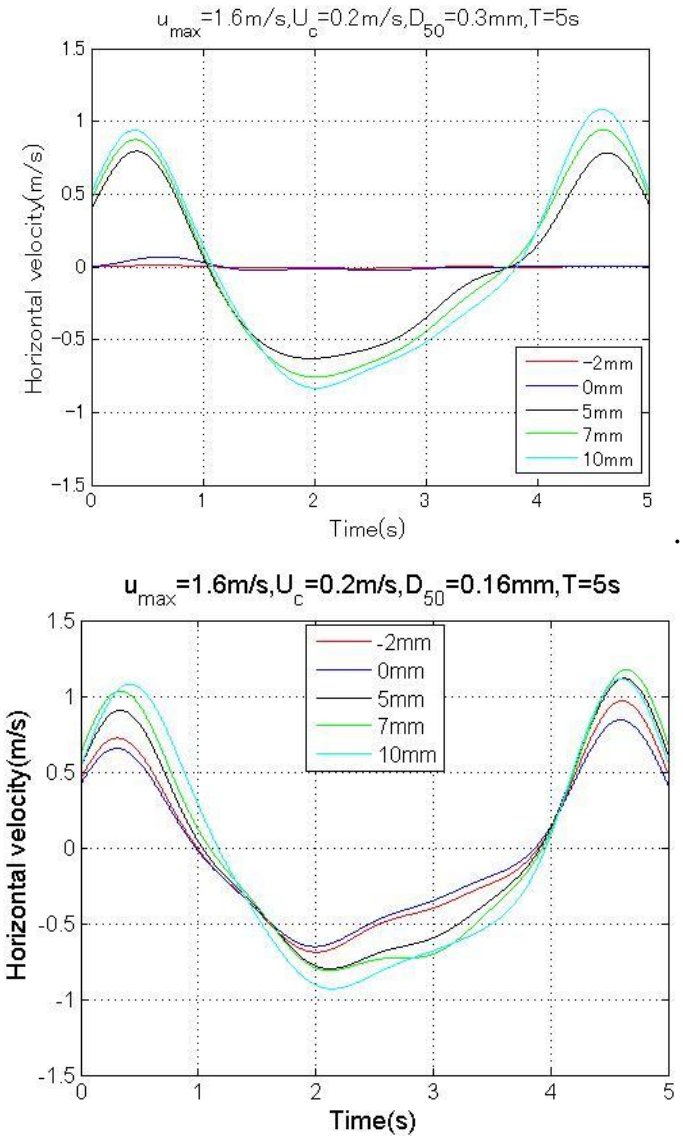

Fig. 4.19. Mean sediment horizontal velocity at different levels

Fig. 4.20 shows the net velocity profile of coarse sand with two different flow velocity conditions of U_c = 0 cm/s. The upper one is with free –stream velocity of 1.0 m/s and 1.4 m/s of wave period 5 s and the lower is wave period of 3 s with u_{max}=1.2 m/s. The near bed mean flow velocity showed similar trend for wave period 5 s. But, the magnitude of mean flow velocity is higher in the case of short wave period compared to long wave period 5 s. From the mean velocity profile, it is found that a very small onshore current exists in the pick-up layer (z < 0 mm). Sand is only mobilized around the time of maximum onshore velocity and the time-averaged velocity is positive (onshore) in this region. An offshore current is detected in the upper sheet-flow layer. The existence of the onshore mean velocity in coarse sand is the reason of wave asymmetry; the lowest levels in the pick-up layer only come into

motion during the peak velocities of the onshore motion but are not mobilized during offshore flow and are therefore not affected by the negative boundary layer streaming (Ribberink et al., 2008).

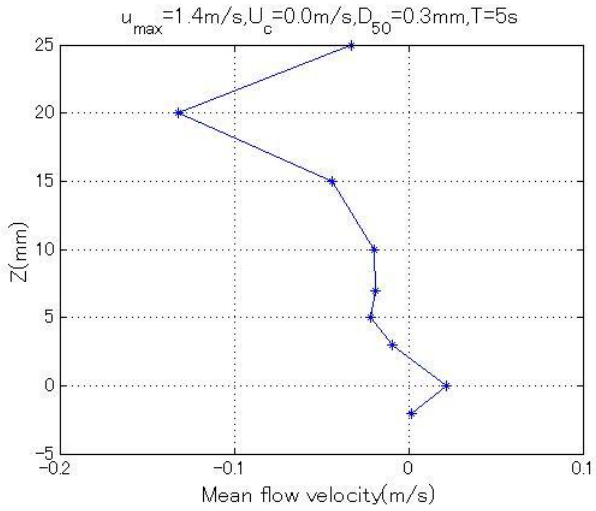

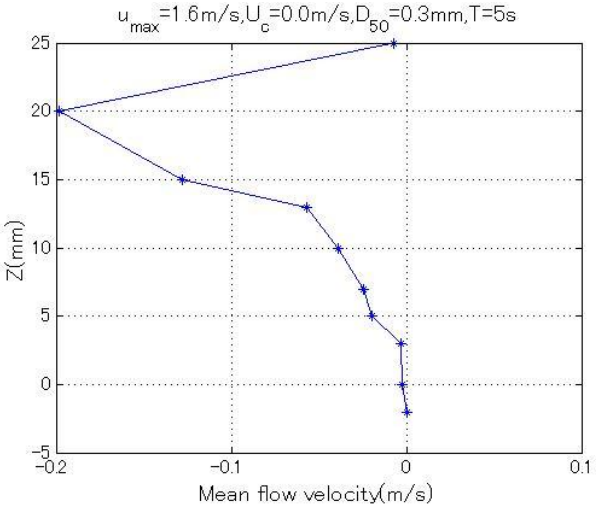

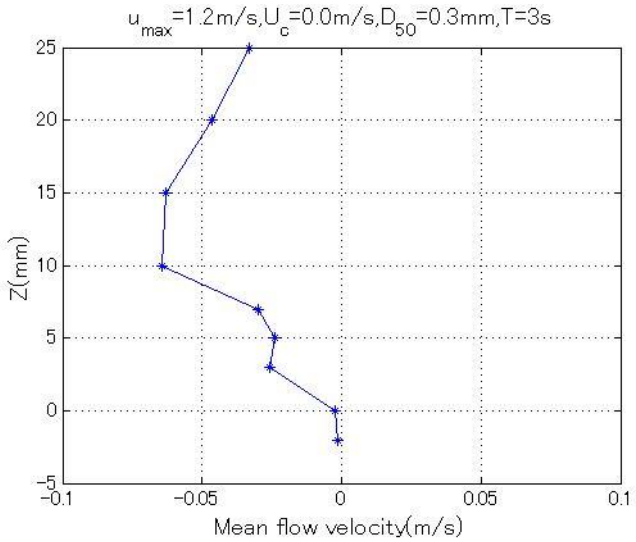

Fig. 4.20. Mean flow velocity profile of coarse sand inside the wave boundary layer (U_c= 0 cm/s)

The mean flow velocity for fine sand with two different wave period of flow velocity (u_{max}=1.0, 1.2 and 1.4 m/s) is described in Fig. 4.21. In fig. 4.21, a negative streaming is induced due to the strong phase-lag effect of fine sand. The positive near-bed streaming is not observed for all cases. The attribution of the time-averaged profile of fine sand is comparable with the trend of coarse sand in the sheet flow layer. The magnitude of negative streaming for coarse sand is smaller than fine sand. In addition, when the depth increases, in the region of suspension layer, the mean flow profile still continues to offshore direction as sand entrained at times of high velocity could not settle back to the bed and transported to the offshore direction. The large phase-lag can induce a negative (offshore) net transport. Thus, the phase-lag effect seems to play an important role for the sediment sheetflow transport in OFT test. All these results are consistently with previous researches (Ribberink et al. 2008).

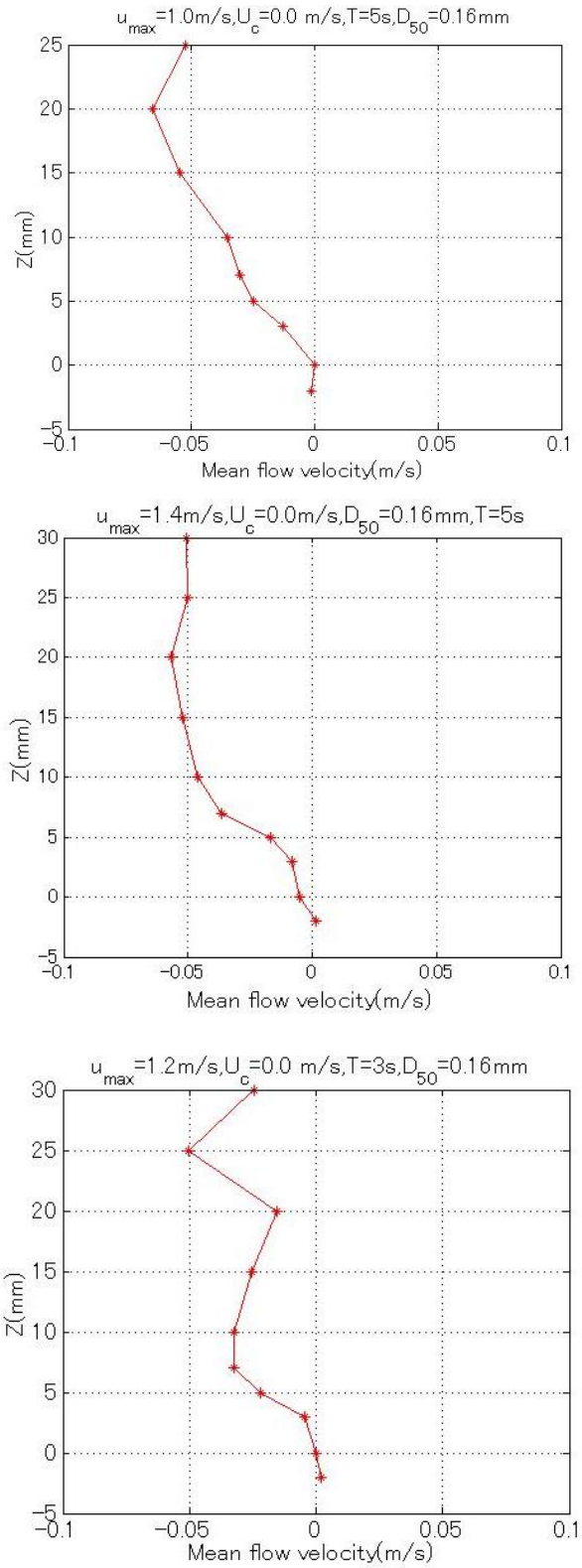

Fig. 4.21. Mean flow velocity profile of fine sand inside the wave boundary layer (U_c=0 cm/s)

4.5.2. Mean flow velocity for combine wave and current

Apart from the mean flow velocities measured under wave, the mean flow velocity profiles are of importance under combined wave and current condition. Fig. 4.22 presents the results for vertical distribution of mean flow velocity of fine sand with a different flow velocities and wave period.

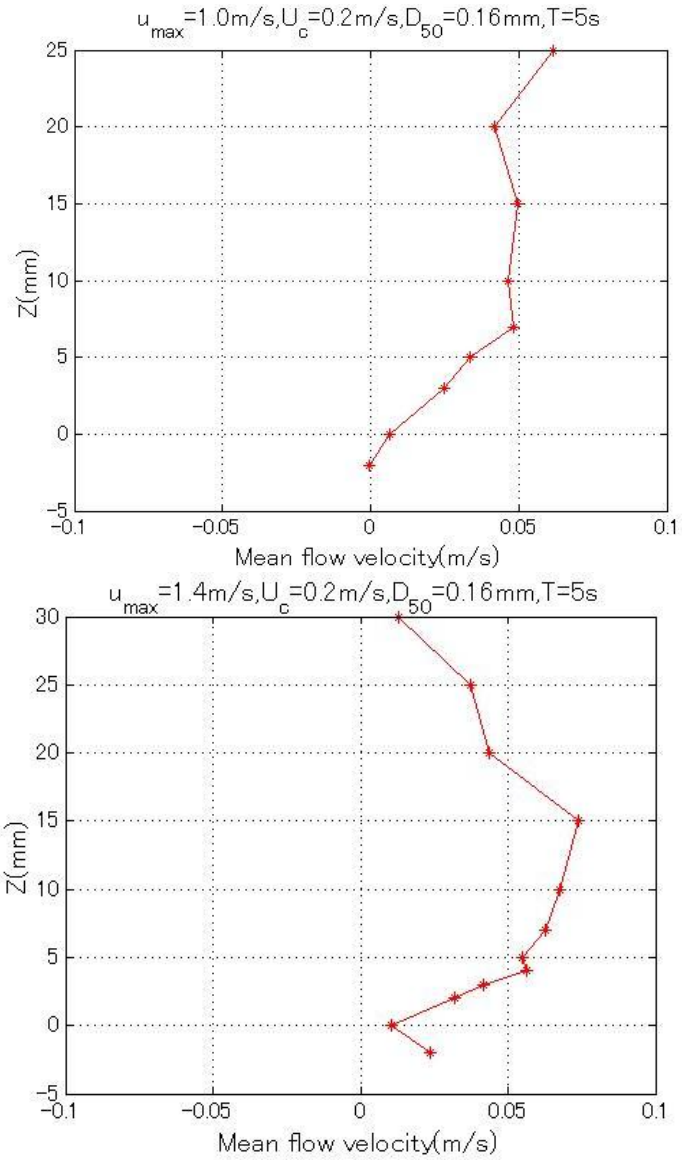

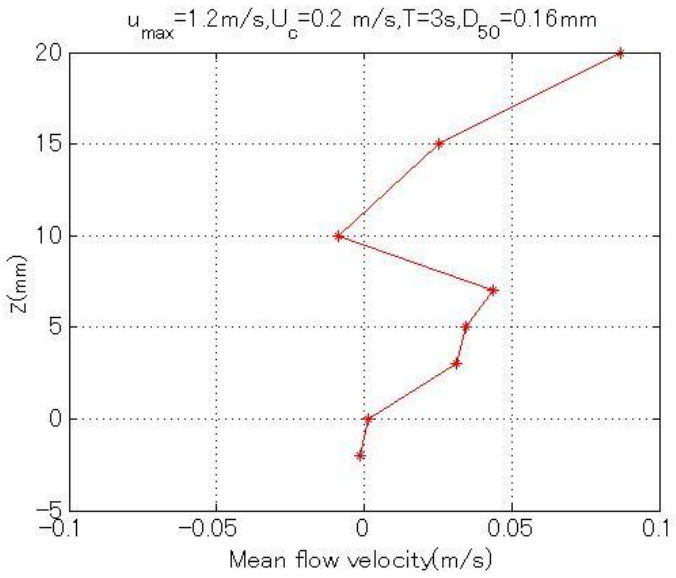

Fig. 4.22. Mean flow velocity profile of fine sand inside the wave boundary layer (U_c = 20 cm/s)

Considering the fine sand with onshore streaming, the mean flow profiles illustrate positive direction in the boundary layer due to the higher concentrations of sand in the suspension layer. The magnitude of velocity is highest in the sheet flow layer for both sands. Fig 4.23 illustrates the mean flow profiles for coarse sand in the case of onshore streaming, U_c = 20 cm/s, with two wave period and different flow velocity.

Taking into account the effect of onshore streaming, in the pick –up layer and sheet flow layer, the positive wave –induced streaming is occurred in case of coarse sand. In the sheet flow layer, more sand is carried relatively high in the flow by the higher onshore velocities than by the lower offshore velocities. However, when the elevation is higher than 15 mm, the mean flow changes its direction from onshore to offshore.

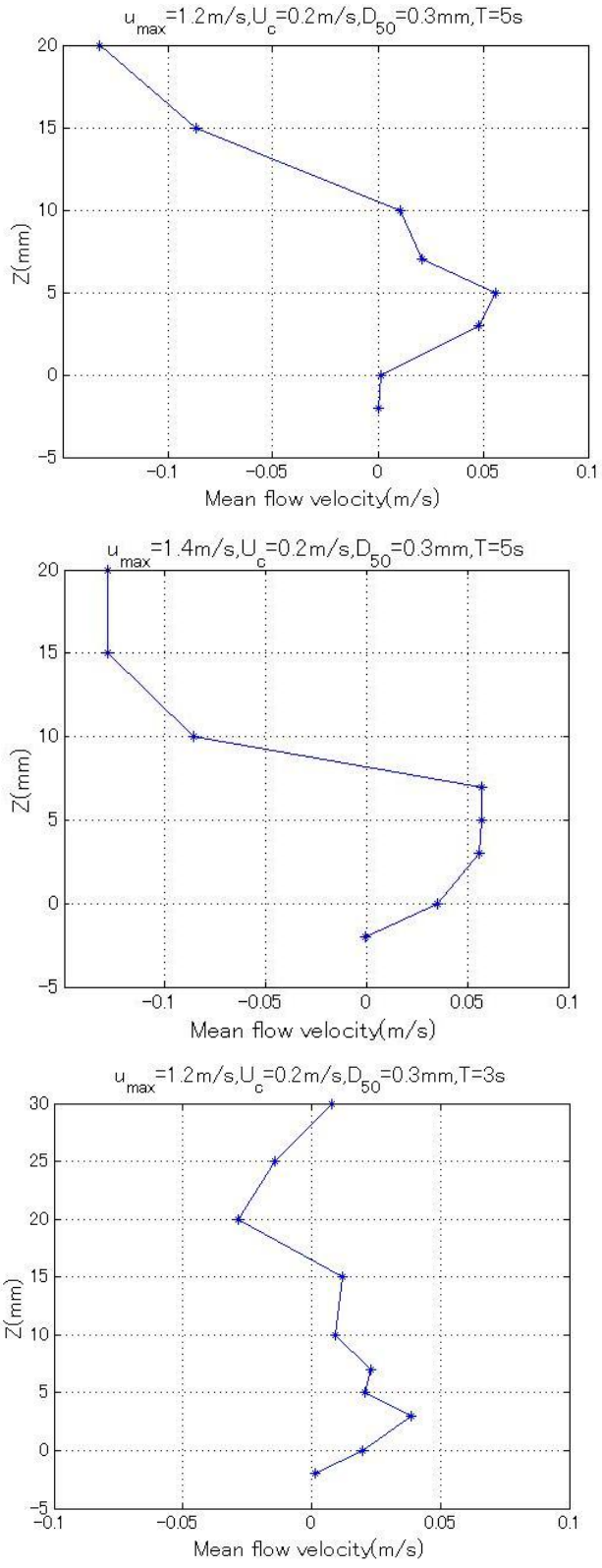

Fig. 4.23. Mean flow velocity profile of coarse sand inside the wave boundary layer (U_c=20 cm/s)

4.5.3. Comparisons of Mean Flow Velocity

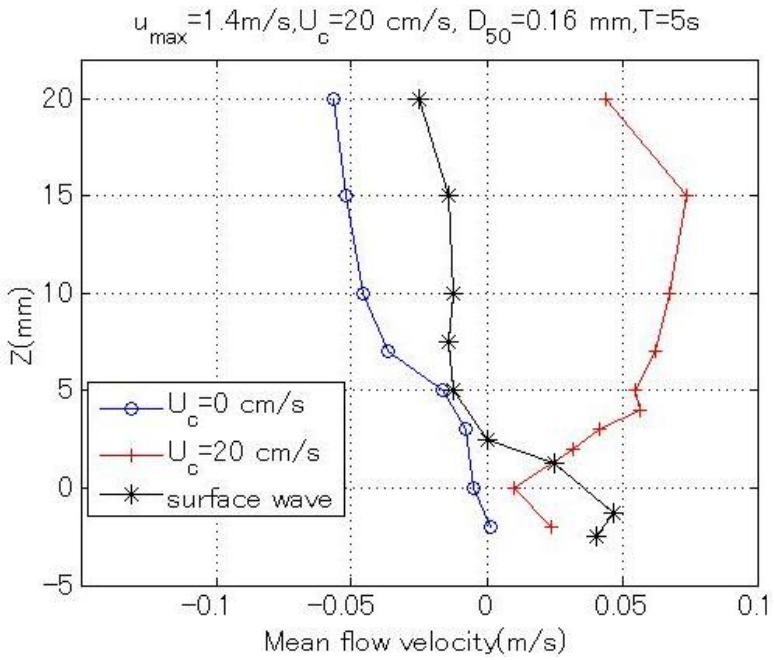

Fig. 4. 24. Comparison of Mean flow velocity profile of fine sand

Fig. 4.24 describes the comparison results of fine sand between the new experiments and surface wave results. It indicates that in surface wave, whatever sand size like medium and fine sand, the trend of mean flow is similar characteristics. They show a consistent behaviour for all wave conditions for both fine and medium sand. However, in oscillatory flow, without onshore streaming (U_c= 0), the positive near-bed streaming is not occurred and for U_c=20 cm/s the mean flow profile can be seen as a positive value in the pick-up and sheet flow layer also. Hence, the contribution of onshore current can be produced the positive streaming in the pick-up layer for the fine sand. Meanwhile, the results for coarse sand were presented in fig. 4.25. The results show that the positive streaming was observed for both without and with onshore current. It is because of wave asymmetry in the pick-up layer, the sand is only mobilized by the onshore velocities and they drive the water particles to onshore direction. And also, in case of without streaming, the mean flow directs to offshore direction which is consistent with the surface wave in the upper layer. However, considering the effect of onshore current, the mean velocity indicates the change of direction from onshore to offshore in the suspension layer. In the fix-bed layer, we may expect that the current profile should be the logarithmic velocity distribution. However, when it considers for mobile bed, the sediment will be mobilized and the

current velocity decreases. If the sediment is coarse enough, the mean flow profile will be negative in upper layer. As a result, the behavior of mean flow profiles for medium and fine sand is different in oscillatory flow tunnel. Correspondingly, the profile is too dependent on sediment size.

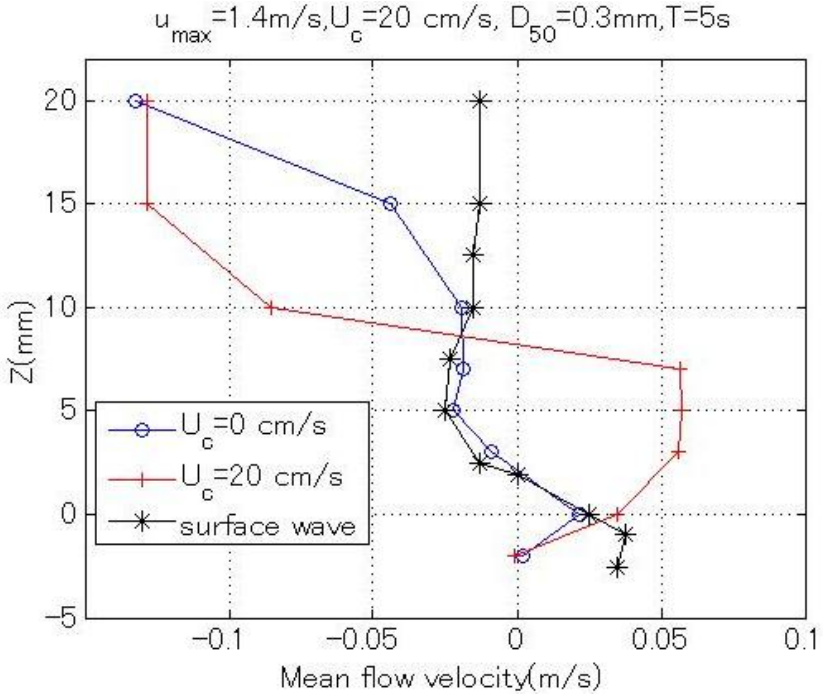

Fig. 4.25. Comparison of Mean flow velocity profile of fine sand

As mentioned before, it can be explained that the difference of net transport rate in OFT and surface wave (LWF) is the cause of onshore directed boundary streaming which only observed in surface wave. On the other hand, taking into considering the measured mean flow profiles under combined wave and current, the profiles in oscillatory flow deviates from the net velocity profiles of surface wave experiments. All the results of the mean profile give a positive value and lead to onshore direction in the sheet flow. The onshore mean flow profiles can distribute the increment of net transport rate in oscillatory flow for most of the cases. Despite an onshore streaming was observed in the boundary layer of fine sand, the offshore net transport rate was still found with the large velocity case due to strong phase-lag effect.

4.6. Erosion Depth

4.6.1. Maximum Erosion Depth

Further comparison between surface wave and oscillatory flow is the difference of erosion depth. In tunnels, despite the fact that free-stream velocity skewness is comparable, the erosion depth under the wave crest ($\delta_{e,crest}$) is almost the same as the erosion depth under the wave trough ($\delta_{e,trough}$) which is explained by phase-lag effects, (Ribberink et al., 2008). However, in the wave flume experiments, Schretlen et al. (2009) found the erosion depth under the wave crest is larger than wave trough for both medium and fine sand experiments, which directly leads to a net onshore velocity in the lowest levels of the sheet-flow layer. They explained that the reason of the difference in erosion depth is due to the contribution of the positive mean wave-Reynolds stress component to the time-dependent bed-shear stress. In order to know the influence of erosion depth, the maximum erosion depth and time-varying erosion depth were measured in the different flow conditions.

In this section, firstly, the maximum erosion depth will be discussed. And then, the temporal distribution of erosion depth will be described focusing on the influence of flow velocity, onshore streaming and wave period as well as sand size on the erosion depth. The variation of bed level was recorded by HSVC and the maximum erosion depth was measured according to Dohmen-Janssen (1999). The difference between the top of bed level at zero and maximum velocity is defined as maximum erosion depth. Previously, several researchers proposed a linear relationship between the relative erosion depth δ_{em}/D_{50} and the maximum Shields parameter θ_m with different linear coefficient.

The measured maximum erosion depth is plotted against the Shields parameter $\theta_{max.}$ in Fig. 4.26 with previous empirical relationships described in Section 2.6. Most of the data exist between the results of Zala-Flores and Sleath (1998) and Asano (1992). The experiment data are in reasonably good agreement with the calculated results for without onshore current and wave period T = 5 s. Dohmen-Janssen *et al*. (2001) showed that measured values of δ_{em}/D_{50} tended to be larger for fine sand than for medium or coarse sand because of transport regime between fine sand and medium sand.

Regardless of measurement results for combined wave and current condition are not within the range, the linear relationship is still observed between maximum erosion depth and Shields parameter. The liner coefficient of fine sand is larger than coarse sand. In this study, a combined wave-current Shields parameter, θ_{cw} was used to be more appropriate to relate values of δ_{em}/D_{50} .

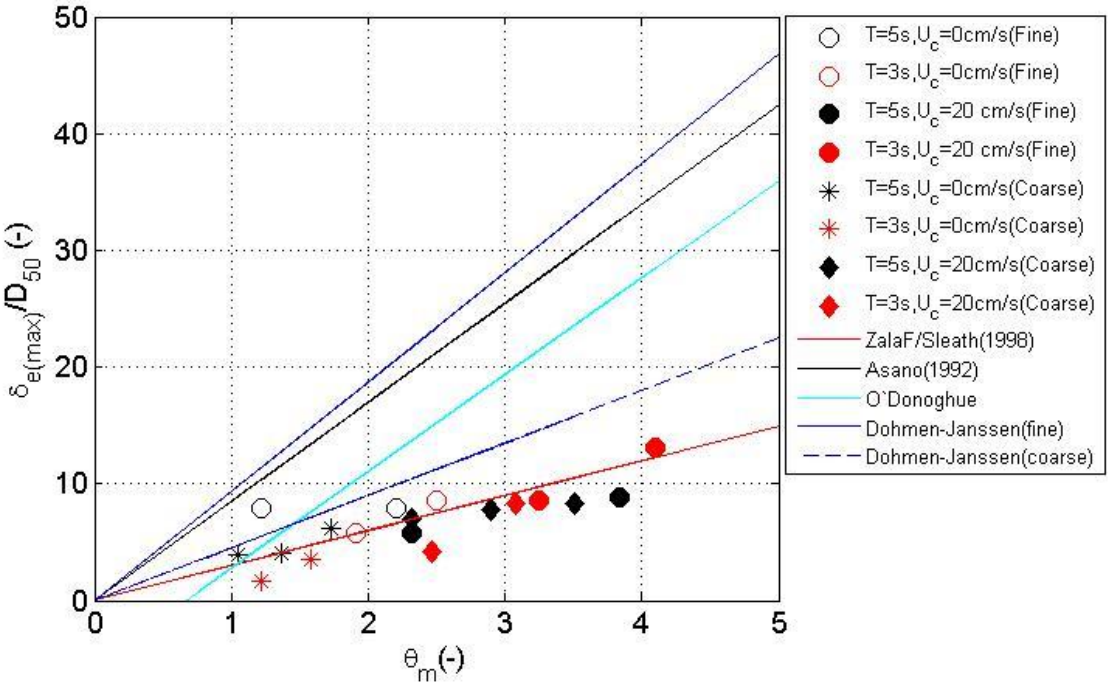

Fig. 4.26. Non-dimensional erosion depth against the Shields parameter

4.6.2. Time –varying Erosion Depth

Temporal variation of erosion depth under different experimental conditions is presented together with free- stream velocity in Fig. 4.27 to represent the influence of onshore streaming. In this figure, the initial bed level is set as equal to 0 (z =0 mm). In Figs.4.26 (a) and (b), in order to know the streaming effect, the time-varying of erosion depth is plotted including the data points for wave period of 3 s and 5 s with and without the onshore streaming. Taking into account the measured erosion depth under the combined wave and current, the erosion depth with onshore streaming U_c = 20 cm/s is larger than compared to U_c= 0 cm/s case. The erosion depth under wave crest is larger than under

wave trough for both types of sand. The asymmetry of erosion depth was observed in the case of combined wave and current conditions.

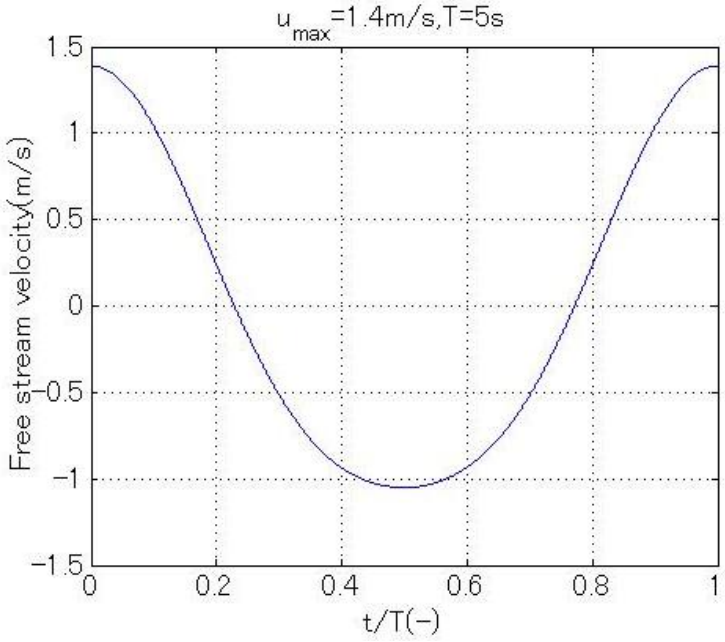

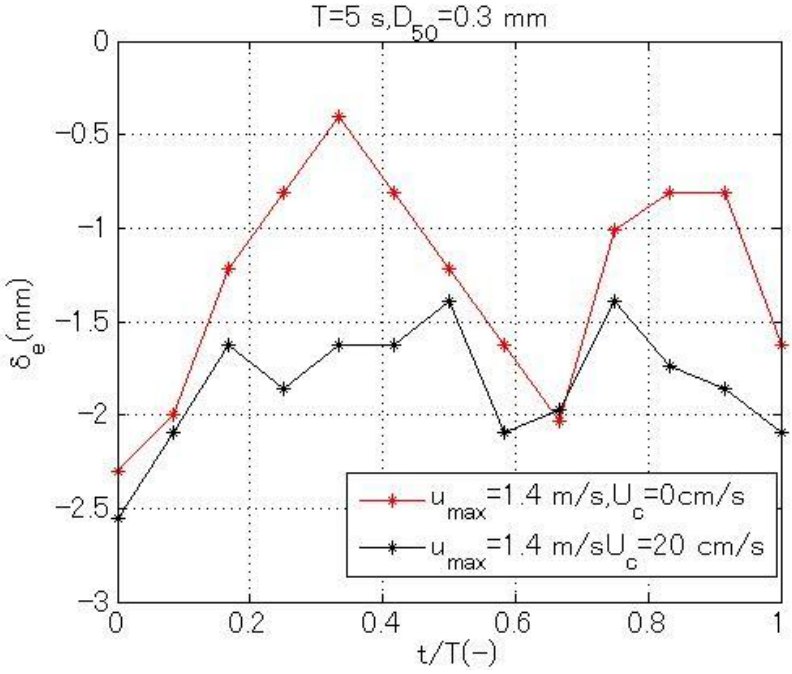

(a)

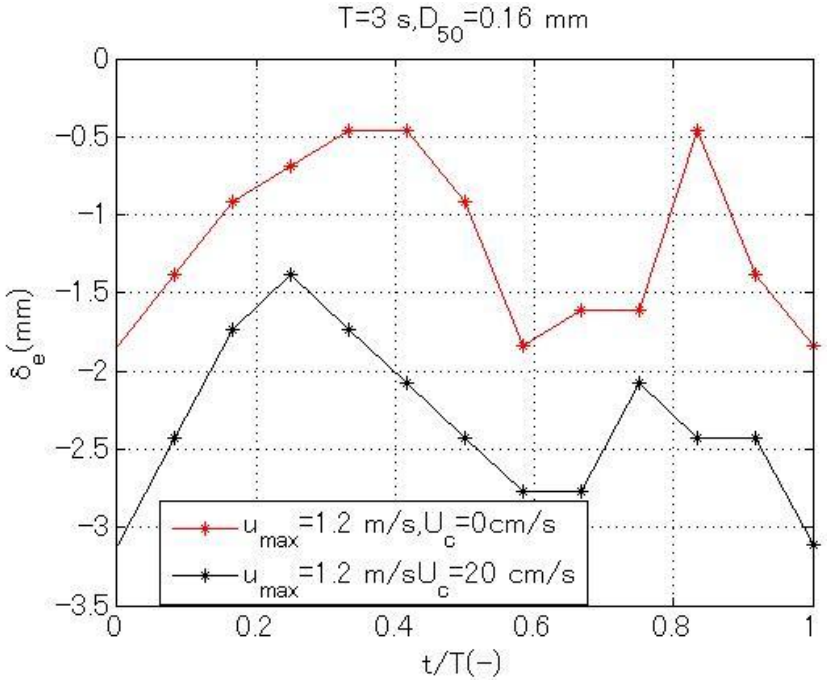

(b)

Fig.4.27. The influence of onshore streaming on time-varying erosion depth

To investigate the effect of flow velocity, the results for fine sand are shown in Figs. 4.28 (a) while the coarse sand in Fig. (b). The results show the erosion depth is increasing for increasing oscillatory velocity for both types of sand due to the increase in the bottom shear.

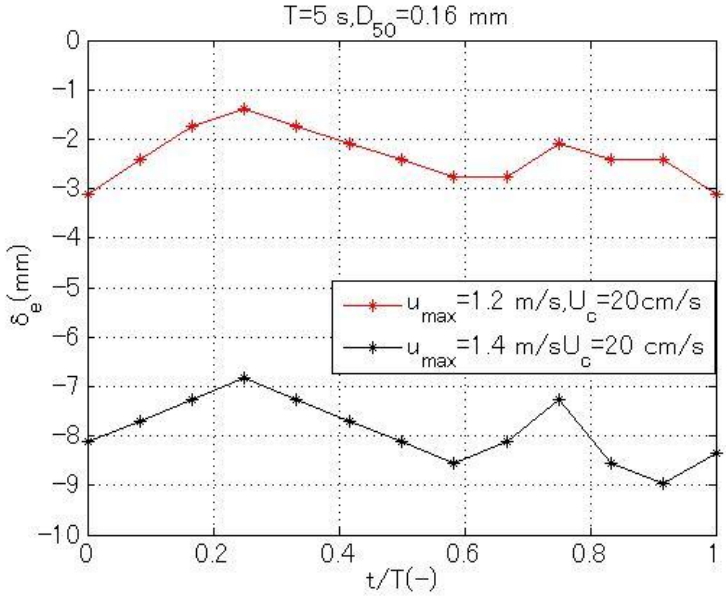

(a)

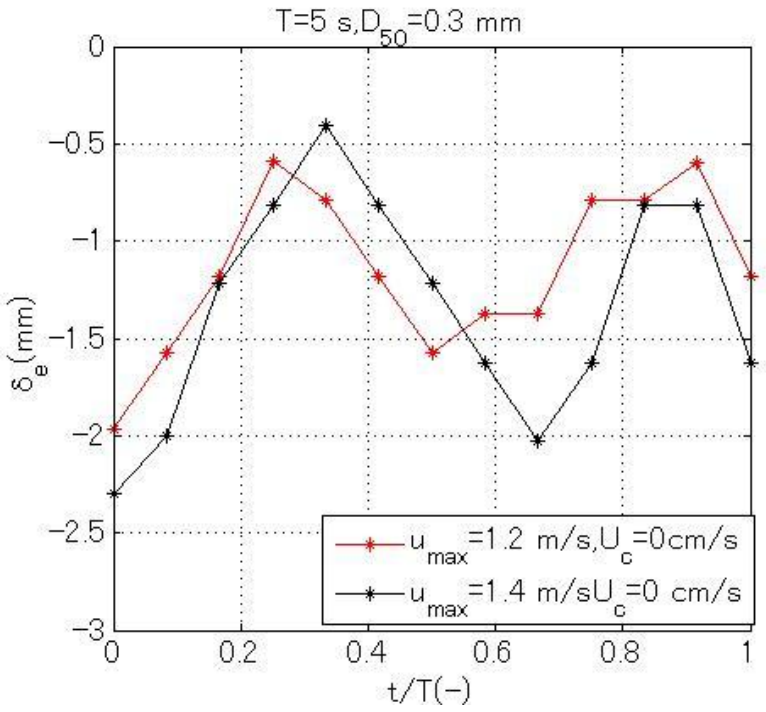

(b)

Fig. 4.28. The influence of velocity amplitude on time-varying erosion depth

The measured time-varying erosion with two different wave period and sand grain size are illustrated in Fig. 4.29 (a) and (b). Again, considering the effect of wave period and san size, the erosion depth for wave period 3 s is smaller than for 5s. And also, we can observe that the time-varying erosion depth increases with grain size due to the increase of the bottom shear stress or the friction factor.

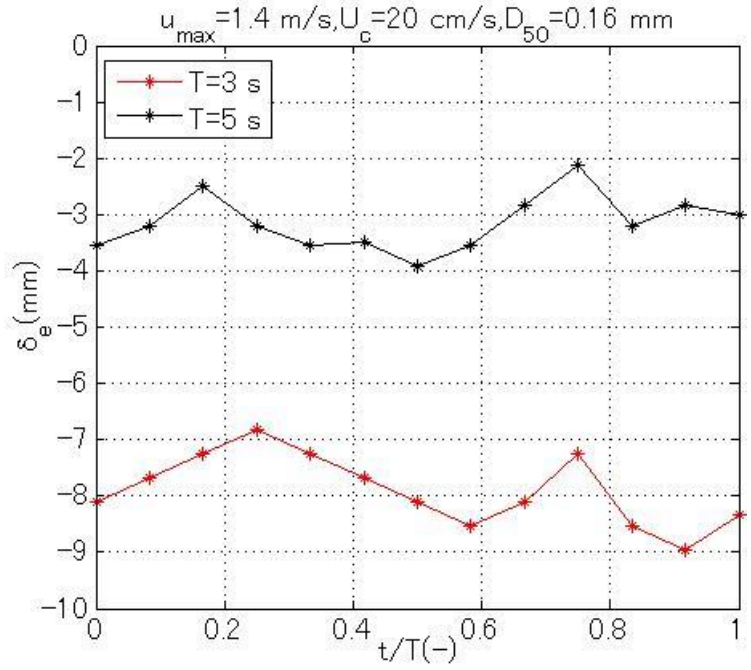

(a)

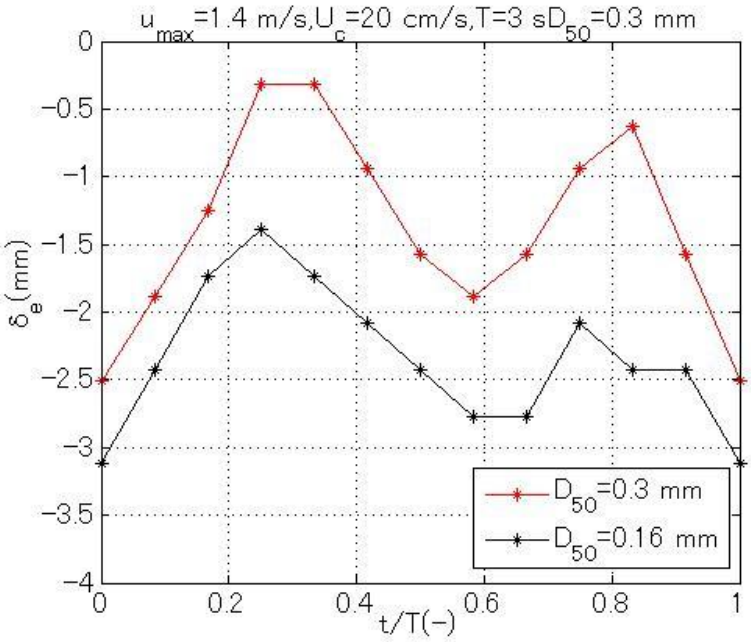

(b)

Fig. 4.29. The influence of wave period and sand size on time-varying erosion depth

CHAPTER 5

Comparison of Experimental Results and Verification of the Models

5.1. Comparison of measured and calculated sand transport rates

In the following section, the comparison is made through the measured net transport rates from the new experiments with existing four sand transport models described in chapter 2. In each figure, 5.1 and 5.2, the predicted transport rate is plotted against the measured transport rate under different flow conditions. In addition, previous experimental data which were collected under similar 2^{nd} -order Stokes wave conditions are incorporated in comparison. The data of Ribberink and Chen (1993), Ribberink and Al-Salem (1994) and O'Donoghue and Wright (2004) are used for comparison analysis.

The practical models, Dabajnia et al. (2001), (DW01), Ribberink (1998), (RB98), Dohmen-Janssen *et al*. (2002), (DM02), and SANTOSS (2010) are applied to verify the measured sediment net transport rates.

5.1.1. Ribberink (1998) and Dohmen-Janssen et al. (2002)

Fig. 5.1 presents the comparison of measured and calculated net transport rate by Ribberink (1998) and Dohmen-Janssen (2002). The solid line indicates a perfect agreement between the measured and predicted net transport rate, and dash lines represent the difference by a factor of two. The upper panel is Ribberink model and the lower is Dohmen-Janssen et al. Both Ribberink and Dohmen-Janssen *et al*. models were originally based on quasi – steady flow conditions. It means the time- dependent transport rate is instantaneously related to some power of the near bed orbital velocity or stress.

Ribberink (1998) and Dohmen-Janssen (2002) models predict well for the estimation on medium and coarse sands which fall within a factor of two. On the other hand, due to the quasi-steady assumption of Ribberink model, it cannot estimate the reasonable results for the magnitude and direction of offshore net transport rate with very fine sand and fine sand with large velocity case. As a result, Dohmen-Janssen's model

cannot be also predicted the offshore net rate properly because the Dohmen-Janssen et al. model was based on the model Ribberink. Although Dohmen-Janssen *et al*. model introduced a phase-lag parameter by considering the phase-lag effect, the model fails to show the offshore direction but it reduces the magnitude of net transport rate. It is confirmed that the two models do not predict the offshore transport for all fine sand cases.

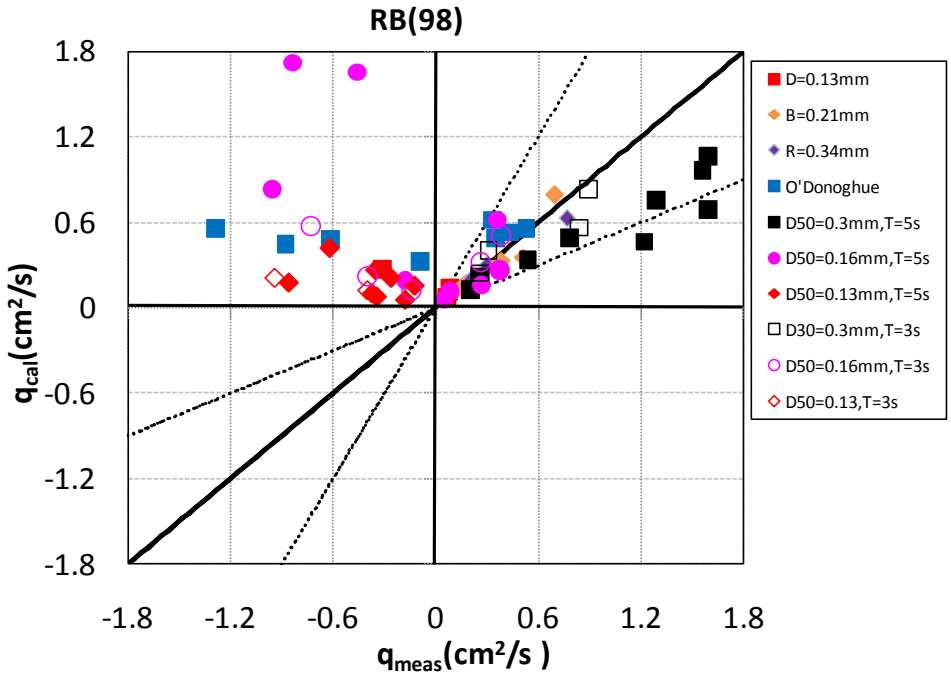

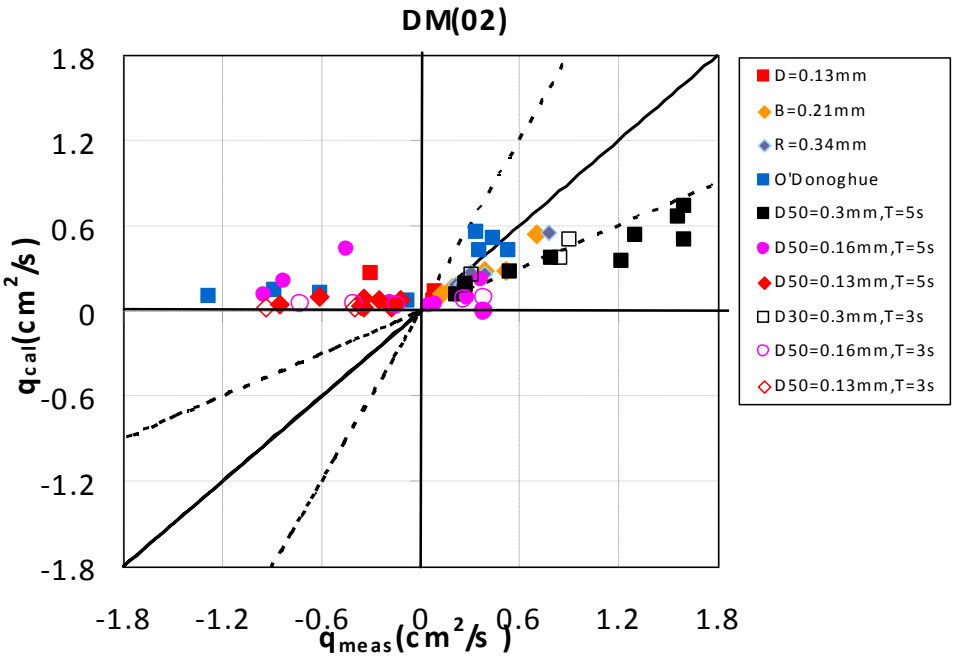

Fig. 5.1. Comparison between measured and predicted net sand transport rates (RB1998) and DM (2002)

5.1.2. Dibajnia et al. (2001) and SANTOSS(2010)

Fig. 5.2 presents the comparison between the test data and the prediction of Dibajnia *et al*. model (2001) and SANTOSS model (2010). The upper panel is Dibajnia et al. model and the lower panel is SANTOSS model. In Dibajnia *et al*. model, good agreements with experimental data for medium and coarse sand can be observed which are almost within a factor of 2 except some scattered values. However, it predicts the wrong direction of the sediment transport for the results with the fine sand data of O'Donoghue and Wright (2004) and with present measurements of fine and very fine sand data under combined wave and current conditions. Using SANTOSS (2010) model, it presents more reasonable results for most of cases. Most of the experiment results drop within in a factor of two and it leads into the accurate direction.

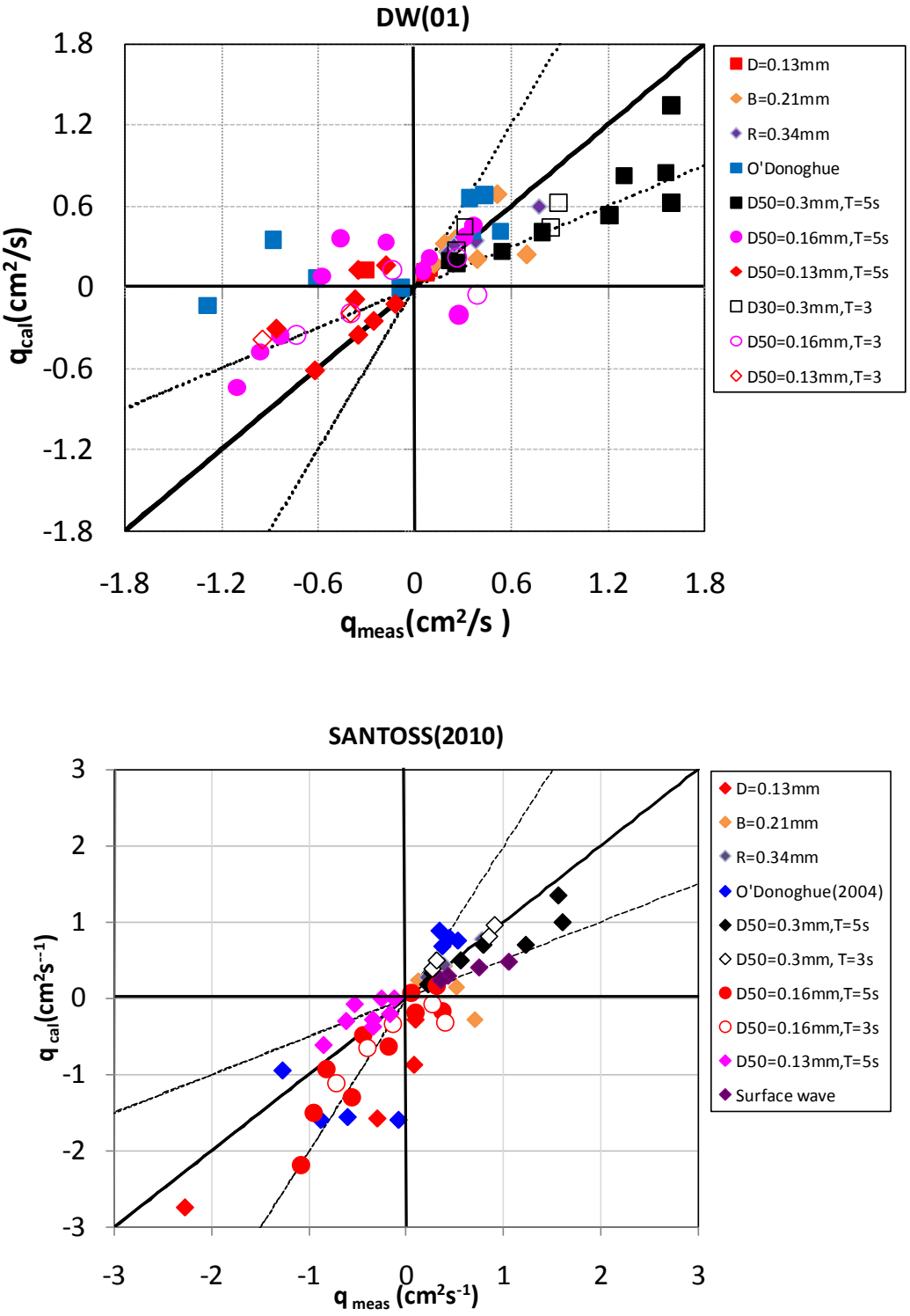

Fig. 5.2. Comparison between measured and predicted net sand transport rates (DW01) and (SANTOSS10)

5.2. SANTOSS Model with Streaming Velocity

Forementioned, the measured net transport rate with an onshore streaming results a larger onshore net transport comparing to that without streaming. It indicates that the contribution of small onshore current enhanced the onshore net rate somewhat. For very fine and fine sand case, the magnitude of net transport rate reduces but the direction still leads to offshore even onshorestreaming is generated with wave propagtion. It seems to be pointed out to study the other dominate factors which causes the difference between the oscillatory flow and surface wave.

As describe in section 5.1, the experimental results were compared with well-known four existing sediment transport models. Among the formulae studied, SANTOSS model gave better reliable results for most of the cases. Here, SANTOSS model is used to validate the measured net transport rate. Because Ribberink *et al*. (2010) modified the SANTOSS model taking into consideration the surface wave effect by incorporating the influence of boundary layer streaming, Lagrangian grain motion and vertical orbital velocity.

In this study, firstly, taking into account the streaming effect, the streaming related bed-shear is calculated based on Nielson (2006). In order to know the Lagrangian motion effect, the time required for wave crest and trough period is estimated based on SANTOSS model (2010). An additional time-averaged shear stress $-(\overline{\tilde{u}\tilde{v}})_\infty$ in terms of wave friction factor, f_w, and wave number, k, is,

$$(\overline{\tilde{u}\tilde{v}})_\infty = \frac{D_E}{\rho c} = \frac{1}{7\pi} A^3 \omega^2 f_e / c \tag{5.1}$$

The non-dimensional the streaming-related Shields parameter for crest and trough is calculated as,

$$\theta_{jsw} = \frac{(u_j^2 + (\overline{\tilde{u}\tilde{v}})_\infty)}{2sgD} \tag{5.2}$$

Here, the coefficient 1/7 is used to increase the bed shear stress.

where A is the near-bed semi-excursion distance and $\omega = \frac{2\pi}{T}$.

$$f_e = \exp\left[5.5\left(\frac{r}{A}\right)^{0.2} - 6.3\right] \tag{5.3}$$

where the roughness is $r = 2.5D_{50}$.

In case of Lagrangian grain motion, the longer crest period (T_{csw}) and the shorter period (T_{tsw}) is estimated according to Ribberink, *et al*. (2010).

$$T_{csw} = T_c + \Delta T_c, \quad T_{tsw} = T_t - \Delta T_c \tag{5.4}$$

ΔT is the ratio of the wave speed and the orbital diameter d_g .

$$\left.\begin{aligned} &\text{The longer wave crest period is} \quad \Delta T_t = \frac{d_g}{c} = \left\{\frac{c}{\zeta U_{rms}}\pi - 2\right\}^{-1} T \\ &\text{The smaller wave crest period} \quad \Delta T_c = \frac{d_g}{c} = \left\{\frac{c}{\zeta U_{rms}}\pi + 2\right\}^{-1} T \end{aligned}\right\} \tag{5.5}$$

The details explanation of various parameters used in SANTOSS model can be seen in section 2.2.4 of Chapter 2. Then, the net transport rate including both streaming effect and Lagrangian grain motion is estimated as,

$$q = \frac{\sqrt{|\theta_{csw}|}T_{c,sw}\left(\Omega_{cc} + \frac{T_{c,sw}}{2T_{cu,sw}}\ \Omega'_{tc}\right)\frac{\theta_{c,sw}}{|\theta_{csw}|} - \sqrt{|\theta_t, sw|}T_{t,sw}\left(\Omega_{tt} + \frac{T_{t,sw}}{2T_{tu}, sw}\Omega'_{ct}\right)\frac{\theta_t, sw}{|\theta_t, sw|}}{T}\sqrt{(s-1)gd_{50}^3} \tag{5.6}$$

This equation is the same as eq. (2.39) except the Shields parameter and the crest wave period and trough period which are calculated into considering the surface wave effect.

In this paragraph, the importance of the streaming component of the SANTOSS model was considered by comparing the computed sand transports with the measured sand transports. Fig. 5.3 (a and b) present the calculated and measured results of sand transport without and with including the effects of boundary layer streaming for two different types of sand under surface wave. Considering without streaming effect, the computed transport rates correspond with the measured data fall within a factor two, however, only small underestimations can be observed in Fig. 5.3. If the streaming effect is included, the performance of the model improves as the calculated net transport rate

with measured net transport lie with a factor of two. Thus, the SANTOSS model predicted well not only the oscillatory flow data but also the surface wave as it considers the relevant surface wave effect such as boundary streaming, Lagrangian motion and vertical orbital velocity effect.

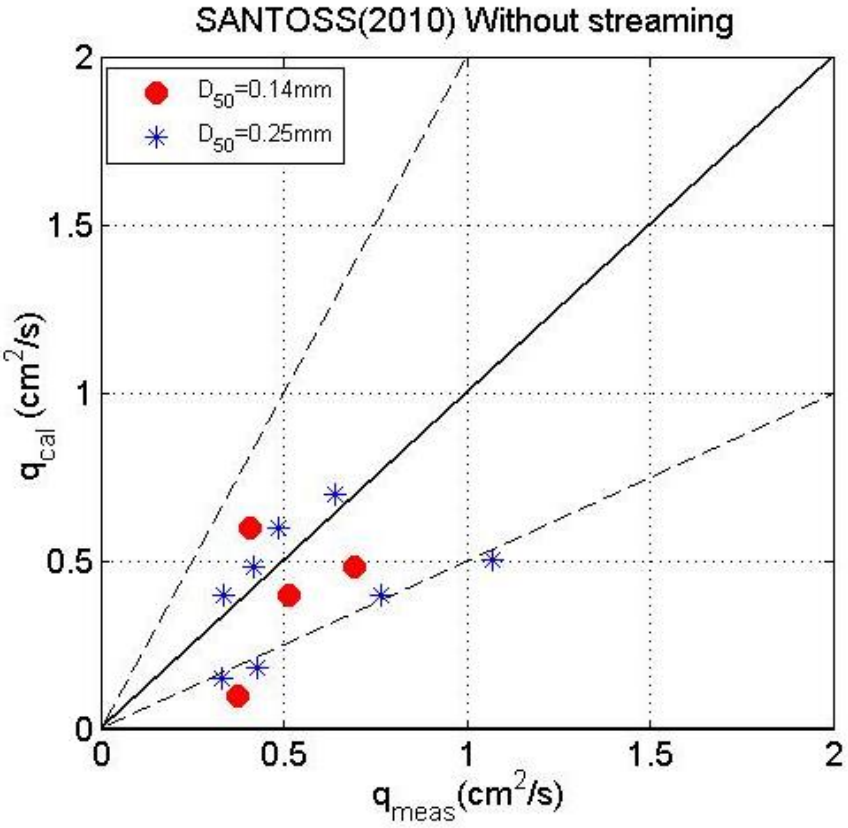

Fig. 5.3 (a). Comparison between measured and predicted net sand transport rates (SANTOSS model without streaming)

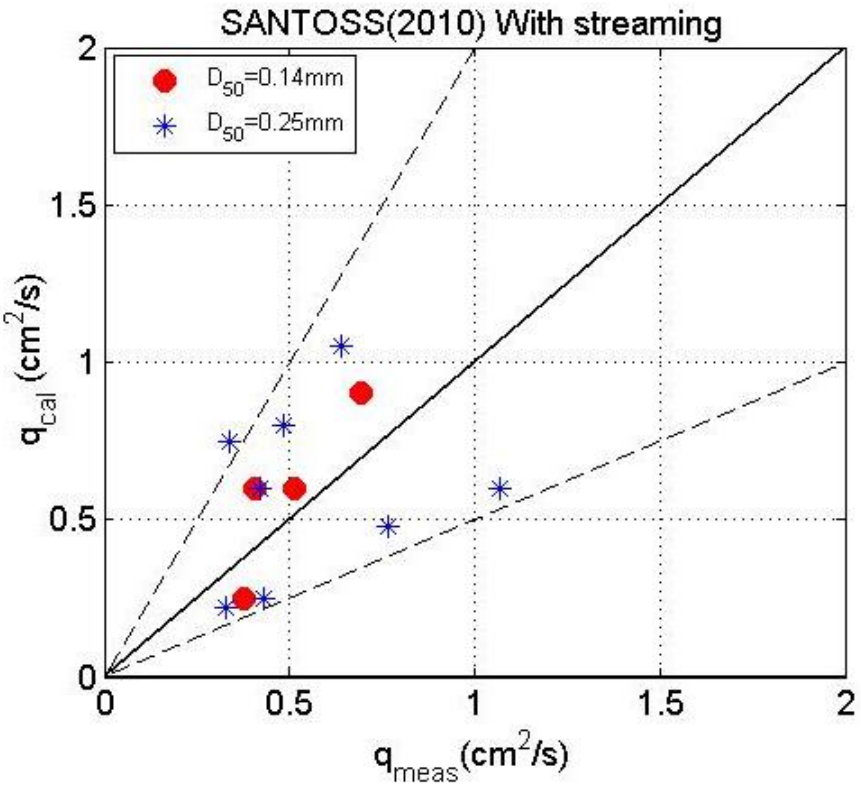

Fig. 5.3 (b). Comparison between measured and predicted net sand transport rates (SANTOSS model with streaming)

5.2.1 Validation of experiment data with SANTOSS model

In order to know how much the distribution of small onshore streaming enhanced the larger net rate, the results of net transport rate with onshore streaming are compared with SANTOSS model which includes surface wave effects. The experimental data sets described in Chapter 4 are applied to validate of SANTOSS model and the comparisons of net transport rate are demonstrated in following section.

The measurements results are compared with calculated results by the application of SANTOSS's model under different wave conditions. And then, to investigate the relative importance of boundary layer streaming effect to sediment transport, SANTOSS model was applied with considering streaming effect. Firstly, the model is regarded as streaming -related model which is incorporated with the boundary layer streaming effect (hereafter STR). And then, the calculated results with streaming effect are compared with the experimental measurements of net transport rate for all cases (U_c = 0,10,20 cm/s). Table

5.1, 5.2 and 5.3 present the measured net sediment transport rate and the predicted net transport rate considering with streaming.

Table 5.1. Comparison of Sediment Transport Rate (D_{50}=0.13 mm)

u_{max} (m/s)	T(s)	q_{net} (cm^2/s) (U_c=*0* cm/s)	q_{net} (cm^2/s) (U_c=*10 c*m/s)	q_{net} (cm^2/s) (U_c=*20* cm/s)	q_{net} (cm^2/s) (STR)
0.8	5	-0.17	-0.12	0.27	0.19
0.9	5	-0.35	-0.25	0.28	0.144
1.0	5	-0.37	-0.35	-	0.16
1.2	5	-0.83	-0.63	-	0.23

Table 5.2. Comparison of Sediment Transport Rate (D_{50}=0.16 mm)

u_{max} (m/s)	T(s)	q_{net} (cm^2/s) (U_c=*0* cm/s)	q_{net} (cm^2/s) (U_c=*10 c*m/s)	q_{net} (cm^2/s) (U_c=*20* cm/s)	q_{net} (cm^2/s) (STR)
0.8	5	0.05	0.28	-	0.544-
1.0	5	0.09	0.38	0.41	0.2
1.2	5	-0.18	0.31	0.56	0.23
1.4	5	-0.57	-0.45	-0.25	0.33
1.6	5	-0.93	-0.83	-0.6	0.44

Table 5.3. Comparison of Sediment Transport Rate (D_{50}=0.3 mm)

u_{max} (m/s)	T(s)	q_{net} (cm^2/s) (U_c=*0* cm/s)	q_{net} (cm^2/s) (U_c=*10 c*m/s)	q_{net} (cm^2/s) (U_c=*20* cm/s)	q_{net} (cm^2/s) (STR)
1.0	5	0.21	-	-	0.9
1.2	5	0.27	1.22	1.3	0.8767
1.4	5	0.54	1.56	1.6	0.99
1.6	5	0.8	1.6	1.85	1.16

In Fig. 5.4, the results of fine sand were described while keep the wave period and grain size considering the streaming effect (hereafter STR). The calculated results were plotted

against the experimental data under different flow conditions. The upper panel is for fine sand, the lower ones are for coarse sand.

The measured results of fine sand showed that all most data lie within a factor of two for all cases with U_c =0,10 and 20 cm/s. When the streaming effect was included, it enhanced the larger onshore net rate and it was consistent with the measured net transport rate with onshore current U_c =10 cm/s. However, for U_c =20 cm/s, the calculated results underestimate compared to the measured results.

In the case of coarse sand, also the SANTOSS's model with boundary layer streaming caused an increment of onshore net transport rate. The measured net transport rates with onshore streaming, U_c = 20 cm/s, are larger than the magnitude of the model results which include streaming effect. In case of U_c=10 cm/s, although the model under predicted, the results are within a range of factor of two. It indicates that the model results with streaming effect under predicted the net transport rate for all two types of grain size. Overall, it is observed that the calculated net transport rates with streaming effect (STR) are in the direction of wave propagation, which contributes to higher onshore sediment transport comparing to without streaming effect. As a result, the enhancement of larger onshore net transport rate by the addition of small onshore current is to be comparable with the prediction of the SANTOSS' model with inclusion of boundary layer streaming.

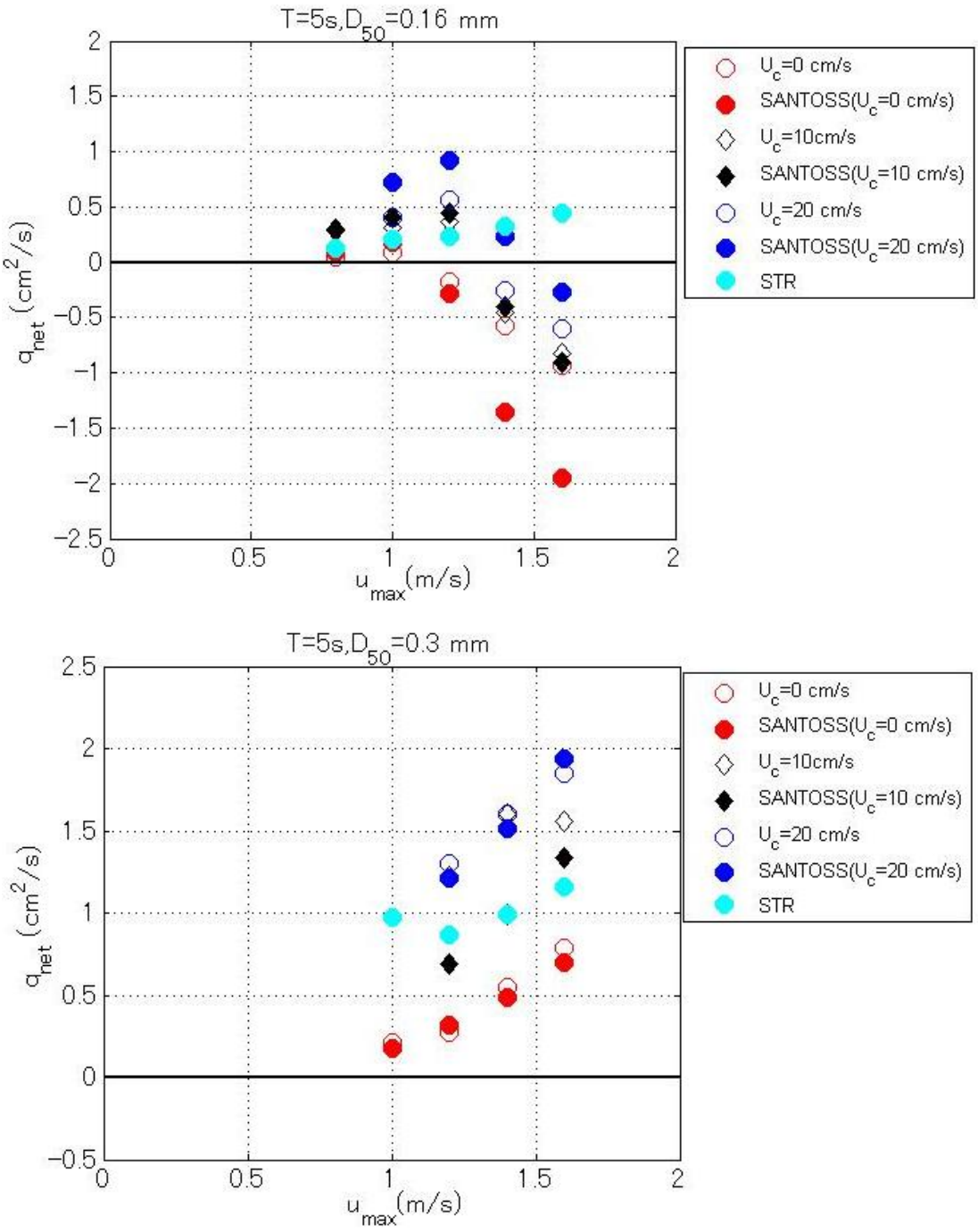

Fig. 5.4 Importance of boundary layer streaming

CHAPTER 6

Conclusions and Recommendations

6.1. Summary and Conclusions of Experimental Works

To answer the question whether the additional net onshore current contributes to a larger onshore net rate and to investigate the behavior of mean flow velocity profiles, a series of experiments was performed in the oscillatory flow tunnel and measurements of the net sand transport rate were conducted under asymmetric waves superimposed with an onshore current. To understand the effect of onshore streaming, a small current of 10 cm/s and 20 cm/s was generated in the onshore direction. Experiment result for small current 10 cm/s shows the magnitude offshore net transport rate reduces and the direction is to the offshore for very fine sand and fine sand with large velocity case. When increasing the small current value to 20 cm/s, the net transport rate of fine and very fine sand increases and changes to onshore direction with small velocity case. But for large velocity case, even though the magnitude of offshore net rate reduces, the direction is still directed to offshore for fine sand case. When the onshore current is contributed, the larger net transport rates of coarse sand are occurred. It is concluded that in general, the measured net transport rate with an onshore streaming results a larger onshore net transport comparing to that without streaming. Several exceptions were confirmed for fine sands under certain free-stream velocity conditions under which onshore streaming even enhances the offshore net transport, which is attributed to the phase-lag effect. The experiment results indicate that the onshore streaming, indeed, enhances the onshore net transport rate. The present experimental study shows the streaming-induced net transport rate is quantitatively affected by various factors, such as the free-stream velocity, wave period and the sand size.

Therefore, we conclude that the additional onshore current in the tunnel does contribute to more onshore sediment transport. Meanwhile, it is also confirmed that the phase-lag effect plays an important role in the sediment transport under the sheetflow conditions, especially for the fine sand case. In order to know the reason of the increment of onshore net transport rate due to the addition of small onshore current, the vertical profiles of mean flow velocity were investigated for all conditions. Sediment particle

velocity within the sand-laden sheetflow layer was measured by means of a PIV technique. From the PIV analysis, in the case of without current, the mean flow velocity, or wave–induced streaming, was directed to the offshore direction in the upper sheetflow layer while in the pick-up layer, a small value of onshore streaming produced for coarse sand. On the other hand, for fine sand case, an onshore mean flow was not observed in oscillatory flow tunnels. The mean flow velocity is always in the offshore direction. However, the mean flow velocity leads to onshore direction in the pick–up layer and sheet flow layer of fine sand and coarse sand in the condition of combined wave and current. In the suspension layer, the mean flow velocity for coarse sand changed from onshore to offshore direction. Under the 2^{nd}- order Stokes wave with onshore current, the boundary layer streaming gives an increase in additional onshore transport. It means the contribution of small onshore current enhances the larger onshore net rate for coarse and fine sand with small velocity case. But for very fine and fine sand with large velocity, even though the offshore net transport rate reduces, they do not show the onshore net rate like surface wave features. Hence, the wave-induced streaming cannot fully give an explanation about the difference of net rate between the oscillatory flow and surface wave. Further investigation is needed.

Under the same conditions of third-power flow velocity moment, $<u^3>$, the net rate of fine sand with onshore streaming, U_c =10 and 20 cm/s in oscillatory flow predicted about 75 % of surface wave experiments under the same conditions, $<u^3>$. Besides, the results for coarse sand with onshore streaming are significantly larger than the surface waves. It means that the onshore streaming of U_c 10 and 20 cm/s is sufficient for very fine and fine sand with small velocity case to produce the larger onshore net rate. For the large velocity case, the larger onshore streaming is needed to be contributed for the small sand-sized case. On the other hand, for the coarse sand, the onshore streaming is still quite large to produce the more onshore net rate. Thus, the contribution of onshore current and the mean flow profile are too much dependent on sediment size and also on the free-stream velocity. It can be drawn the conclusions from that results is that not only the streaming effect and also other effect may cause the difference of net transport rate between the oscillatory flow and surface wave.

SANTOSS model was applied in this study to investigate the relative importance

of effect boundary layer streaming. From the comparison results, measured net transport rates for combined wave-current can be comparable with the calculated results with the inclusion of the effect of boundary layer streaming. The model predicted more onshore sediment transport when it considers the streaming effect.

From the measurement of erosion depth, the erosion depth was found to be larger for a smaller wave period and small grain size due to the increase in the bottom shear stress or the increase in the friction factor. Taking into account the erosion depth under combined wave and current condition, the maximum erosion depth under wave crest, $\delta_{e,crest}$, was larger than the maximum erosion depth under wave trough, $\delta_{e,trough}$, for fine sand and coarse sand, it leads to a asymmetry of bed-shear stress resulting in a increase of net transport rate.

6.2. Recommendations

For future research, recommendations from the present study are expressed in this section. The following important aspect and work will be required to study.

-To verify the results of measured net transport, SANTOSS model was utilized in this study. To account the influence of boundary layer streaming, the time–averaged shear stress is simply added to this model. It is further necessary to improve the model which needs further specifications to cause an enhancement of onshore net rate.

- Here in, the onshore current was used only constant value of U_c = 10 and 20 cm/s. In order to know the effect of streaming, the amount of onshore current should be applied based on the free-stream velocity and sand size. Longer wave period should be approved to compare the surface experiment and to identify the effect of wave period.

-In this study, the sediment particles were measured by using PIV technique and also erosion depth was determined by image analysis. The reliable quantitative measurement s of concentration and velocity inside the sheetflow are needed by applying new measuring technique.

-The experimental approach is adopted and performed experiments in this study. And then, the analytical model is used to validate the present measured results. Further development of numerical modeling is necessary to implement the simulation considering the significant effects which dominate the difference between the oscillatory flow and

surface waves.

-In the present study, only the results for net transport rate and mean flow profile is achieved to compare with the surface wave experiment. Further comparisons of concentration and sediment flux between the oscillatory flow and surface waves should be investigated in details.

Bibliography

Ahmed, A.S.M., Sato, S., 2001. Investigation of bottom boundary layer dynamics of movable bed by using enhanced PIV technique. Coastal Eng. J., 43 (4), 239-258.

Ahmed, A.S.M., 2002. Sheet Transport Mechanism of the heterogeneous sands under nonlinear oscillatory sheetflows. Ph.D thesis. University of Tokyo,Japan.

Ahmed, A.S.M., Sato, S., 2003a. A sheetflow transport model for asymmetric oscillatory flows - part I: uniform grain size sediments. Coastal Eng. J., 45 (3), 321-337.

Ahmed, A.S.M., Sato, S., 2003b. A sheetflow transport model for asymmetric oscillatory flows - part II: mixed grain size sediments. Coastal Eng. J., 45 (3), 339-361.

Asano, T., 1990. Two-phase flow model on oscillatory sheet-flow. ASCE, Proceedings of the 22nd Inter. Conf. on Coastal Eng., 2372-2384.

Bailard, J.A., 1981. An energetic total load sediment transport model for a plane sloping beach. J. Geophys. Res., 86 (C11), 10938-10954.

Davies, A.G., Li, Z., 1997. Modelling sediment transport beneath regular symmetrical and asymmetrical waves above a plane bed. Cont. Shelf Res., 17(5), 555-582.

Davies, A.G., Ribberink, J.S., Temperville, A., Zyserman, J.A., 1997. Comparisons between sediment transport models and observations made in wave and current flows above plan beds. Coastal Eng., 31, 163-198.

Davies, A.G., Van Rijn, L.C., Damgaard, J.S., Van de Graaff, J., Ribberink, J.S., 2002. Intercomparison of research and practical sand transport models. Coastal Eng., 46, 1-23.

Dibajnia, 1991. Study on nonlinear effects in beach processes. PhD thesis, University of Tokyo, September 1991, 105 pp.

Dibajnia, M., Watanabe, A. 1992. Sheet flow under nonlinear waves and currents. ASCE, Proceedings of the 23rd Inter. Conf. on Coastal Eng., 2015-2028.

Dibajnia, M., Shimizu, T., Watanabe, A., 1994. Profile change of a sheet flow dominated beach. ASCE, Proceedings of the 24th Inter. Conf. on Coastal Eng., 1946-1960.

Dibajnia, M., 1995. Sheet flow transport formula extended and applied to horizontal plan problems. Coastal Eng. in Japan, 38(2), 179-194.

Dibajnia, M., Watanabe, A., 1996. A transport rate formula for mixed-sized sands. ASCE, Proceedings of the 25th Inter. Conf. on Coastal Eng., 3791-3804.

Dibajnia, M., Moriya, T., Watanabe, A., 2001. A representative wave model for estimation of nearshore local transport rate. Coastal Eng. J., 43(1), 1-38.

Dohmen-Janssen, C.M. (1999). Grain size influence on sediment transport in oscillatory sheet flow. Phase-lags and mobile-bed effects. PhD thesis, Delft Univ. of Tech., the Netherlands, ISBN 90-9012929-4.

Dohmen-Janssen, C.M., Hassan, W.N., Ribberink, J.S., 2001. Mobile-bed effects in oscillatory sheet flow. J. Geophys. Res., 106 (C11), 27103-27115.

Dohmen-Janssen, C.M., Kroekenstoel, D.F., Hassan, W.N., Ribberink, J.S., 2002. Phase lags in oscillatory sheet flow: experiments and bed load modeling. Coastal Eng.,46, 61-87.

Dohmen-Janssen, C.M., Hanes, D.M., 2002. Sheet flow dynamics under monochromatic nonbreaking waves. J. Geophys. Res., 107 (C10), 27103-27115.

Dohmen-Janssen, C.M., Hanes, D.M., 2005. Sheet flow and suspended sediment due to wave groups in a large wave flume. Cont. Shelf Res., 25(3), 333-347.

Dong, P., Zhang, K., 1999. Two-phase flow modelling of sediment motions in oscillatory sheet flow. Coastal Eng., 36, 87-109.

Dong, P., Zhang, K., 2002. Intense near-bed sediment motions in waves and currents. Coastal Eng., 45, 75-87.

Fuhrman D.R., Sumer B. M. , and Fredsøe1 J., 2011. Roughness -induced streaming in turbulent wave boundary layers. J. Geophys. Res., 116, C10002.

Gui, L., Merzkirch, W., 1996. A method of tracking ensembles of particle images. Experiments in Fluids, 21, 465-468.

Holmedal, L.E., Myrhaug, D., 2009. Wave-induced steady streaming, mass transport and net sediment transport in rough turbulent ocean bottom boundary layers.Continental Shelf Research, 29, 911-926.

Horikawa, K., Watanabe, A., Katori, S. 1982. Sediment transport under sheet flow condition. ASCE, Proceedings of the 18th Inter. Conf. on Coastal Eng., 1335-1352.

Janssen, C.M., Ribberink, J.S., 1996. Grain-size influence on sand transport in oscillatory sheet flow. ASCE, Proceedings of the 25th Inter. Conf. on Coastal Eng., 4779-4792.

Jensen, B.L., Sumer, B.M., Fredsøe, J., 1989. Turbulent oscillatory boundary layers at high Reynolds numbers. J. Fluid Mech., 206, 265-297.

Liu, H., Sato, S., 2005. Laboratory study on sheetflow sediment movement in the oscillatory turbulent boundary layer based on image analysis, Coastal Eng. J.47(1), 21-40.

Liu, H., 2005.Laboratory Experiments and Numerical Simulation on Sheetflow Sediment Movement, PhD Thesis, University of Tokyo

Longuet-Higgins, M.S., 1953. Mass transport in water waves. Phil. Trans. R. Soc. Lond. A, 245, 535-581.

Longuet-Higgins, M.S., 1957. The mechanics of the boundary layer near the bottom in a progressive wave (Appendix to a paper by R.C.H. Russel and J.D.C. Osorio). Proc. 6th Conf. on Coastal Eng., Miami, ASCE, 184-193.

Longuet-Higgins, M.S., 2005. On the wave set-up in shoaling water with a rough sea bed. J. Fluid Mech., 527, 217-234.

Madsen, O.S., Grant, W.D., 1976b. Sediment transport in the coastal environment, Rep. 209. Ralph M. Parsons Lab. For Water Resour. And Hydrodyn., Dept. of Civil Eng., Mass. Inst. of Technol., Cambridge, pp 105.

Meyer-Peter, E., Muller, R., 1948. Formulas for bed-load transport. Proc. 2nd Congr. Int. Assoc. Hydr. Struct. Res., Stockholm, Sweden, 39-64.

Nielsen, P., 1992. Coastal Bottom Boundary Layers and Sediment Transport. World Scientific, Singapore. 324 pp.

Nielsen, P., You, Z.-J., 1996. Eulerian mean velocities under non-breaking waves. Proc. 25th Conf. on Coastal Eng., Orlando, ASCE, 4066-4078.

Nielsen, P., 2002. Shear stress and sediment transport calculations for swash zone modeling. Coast. Eng. 45, 53– 60.

Nielsen, P., Callaghan, D.P., 2003. Shear stress and sediment transport calculations for sheet flow under waves. Coastal Engineering, 47, 347-354.

Nielsen, P, 2006. Sheet flow sediment transport under waves with acceleration skewness and boundary layer streaming. Coastal Engineering, 53, 749-758.

O'Donoghue, T., Clubb, G.S., 2001. Sand ripples generated by regular oscillatory flow. Coastal Eng., 44, 101-115.

O'Donoghue, T., Wright, S., 2004a. Concentrations in oscillatory sheet flow for well sorted and graded sands. Coastal Eng., 50 (3), 117-138.

O'Donoghue, T., Wright, S., 2004b. Flow tunnel measurements of velocities and sand flux in oscillatory sheet flow for well-sorted and graded sands. Coastal Eng., 51 (11-12), 1163-1184.

Ribberink, J.S., Al-Salem, A.A., 1994. Sediment transport in oscillatory boundary layers in cases of rippled beds and sheet flow. J. Geophys. Res., 99 (C6),12707-12727.

Ribberink, J.S., Al-Salem, A.A., 1995. Sheet flow and suspension of sand in oscillatory boundary layers. Coastal Eng., 25, 205-225.

Ribberink, J.S., 1998. Bed-load transport for steady flows and unsteady oscillatory flows. Coastal Eng., 34, 59-82.

Ribberink, J.S., Dohmen-Janssen C.M., Hanes D.M., Mclean S.R. Vincent C., 2000. Near-Bed sand transport mechanisms under waves

Ribberink, J.S., Van der Werf J.J., and O'Donoghue, T., 2008. Sand motion induced by oscillatory flows; sheet flow and vortex ripples. Journal of Turbulence, Vol. 9, No. 20. 477, The Netherlands.

Ribberink, J.S., Van der A, D.A., Buijsrogge, R.H., 2010. SANTOSS transport model – A new formula for sand transport under waves and currents. Report SANTOSS_UT_IR3, University of Twente, The Netherlands.

Sato, S., Horikawa, K., 1986. Laboratory study on sand transport over ripples due to asymmetric oscillatory flows. ASCE, Proceedings of the 20th Inter. Conf. on Coastal Eng., 1481-1495.

Scandura, P., 2007. Steady streaming in a turbulent oscillating boundary layer. J. Fluid Mech., 571, 265-280.

Schretlen, J.J.L.M., Ribberink, J.S., O'Donoghue, T., 2009. Sand transport under full-scale surface waves. Proc. 6th Conf. on Coastal Dynamics, Tokyo, Paper 123.

Schretlen, J.J.L.M., Ribberink, J.S., and O'Donoghue. T., 2010. Boundary layer flow and sand transport under full scale surface waves, Proceedings of the 32nd Inter. Conf. on Coastal Eng.,337

Trowbridge, J., Madsen, O.S., 1984. Turbulent wave boundary layers 2. Second- order theory and mass transport. Journal of Geophysical Research 89 (C5), 7999–8007.

Van der A, D.A., O'Donoghue , T., Ribberink, J.S.,2009. Measurements of sheet flow transport in acceleration-skewed oscillatory flow and comparison with practical formulations. Coastal Eng.J.,(2009)

Van der A, D.A., Ribberink O'Donoghue, T., Wright, and. Van der Werf, J.J., 2010. New practical model for sand transport induced by non-breaking waves and currents, Proceedings of the 28th Inter. Conf. on Coastal Eng., 273,331-342.

Van der Werf, J.J., Ribberink J.S. and O'Donoghue T., 2007. Development of a new practical model for sand transport induced by non-breaking waves and currents. Coastal Sediments '07, ASCE, 42-55.

Van der Werf, J.J., Schretlen, J.J.L.M Ribberink J.S., and O'Donoghue.T.,2009. Database of fullscale laboratory experiments on wave-driven sand transport processes, Coastal Engineering, 56, 726-732.

Wright, S., 2002. Well-sorted and Graded Sands in Oscillatory Sheet-flow, PhD Thesis, University of Aberdeen.

Wright, S., O'Donoghue, T., 2002. Graded sediments in oscillatory sheet flow. ASCE, Proceedings of the 28th Inter. Conf. on Coastal Eng., 2638-2650.

Wouter Kranenburg1, Ribberink1, J.S., and Rob Uittenbogaard., 2010.Sand transport by surface wave. Proceedings of the 32nd Inter. Conf. on Coastal Eng., Paper 337

Xiao Yu, Tian-Jian Hsu, and Daniel M. Hanes., 2010. Sediment transport under wave groups: Relative importance between nonlinear wave shape and nonlinear boundary layer streaming.,J. Geophys. Res., 115(C0203),.

Zala-Flores, N., Sleath, J.F.A., 1998. Mobile layer in oscillatory sheet flow. J. Geophys. Res., 103 (C6), 12783-12793.